Yttrium, Gadolinium and Lutetium Based Endohedral Metallofullerenes: From Synthesis to Application

Jianyuan Zhang

Dissertation submitted to the Faculty of Virginia Polytechnic Institute and State University in partial fulfillment of the requirements for the degree of

Doctor of Philosophy

In

Chemistry

Harry C. Dorn

Harry W. Gibson

Paul R. Carlier

Webster L. Santos

Dec. 4, 2013 Blacksburg, Virginia

Key words: Endohedral Metallofullerene, Metal Carbide Cluster, Trimetallic Nitride Template, Clusterfullerene, “Top-down” Fullerene Formation, Isolated Pentagon Rule, Contrast Agent

Yttrium, Gadolinium, and Lutetium Based Endohedral Metallofullerenes: From Synthesis to Application

Jianyuan Zhang

Abstract

Endohedral metalofullerenes (EMFs) have emerged as an important class of nanomaterials with vast promise in applications of molecular devices and nanomedicines. This dissertation addresses the EMF research span from synthesis to application, with an emphasis of work on trimetallic nitride template (TNT) EMF and carbide clusterfullerenes (CCFs).

As a general introduction, chapter 1 reviews the main literature in TNT EMF studies. Also key works in CCF area are highlighted to show the common feature and uniqueness of this class of EMF in comparison with other EMFs. In the last part of the chapter a list of milestone progress in EMF area has been summarized.

Chapter 2 is devoted to the synthetic work on EMFs. Especially, for isotopic modification, the trial and actual EMF syntheses in efforts to introduce ^{13}C, ^{89}Y and ^{177}Lu are described.

The next three chapters address the structural characterization of EMFs. Chapter 3 focuses on structural studies of CCFs. With detailed interpretation of ^{13}C NMR and DFT computational results for selected members of the $Y_2C_2@C_{2n}$ family, the influence of fullerene cage on the size and shape of the yttrium carbide cluster $(Y_2C_2)^{4+}$ is investigated. It has also been established that the carbide cluster prefers a linear shape in sufficiently large fullerene cages but adopts a compressed butterfly shape in smaller cages where space is constrained.

Chapter 4 presents a systemic examination of dipole moments in TNT EMFs. The first ^{13}C NMR study of $M_3N@C_2(22010)\text{-}C_{78}$ is achieved on $Y_3N@C_2(22010)\text{-}C_{78}$. In addition, dipole

moments of the $M_3N@C_{2n}$ (n=39-44) family are probed by interpretation of chromatographic retention behavior, DFT computational results and single-crystal data. It has been found that TNT EMFs with pentalene motifs exhibit enhanced dipole moments due to the cluster-cage interplay.

Chapter 5 provides full characterization of the $M_2C_2@C_1(51383)$-C_{84} (M=Y, Gd) molecule, which contains the first example of an asymmetric fullerene cage with fused pentagons. Furthermore, it is suggested that the $C_1(51383)$-C_{84} cage is capable of a cascade of rearrangements into high symmetry and stable fullerene cages via well-established mechanistic steps, namely, extrusion of C_2 units from pentalene or indene motifs and Stone-Wales transformations. As an important intermediate in the formation of high symmetry fullerene cages, the $C_1(51383)$-C_{84} represents a missing link that implies the "top-down" fullerene formation mechanism.

Chapter 6 describes the endeavor to functionalize two exotic EMFs, the room-temperature radical heterometallofullerene $Gd_2@C_{79}N$, and the egg-shaped TNT EMF $Gd_3N@C_{84}$. The reactivity of $Gd_2@C_{79}N$ is directly compared to $Y_2@C_{79}N$, $Gd_3N@C_{80}$ and $Sc_3N@C_{80}$ in two reactions and the paramagnetic $Gd_2@C_{79}N$ is proven to be very inert toward many known common fullerene cage reactions. Eventually both EMFs have been successfully functionalized via the Bingel reaction, and the derivatives are characterized with HPLC and mass-spectrometry.

Chapter 7 compares the effective magnetic moment of $Gd_3N@C_{80}$ and $Gd_3N@C_{84}$, together with the previously reported $Gd@C_{82}$. The magnetic moment has a second-order contribution to the T_1 relaxivity and thereby is an important factor to evaluate an EMF's value in application as MRI contrast agents. Furthermore the influence of cluster motion to magnetic behavior in TNT EMF is discussed.

Acknowledgement

Several lines in the dissertation acknowledgement will not be able to fully express my deepest and most sincere appreciation to my research advisor, Dr. Harry Dorn, for his inspiration, guidance, support and friendship. I appreciate him as a mentor, who provides me with valuable academic training and advice when I explore the world of NMR and metallofullerenes. I also appreciate him as a captain, who works together with me when we probe into the area that is unknown to both of us, and gives me numerous inspirations in science and morale all the time. Finally, I appreciate him as a lead, whose academic dedication and scientific curiosity set up an example to follow for the rest of my career and life.

I also would like to thank my advisory committee for their time, patience, encouragements and suggestions. Dr. Harry Gibson has been an inexhaustible source of literature and ideas. Every time I talk to him I gain knowledge and realize there is more reading to do. Meanwhile, his care reaches smallest details. I can still remember when I proposed a click reaction in group meeting that he was present, in 30 minutes he sent me an instruction of how to safely handle sodium azide. Dr. Paul Carlier and Dr. Webster Santos have given me valuable training class in organic chemistry. Moreover, I used to be overly cautious in research protective to samples. After Dr. Carlier and Dr. Santos encouraged me to be "bolder" in research, I have become more aggressive and obtained many valuable results thanks to that. As an expert in inorganic lanthanides, Dr. Reineke has also provided many insightful suggestions to my work on lanthanide-based endohedral metallofullerenes.

I gratefully thank other faculty members and colleagues in Virginia Tech who has been so helpful. Thanks Dr. Paul Deck for the guidance in departmental policies and generous help with vacuum system. Thanks Dr. Patricia Amateris and Dr. John Morris for their instructions to help me become a better teaching assistant. Thanks Dr. Yee for his kind instruction and cooperation in the magnetic research (Chapter 7). Thanks Dr. Wi and Dr. Azurmendi for their help in NMR study. Thanks Dr. Keith Ray and Mr. Kim Harich for mass-spectral work. Thank Dr. Mehdi Ashraf-Khorassani for his help with HPLC. Thanks Dr. James Mahaney for his help with EPR. Thanks Tom Wertalik for his glass craftsmanship that is important to my research. I also thank the help from Wenyu Zhang, Daniel Schoonover, Dave Hobart, Ying Chen, Charles Carfagna Jr., Dr. Zhenbin Niu, Dr. Daiqiang Xu, Dr. Lesley Owens, Dr. Jianbo Hou, Dr. Ming Ma and other friends.

I also thank the collaborative support outside the University. Especially, I sincerely thank Dr. Daniel Bearden from Hollings Marine Laboratory, NIST, SC, for his long time NMR collaboration, which provided key results for Chapter 3, Chapter 4 and Chapter 5. Thanks Dr. James Duchamp from Emory Henry College, VA for his instructions in metallufullerene synthesis, which enabled my work described in Chapter 2. Thank Dr. Alan Balch, Dr. Marylin Olmstead and Faye Bowles from UC Davis, CA for their single-crystal collaboration, which substantially contribute to the work in Chapter 5. Thanks Dr. Panos Fatouros, Dr. Mike Shultz, Dr. Minghao Sun and other colleagues from Virginia Commonwealth University for their collaboration in medical application of metallofullerenes. I also thank the scientists in *Luna Innovations* for their help in large-quantity sample synthesis.

My work could not have been done without the support from the Dorn group members. I enjoy the collaborative atmosphere in the group and thank the help from Dr. Wujun Fu, Dr. Jianfei Zhang, Dr. Tim Fuhrer, Dr. Chunying Shu, Dr. Jiechao Ge, Hunter Champion, Kaitlyn Dixon,

Chris Pregot, Xiaoling Wang, Sarah Black, Jonathon Reid, Tinghui Li, and specially, our administrative assistant, Stephanie Hurt. In addition, many alumni that did not overlap with me in the group, including Dr. Ting Cai, Dr. Liaosa Xu and Dr. Tianming Zuo, have also provided important help.

I would like to give special thanks to my family members in China, especially my mother Decong Cai and my father Xian Zhang. They have always been supportive to me. Finally, I thank my fiancé Youqing Ye. Her company has made my Ph. D a much more wonderful experience.

Yttrium, Gadolinium and Lutetium Based Endohedral Metallofullerenes: From Synthesis to Application

Chapter 1 Nitride and Carbide Clusterfullerenes

Chapter 2 Introduction of Special Isotopes to Endohedral Metallofullerenes

List of Figures

Chapter 1 Nitride and Carbide Clusterfullerenes

Chapter 2 Introduction of Special Isotopes to Endohedral Metallofullerenes

Chapter 3 Nanoscale Fullerene Compression of an Yttrium Carbide Cluster

Chapter 5 A Missing Link in the Transformation from Asymmetric to Symmetric Metallofullerene Cages Implies a Top-Down Fullerene Formation Mechanism

Chapter 6 Functionalization of Gadolinium Based Endohedral Metallofullerenes with Bingel Reaction

Chapter 7 Magnetic Moments of Gadolinium Endohedral Metallofullerenes

List of Tables

Chapter 1 Nitride and Carbide Clusterfullerenes

Part of this chapter is adopted from a manuscript published on *Accounts of Chemical Research* with appropriate modifications under the permission of the American Chemical Society. Full text of the published manuscript, entitled "*Trimetallic nitride template endohedral metallofullerenes: discovery, structural characterization, reactivity, and applications*" by Jianyuan Zhang, Steven Stevenson and Harry C. Dorn, can be obtained at http://pubs.acs.org/doi/pdf/10.1021/ar300301v.

1.1 Chapter overview

Upon discovery of the new carbon allotrope, the fullerene C_{60},[1] it was recognized that the hollow spheroidal shape could accommodate metal atoms or clusters, which quickly led to the discovery of endohedral metallofullerenes (EMFs).[2] In the past two decades, EMFs have attracted broad interest in different areas of chemistry, including inorganic chemistry, organic chemistry, materials chemistry and biomedical chemistry due to their unique features.[3] For example, certain EMFs provide new clusters that do not exist outside of a fullerene cage, and some enable 10-50 times more efficient magnetic resonance (MR) imaging compared to commercial contrast agents.[3] EMFs that encapsulate only metal ion(s) are referred as "traditional metallofullerenes", and that encapsulate metal-nonmetal clusters are called clusterfullerenes, which can be further classified as based on the type of the encapsulated clusters, into trimetallic nitride template endohedral metallofullerenes (TNT EMFs, or nitride clusterfullerenes, NCFs), carbide clusterfullerenes (CCFs), oxide clusterfullerenes (OCFs), sulfide clusterfullerenes (SCFs) and others. In this chapter, I introduce the discovery of clusterfullerenes and then describe the progression of EMF research from synthesis to applications, using trimetallic nitride template (TNT) EMFs as typical examples. First, I describe the synthetic methodology for several TNT EMFs with an emphasis on chemically adjusting plasma temperature, energy and reactivity (CAPTEAR) tuning to optimize the type and yield of TNT EMFs produced. Second, I review approaches used to separate and purify pristine TNT EMF molecules from their corresponding

product mixtures. Although early separations were achieved by high performance liquid chromatography (HPLC), facile separations based on the reduced chemical reactivity of the TNT EMFs are now commonly employed. The improved production yields and separation protocols have been recently realized for industrial production of TNT EMFs. Third, I summarize the structural features, including cage structures, cluster arrangement and dynamics of individual members of the TNT EMF class. Fourth, I illustrate typical functionalization reactions of the TNT EMFs and corresponding characterization of their derivatives. Two major chemical reaction categories are cycloaddition and radical reactions. Fifth, I use selected examples to illustrate the unique magnetic and electronic properties of certain TNT EMFs for biomedicine and molecular device applications. Then, I cover the studies performed on CCFs which represent another important class of molecules in this dissertation. Finally, I summarize the important work related to EMFs in a chronological order.

1.2 Discovery and a brief introduction to clusterfullerenes

Discovered in the dawn of fullerene study, endohedral metallofullerenes (EMFs) attracted tremendous scientific attention in the 1990s.[4] Although the yields of EMFs were typically as low as 1% of the empty cage C_{60} and extensive and tedious high performance liquid chromatography (HPLC) separation was required to obtain isomerically pure EMF samples, a number of monometallic fullerenes and dimetallic fullerenes (now referred as "traditional metallofullerenes" or "traditional EMFs" in distinction with clusterfullerenes) had been synthesized and isolated. Since then, a new molecular formula $X@C_{2n}$ has been adopted to denote EMFs, in which the X is the encapsulataed species and the C_{2n} is the fullerene cage. Due to the large number of isomers for a certain fullerene formula, numbers and symmetry point

groups are often added to show the cage structure. For example, $Y_2@C_{3v}(8)$-C_{82} denotes an EMF with two yttrium ions encapsulated in a C_{82} fullerene cage that has a C_{3v} symmetry and numbered 8 in the numbering system presented in "*An Atlas of Fullerenes*"[5] by Fowler and Manolopoulos.

The research on EMFs was great enhanced by the discovery of the first clusterfullerene, $Sc_3N@C_{80}$, by Stevenson and Dorn in 1999.[6] During their studies of scandium metallofullerenes, they constantly observed a mass-spectrometry peak of 1109 in the toluene soluble soot product[7] which remained unidentified for 5 years. In the fall of 1998, they were able to determine the molecular formula for that mass peak as $Sc_3C_{80}N_1$ based on the isotopic distribution in high resolution mass spectral data for both natural abundance and ^{13}C enriched sample. Moreover, the molecule was assigned as $Sc_3N@C_{80}$ based on HPLC retention time and the single peak in ^{45}Sc NMR. Furthermore they predicted the cage to be $I_h(7)$-C_{80} which was subsequently confirmed by a two line pattern obtained for the 150 MHz ^{13}C NMR spectrum (Figure 1) which required nearly 1 week of scan time utilizing a 600 MHz (14.1 T) NMR instrument (Roy Bible, G. D. Searle). The appearance of nitrogen in the molecule was unexpected since no nitrogen source was provided in the starting materials (graphite, scandium oxide and helium gas), and it was attributed to the small leak of air into the Krätschmer-Huffman (K-H) electric-arc reactor,[8] which naturally led to the intentional introduction of nitrogen gas into the reaction. The resulting soot contained a significantly increased amount of $Sc_3N@C_{80}$ whose yield exceeded the empty cage fullerene C_{84} and was only second to C_{60} and C_{70}, which is a historical milestone of EMF research that for the first time the yield of EMF is comparable to that of the empty cages. With larger quantities of samples the X-ray single-crystal study was performed and confirmed the structure of $Sc_3N@I_h(7)$-C_{80} (Figure 1). The serendipitous discovery was seemingly

predetermined when it was later realized the coincidence that the Dorn office number in Virginia Tech Hahn Hall was 1109, matching the mysterious molecular weight that led to the discovery.*

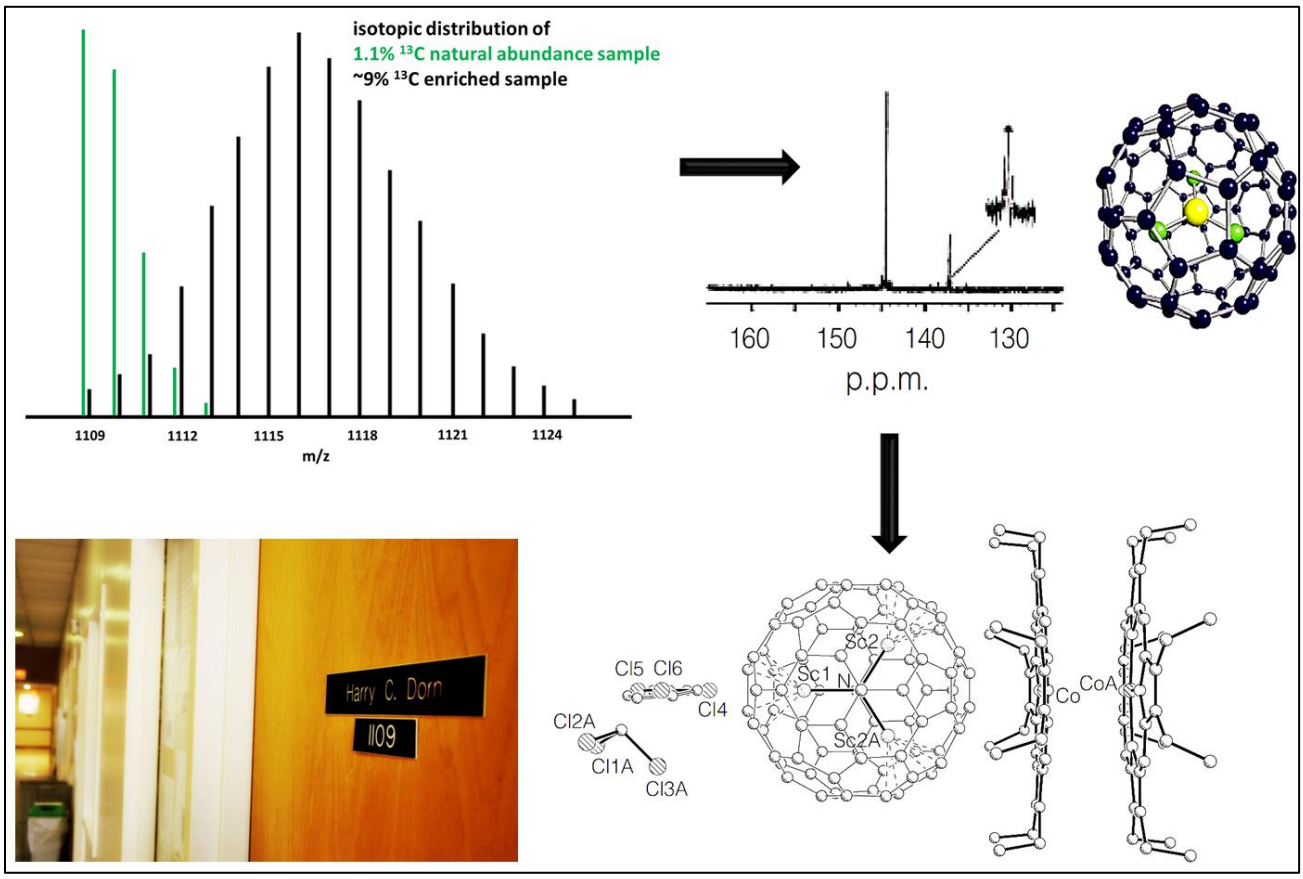

Figure 1. Mass spectral isotopic distribution of natural abundance and ^{13}C enriched $Sc_3N@C_{80}$; the ^{13}C NMR and single crystal x-ray structural data for $Sc_3N@C_{80}$; H.C.D's Virginia Tech office number, Hahn Hall 1109.

The first type of clusterfullerenes was named trimetallic nitride template endohedral metallofullerenes (TNT EMFs). The TNT EMF family also allows "mixed" metal formation, $A_{3-x}B_xN@C_{2y}$ (x = 0-3, A,B = metal).[6] Later it was found that other fullerene cages would also

* The coincidence of 1109 is devoted as a sentimental commemoration after my advisor, Prof. H. C. Dorn moved out his Hahn 1109 office for his position in the Carilion Research Institute of Virginia Tech in the summer of 2012.

accommodate the Sc_3N cluster, including a second isomer for the C_{80} cage, $Sc_3N@D_{5h}$-C_{80},[9] a slightly smaller cage, $Sc_3N@D_{3h}$-C_{78},[10] and a small cage with fused pentagons, $Sc_3N@D_3$-C_{68}.[11] With yttrium and lanthanide metal ions, a whole family of TNT EMFs, $A_3N@C_{2n}$ (A=Sc, Y, Gd, Tb, Dy, Ho, Er, Tm, Lu, Pr, Ce and La, n=34,35, 39-55) have been produced and characterized in the laboratories of Dorn, Echegoyen, Balch, Dunsch, Stevenson, Yang, and others.[3,12-14] The elements that have been encapsulated in TNT EMFs are summarized in Figure 2.

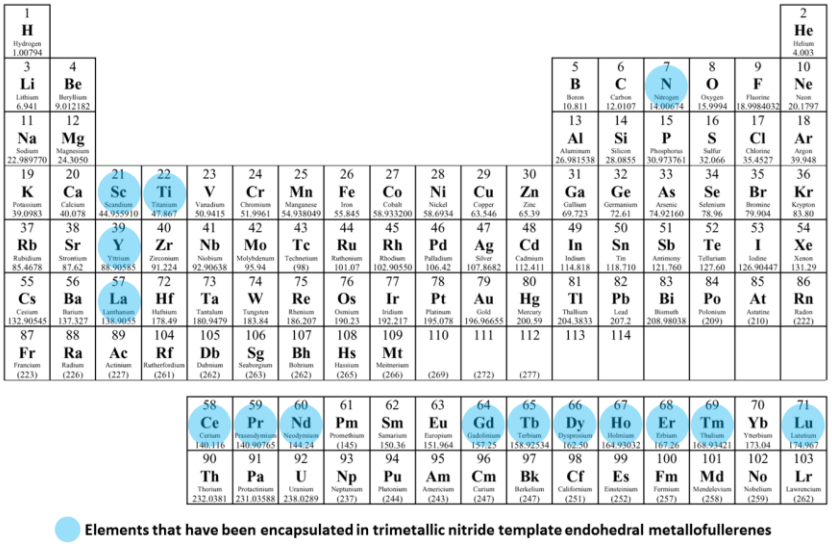

Figure 2. Elements that have been encapsulated in TNT EMFs.

Significant progress in clusterfullerenes has been made after the discovery of TNT EMFs. The first structural elucidation of carbide clusterfullerene (CCFs) $Sc_2C_2@C_{84}$, was achieved in 2001 by Shinohara and coworkers.[15] Unlike TNT EMFs, the CCFs share the same synthetic conditions with traditional EMFs (metal source, helium gas and graphite, no nitrogen needed). However, their existence could be masked by traditional EMFs due to the shared formula. For example, the first characterized CCF $Sc_2C_2@C_{84}$ was thought to be $Sc_2@C_{86}$; however, its ^{13}C NMR didn't resemble any available C_{86} structure but suggested $D_{2d}(23)$-C_{84} fullerene cage,[15] which leads to the discovery of CCFs. Soon after the discovery, many other groups joined the rush to reexamine traditional EMFs, during which many $M_2@C_{2n}$ molecules were proposed as $M_2C_2@C_{2(n-1)}$ *vide*

infra. Due to generally lower yields and being unidentifiable simply by mass-spectrometry, the development of CCFs was much slower than TNT EMFs. Nevertheless, up to date many metals have been encapsulated in fullerene cages as metal carbide cluster as seen in Figure 3.

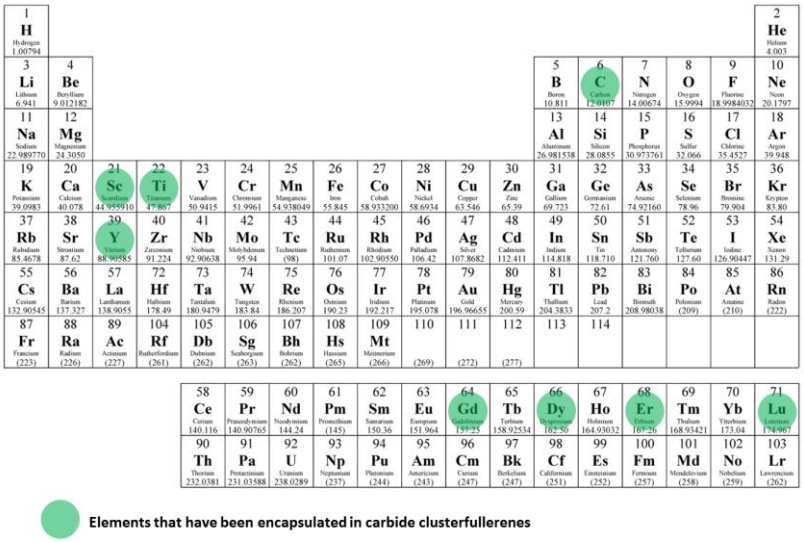

Figure 3. Elements that have been encapsulated in CCFs.

The oxide clusterfullerenes (OCFs) were discovered by the Stevenson group as $Sc_4O_2@I_h(7)$-C_{80} in 2008 using air as the oxygen source.[16] Interestingly, following reports of $Sc_4O_3@I_h(7)$-C_{80},[17] $Sc_2O@C_s(6)$-C_{82},[18] they show even larger diversity in the cluster than in the cage. The sulfide clusterfullerenes (SCFs) were first proposed in 2010 by Dunsch and coworkers with $Sc_2S@C_{82}$[19] and closely followed by Echegoyen et al. with two isomers of the same formula[20] by introducing SO_2 into the reaction chamber. However, it was not until one year later that the first unambiguous structural elucidation of SCFs was achieved by Balch and coworkers[21] on the samples synthesized by Echegoyen group.[20] Recently two smaller cages with fused pentagons were also found to host Sc_2S cluster.[22,23] Compared to TNT EMFs (NCFs) and CCFs, the studies on OCFs and SCFs are only in their infant stage.

1.3 The isolated pentagon rule in EMFs

One of the Nobel laureates for fullerene discovery, Sir Harold Kroto, predicted that pristine fullerenes should not have pentagons fused together, which is referred as the "isolated pentagon rule (IPR)".[24] The IPR strictly applied to all pristine (empty-cage, unfunctionalized) fullerenes through the recent decades. However, when the rule is extended to EMFs, two exceptions were independently reported by Shinohara [$Sc_2@C_{2v}$(4348)-C_{66}][25] and Dorn [$Sc_3N@D_3$(6140)-C_{68}][11] in 2000, with many other examples following.[26] This can be explained by the electron transfer from the encapsulated species to the cage. In all EMFs, the endohedral metal ions or clusters bear positive formal charges while the fullerene cages bear negative formal charges.[3] For example, $Sc_3N@C_{80}$ can be described in an ionic model as $(Sc_3N)^{6+}@C_{80}^{6-}$. Although the fused pentagons (pentalene motifs) are energetically punished for being 8π-anti-aromatic in pristine fullerenes, they can be stabilized by the extra electrons in EMFs. Therefore, the EMFs have a profound influence by drastically increasing the diversity of possible fullerene cages by thousands of times, as listed below in Figure 4 the number for possible non-IPR and IPR isomers from C_{62} to C_{100}.[5]

n	Non-IPR	IPR
62	2,385	0
64	3,465	0
66	4,478	0
68	6,332	0
70	8,148	1
72	11,189	1
74	14,245	1
76	19,149	2
78	24,104	5
80	31,917	7
82	39,710	9
84	51,568	24
86	63,742	19
88	81,703	35
90	99,872	46
92	126,323	86
94	153,359	134
96	191,652	187
98	230,758	259
100	285,463	450

Figure 4. Number of non-IPR and IPR isomers for fullerene C_{62} to C_{100}.

1.4 The TNT EMFs

1.4.1 Synthesis of TNT EMFs

In most preparations to date, TNT EMFs are produced in a K-H electric-arc reactor.[8] Although the geometrical dimensions the K-H reactor vary, a typical apparatus is shown in Figure 5a, b. The soot containing the TNT EMFs is produced from the electric-arc-vaporization of a core-drilled graphite rod that is packed with a desired metal to be encapsulated. The resulting arc-plasma is shown in Figure 3c.

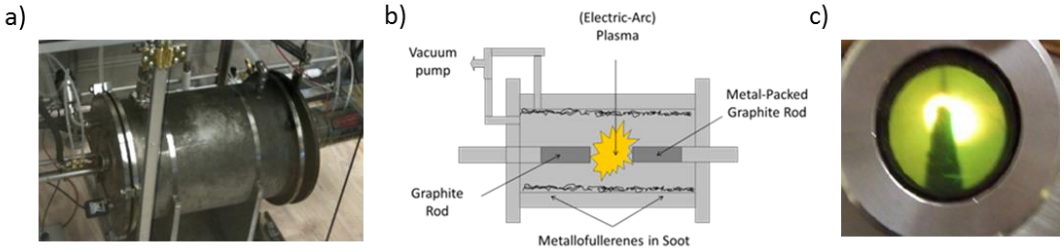

Figure 5. Fullerene and EMF generator. a) An electric-arc reactor (chamber size about 30 cm in diameter and 60 cm in length) b) drawing. and c) the plasma.

As described above, the original production method of TNT EMFs was accomplished with Sc_2O_3 packed rods being vaporized under a mixture of N_2 and He.[6] The soot extract contained predominantly empty-cage fullerenes (e.g., C_{60}, C_{70}) which had to be removed during the purification process. Subsequently, a more reactive gas atmosphere was reported by Dunsch who introduced NH_3 into the K-H reactor as the nitrogen source.[27] The Dunsch method and its reducing atmosphere provided samples depleted in C_{60} and C_{70} and enriched in TNT EMFs. In later studies, an oxidizing atmosphere was reported by Stevenson who introduced O_2 and NO_x vapor via the decomposition of $Cu(NO_3)_2$, in which the product distribution can be tuned by chemically adjusting plasma, temperature, and reactivity (CAPTEAR).[28] Moreover, the

Stevenson laboratory also showed that the yields of TNT EMFs can be increased by 3-5 times in the presence of Cu.[29]

1.4.2 Purification of TNT EMFs

The first TNT EMFs were isolated and purified by HPLC, but these efforts were time-consuming and limited the quantity level of TNT EMFs. During TNT EMF studies, it was found that EMFs are more reactive towards electron acceptors but relatively inert towards electron donors, with empty-cage fullerenes having the opposite effect. Based on this, various chemical reactivity approaches have been developed for TNT EMF purification including selective oxidation[30] and taking advantage of the reactivity differences.[31-35] One of the more facile separation reported to date is the treatment with either Lewis bases or Lewis acids to selectively bind the more reactive species (Figure 6). As a typical example, via the "Stir And Filter Approach" (SAFA, Figure 5a) developed by Stevenson group,[32,33] empty-cage fullerenes bind readily to aminosilica (Lewis base) with the more chemically inert TNT EMFs remaining in solution. The most unreactive component, $Sc_3N@I_h$-C_{80}, eventually is the only species remaining in solution, and is readily isolated in isomeric purity simply by filtration (figure 6b). On contrary, when metal chlorides (Lewis acids) are used, after stirring the EMFs were selectively bound to the insoluble (Figure 6c), which can be recovered from the precipitate with pure I_h-isomer obtained by adjusting the identity and amount of Lewis acids (Figure 6d).[35]

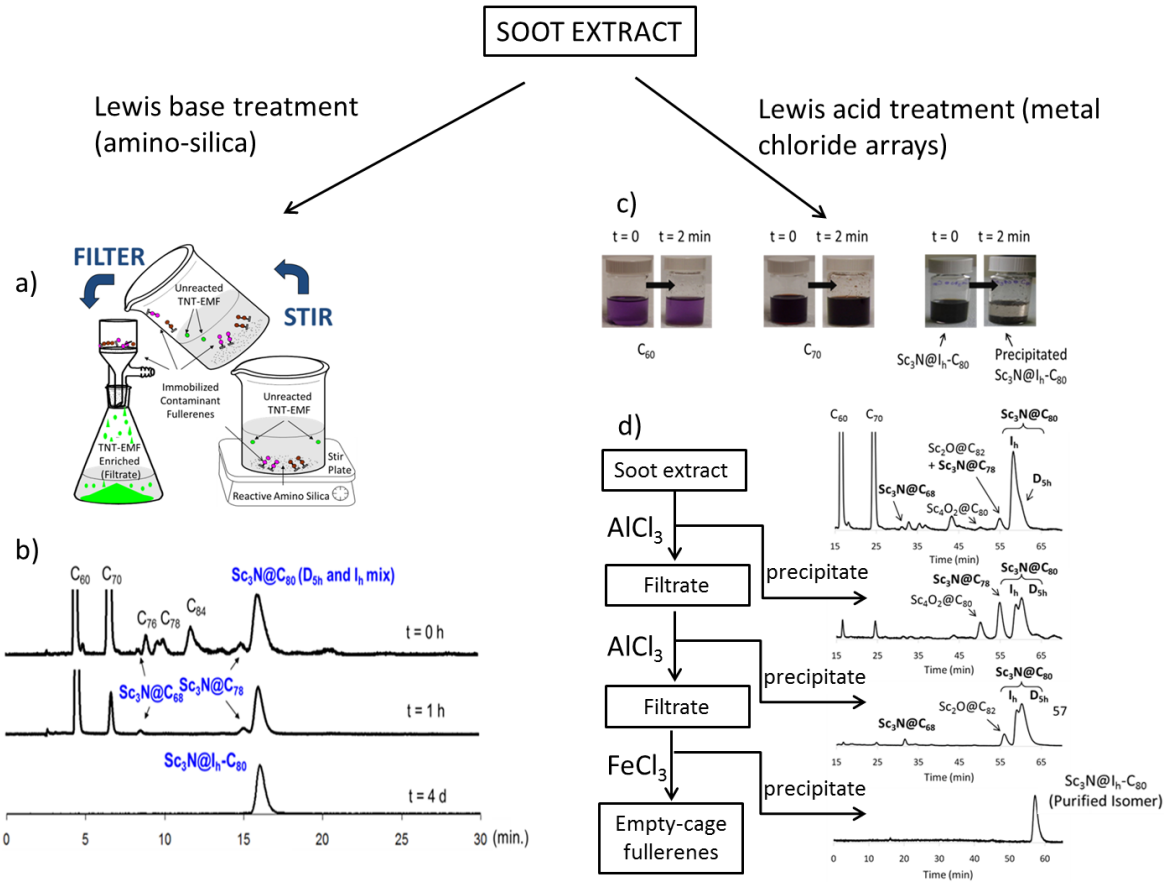

Figure 6. Lewis Acid and Base Reactivity Separations of TNT EMFs.

1.4.3 Structural Characterization of TNT EMFs

As aforementioned the first definitive structural confirmation of the TNT EMF, $Sc_3N@I_h$-C_{80}, was obtained by both single crystal analysis and ^{13}C NMR spectroscopy,[6] which are considered as the "gold standards" for structural characterization of EMFs. For the I_h-C_{80} cage, although it commonly encapsulates planar $(A_3N)^{6+}$clusters, deviations from triangular planarity are observed for larger lanthanide atoms. For example, a cluster that deviates strongly from planarity was found for $Gd_3N@I_h$-C_{80}, in which the N atom deviates from the tri-gadolinium plane by a distance of ~0.5 Å, forming an ammonia-like pyramid.[36]

Several other members of the TNT EMF class have unique structural features that are rarely seen in other fullerenes and metallofullerenes (Figure 6). For the C_{78} cage, two isomeric fullerene cages are found for the trimetallic nitride $(A_3N)^{6+}$ cluster. One is the D_{3h}-C_{78} cage, represented by $Sc_3N@D_{3h}$-C_{78},[10] that is unique for the smaller $(Sc_3N)^{6+}$ cluster and different from any other reported empty-cage C_{78} fullerene. Larger lanthanide metals including Gd, Tm, Dy and Y prefer the non-IPR $A_3N@C_2$(22010)-C_{78} cage[37-39] which has a "flatter flying saucer" shape to host larger planar clusters.[38] This distorted shape of the C_{78} cage conserves the large clusters from pyramidalization and thereby stabilizes the molecule by 140-160 kJ/mol.[37] The A_3N cluster also adopts a non-IPR C_{82} cage, namely, the C_s(29663)-C_{82}, as found in the single crystal structure of $Gd_3N@C_{82}$, where one of the Gd^{3+} ions was close to the site of the fused pentagons.[40] The non-IPR $A_3N@C_{82}$ system was confirmed by a ^{13}C NMR study of $Y_3N@C_{82}$, in which a highly deshielded ^{13}C signal was observed at 165.7 ppm, corresponding to the two carbon atoms fusing the pentalene unit.[41] Also noteworthy is that major isomers of all $A_3N@C_{84}$ (A=Tb, Tm, Gd, Y) EMFs adopt an egg-shaped non-IPR C_s cage, the C_s(51365)-C_{84},[41-43] although there are 24 IPR-obeying options available for C_{84}. The special elliptical shape of the cage is capable of hosting the planar $(A_3N)^{6+}$ cluster and the only pentalene group is located on the "tip" of the "buckyegg". The ^{13}C NMR results of $Y_3N@C_{84}$ also confirm the cage symmetry and the existence of the pentalene motif.[41] The reported $A_3N@C_{86}$ species, where A includes Tb, Gd and Y, share the same fullerene cage, namely, the D_3(17)-C_{86}, as proved by single crystal analysis[44,45] and ^{13}C NMR.[41] The $M_3N@C_{88}$ EMFs are the largest TNT EMFs with crystal structures assigned. D_2(35)-C_{88} cage is the common host for both Tb_3N, Gd_3N and Y_3N clusters.[44,46]

The smallest and largest isolated TNT EMFs are $Sc_3N@C_{68}$[11] and $A_3N@C_{96}$ (A=Pr, Ce and La),[47] respectively. The 12 peaks in the ^{13}C NMR spectrum of $Sc_3N@C_{68}$ and symmetric single

^{45}Sc signal suggested a D_3-C_{68} cage,[11] which was later confirmed by single crystal study.[48] Regarding the larger TNT EMFs, in the soot extract for a lanthanum based TNT EMF synthesis, a mass-spectral peak corresponding to $La_3N@C_{110}$ was observed, which represents the largest TNT EMF reported to date.[47]

NMR investigations of the nuclei in the $(A_3N)^{6+}$ cluster provide additional information regarding cluster dynamics. The ^{45}Sc NMR data was the first NMR information obtained from TNT EMFs (earlier than ^{13}C) and made important contributions to the discovery of the class. Also, the ^{89}Y NMR of $Y_3N@C_{2n}$ (n=40, 42, and 43) series revealed that while in $Y_3N@C_{84}$ the pentalene group fixes one yttrium atom and prevents cluster rotation, in IPR-obeying $Y_3N@C_{80}$ and $Y_3N@C_{86}$ the cluster undergoes free rotation.[41] Moreover, a comprehensive ^{14}N NMR study on $A_3N@C_{80}$ (A=Sc, Y, Lu) was accomplished by Dorn et al. suggesting that the rotational barriers of the clusters are dependent on the ionic radius of the metals.[49]

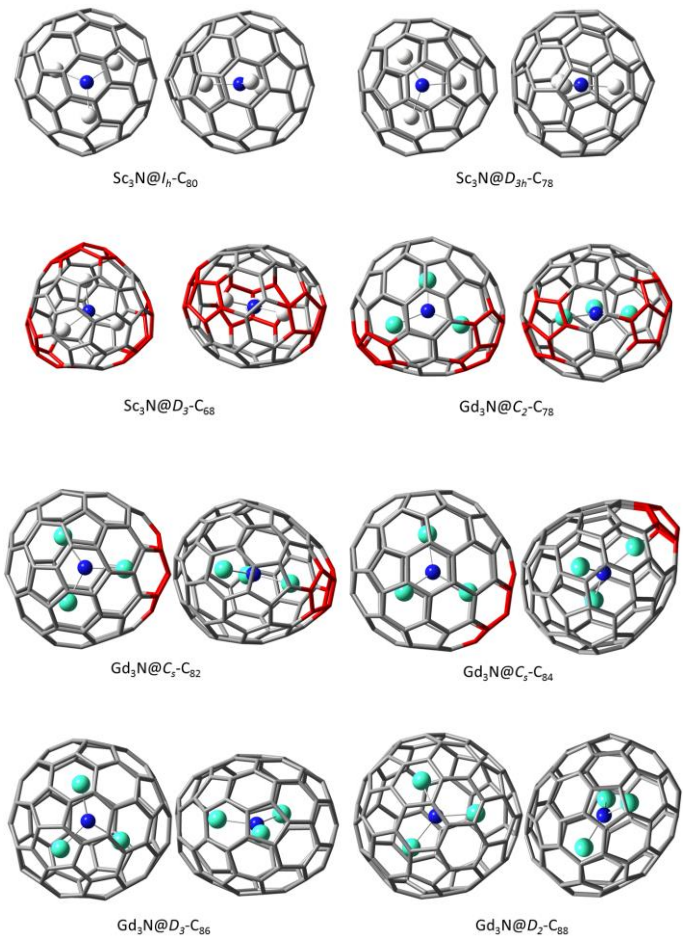

Figure 7. Structures of TNT EMFs based on single crystal analysis. The red portions of the molecules denote pentalene site.

Over the last 10-12 years, the structural characterization of the TNT EMFs has been supported by several seminal computational studies. For example, early computational results by Nagase supported significant charge transfer of ~6 electrons to the icosahedral I_h-C_{80} cage and predicted a relatively large (6.5 eV) band-gap in archetypal, $Sc_3N@I_h$-C_{80}.[50] Also, Aihara predicted exceptional stability for the I_h-C_{80} cage based on a Hückel minimum bond resonance energies (min BRE) approach.[51] More recently, Poblet and coworkers have advanced a rule based on a simple ionic model for transfer of 6 electrons from the trimetallic nitride cluster for $Sc_3N@D_3$-C_{68}, $Sc_3N@D_{3h}$-C_{78} and $Sc_3N@I_h$-C_{80}.[13,52] This rule predicts that a suitable fullerene must host

three low-lying unoccupied molecular orbitals and there must be sizable gap between the LUMO-4 and LUMO-3 orbitals where LUMO-n is the nth-lowest unoccupied MO. A very detailed DFT study by Popov and Dunsch has shown that for the isomers of $A_3N@C_{2n}$ (A= Sc and Y, n=68-98) based on the most stable $(C_{2n})^{6-}$ the lowest energy isomers for $Sc_3N@C_{68}$, $Sc_3N@C_{78}$, $Sc_3N@C_{80}$, $Y_3N@C_{80}$, $Y_3N@C_{84}$, $Y_3N@C_{86}$ and $Y_3N@C_{88}$ are the same ones found from the single-crystal X-ray studies *vide supra*.[53]

1.4.4 Cage surface functionalization reactions of TNT EMFs

Exohedral chemical functionalization of TNT EMF surface is a prerequisite for many potential applications. The TNT EMF cages have sp^2 carbons that undergo cycloaddition and radical reactions, in resemblance to the double bond of alkenes and aromatic rings in small molecules.

Most functionalization studies to date have focused on the $A_3N@I_h$-C_{80} system. The first reported derivative of a TNT EMF was a Diels-Alder addition to $Sc_3N@I_h$-C_{80},[54] reported by Dorn's laboratory and subsequently a single crystal X-ray crystallographic structure of the isochromanone derivative was obtained by Balch's laboratory.[55] The Diels-Alder addition also gave the first derivative of the highly promising candidate of next generation of magnetic resonance imaging contrast agent $Gd_3N@C_{80}$.[56]

The classical 1,3-dipolar cycloaddition on empty-cage fullerenes was first performed on TNT EMFs by Echegoyen and coworkers[57] who concluded that addition on $Sc_3N@I_h$-C_{80} was across a [5,6] bond while on $Y_3N@I_h$-C_{80} it was on a [6,6] bond.[58] Later, the Dorn group found that both [5,6] and [6,6] addition could happen to $Sc_3N@I_h$-C_{80}.[59] The kinetically favored [6,6] product dominates after short reaction time, while the thermodynamically favored [5,6] product gradually becomes the main product when the reaction proceeds longer. The products were differentiated

by monitoring the ^{13}C NMR signal for the methylene groups attached to the cage. The [5,6] addition gives symmetric methylene groups and show only one signal between 50 and 70 ppm in ^{13}C NMR spectrum, in contrast to the [6,6] addition giving asymmetric methylene groups and thereby show two NMR signals (Figure 8). Meanwhile, upon heating the kinetically favored [6,6] product could be converted to the thermodynamically favored [5,6] product. Interestingly, Chen et al. investigated the influence of cluster size on the reaction sites for the $Sc_xGd_{3-x}N@C_{80}$ (x=0-3) series with a similar 1,3-dipolar cycloaddition reaction.[60] They found larger cluster size leads to higher stability of the [6,6] product, and after interconversion at elevated temperature the [6,6] product dominated for $Gd_3N@C_{80}$ while the [5,6] product dominated in other ($Sc_3N@C_{80}$, $ScGd_2@C_{80}$ and $Sc_2Gd@C_{80}$) cases.

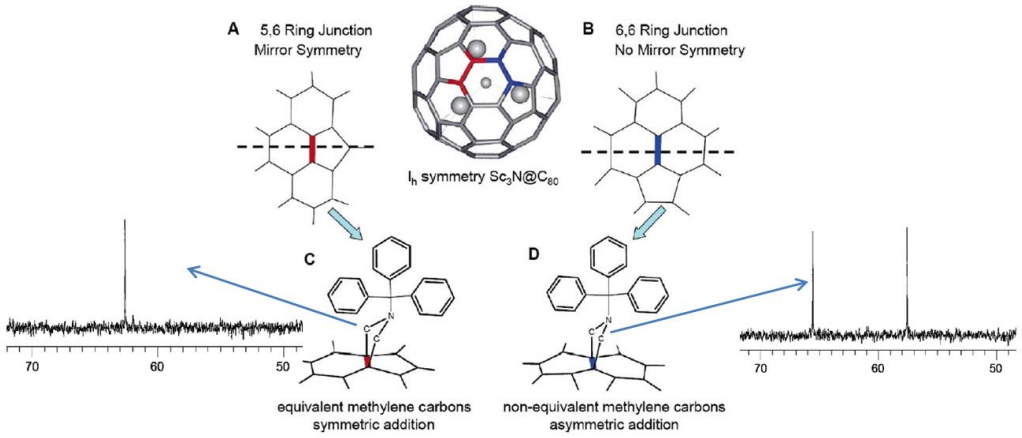

Figure 8. The ^{13}C NMR spectral differences between the [5,5] and [5,6] 1,3-dipolar derivatives of $Sc_3N@C_{80}$.

The Bingel reaction also gives a series of important TNT EMF derivatives; among them is the important open-cage Bingel derivative of $Y_3N@I_h$-C_{80} via bromomalonate addition by Echegoyen group.[61] The open-cage product was characterized by both HMQC NMR and single crystal study. The authors also found one yttrium atom (Y_1) was fixed near the open site while

the other two yttrium atoms (Y_2 and Y_3) were still rotating about the Y_1-N axis (Figure 9). Although it was earlier reported that $Sc_3N@I_h$-C_{80} was unreactive toward in the usual Bingel reaction conditions,[58] the Dorn laboratory synthesized a cyclopropanyl adduct of $Sc_3N@I_h$-C_{80} with catalytic manganese (III) via a radical mechanism.[62] Alternatively, the Echegoyen laboratory has shown that in the presence of DMF $Sc_3N@I_h$-C_{80} can also react with bromomalonate to form Bingel adducts in similar fashion to the $Y_3N@I_h$-C_{80}.[63]

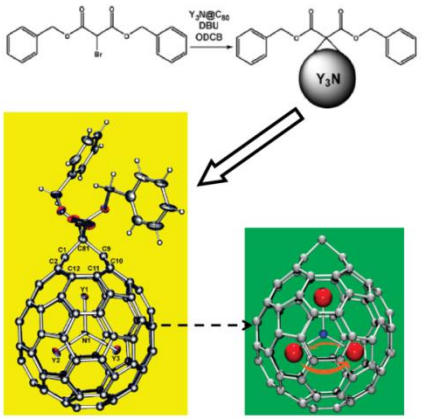

Figure 9. Preparation and Crystallographic study of the Bingel adduct of $Y_3N@I_h$-C_{80}.

Two other important reactions on empty-caged fullerenes are also sucessful for $A_3N@I_h$-C_{80} EMFs. The 1,3-dipolar addition diazo reaction has been reported in two independent studies yielding phenyl-A_3NC_{81}-butyric methylate (A=Lu, Sc, Y) TNT EMF derivatives which are important new materials as electron acceptors for heterjunction photovoltaic solar cell devices.[64,65] Echegoyen and coworkers have also reported the interesting [2+2] reaction of isoamyl nitrite and anthranilic acid with $Sc_3N@I_h$-C_{80} that leads to a benzyne intermediate with formation of monoadducts with a four-membered ring attached to the cage surface with both [5,6] and [6,6] ring addition.[66] It is noteworthy that in the [2+2] reaction the TNT EMF acts as an electron donor, as opposed in most other reactions the EMFs act as electron acceptors.

Organic functionalization have also been performed on other TNT EMFs besides $A_3N@I_h$-C_{80}. In 2005, the Dorn laboratory demonstrated that $A_3N@D_{5h}$-C_{80} (A=Sc, Lu) has higher reactivity towards Diels-Alder reaction and 1,3-dipolar reaction than the I_h isomer.[67] The two 1,3-dipolar addition products for $A_3N@D_{5h}$-C_{80} were assigned by ^{1}H NMR, but an alternative assignment has been advanced for one of these products in a recent computational report.[68] The smaller TNT EMF, $Sc_3N@D_{3h}$-C_{78} was also functionalized with a 1,3-dipolar reaction[69] and the Bingel reaction.[70] In the latter both mono- and bis-adducts were isolated and characterized. In this case, ^{1}H NMR spectra of the mono- and bisadducts turned out to be identical, excluding many but 5 possible reaction sites for the second addition to happen (demostrated in Figure 10a). Furthermore, the ^{13}C NMR for the bisadduct suggested the molecule retained C_{2v} symmetry; therefore, it was revealed that the second addition occurs on the same side of the first reaction site (Figure 10b).

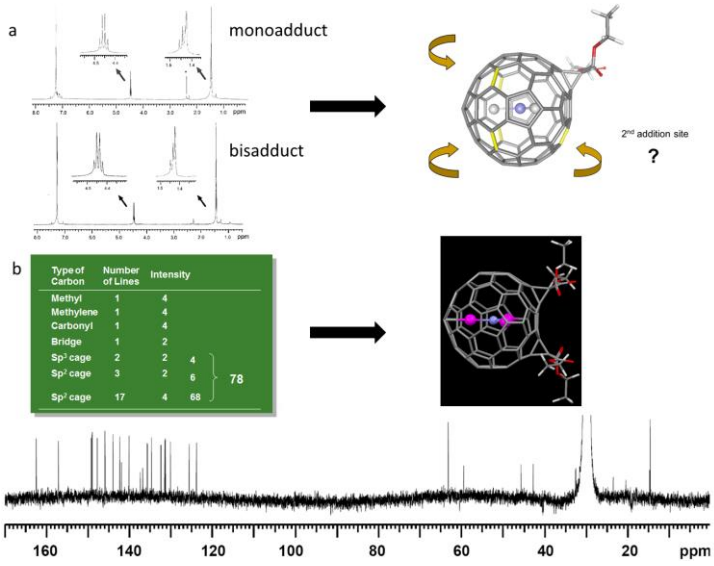

Figure 10. Structural characterizaion of the Bingel bisadduct of $Sc_3N@C_{78}$ with NMR.

Some non-IPR TNT EMFs, including $Sc_3N@D_3$-C_{68}, $Gd_3N@C_s$-C_{82}, $Gd_3N@C_s$-C_{84}, are also reactive towards the Bingel reaction;[71-73] however the structural characterization of products revealing the addition sites are largely limited to theoretical calculations, and there has not been an unambiguously characterized structure of a non-IPR TNT EMF derivative. The major cycloaddition reactions on TNT EMFs are summarized in Figure 11 below.

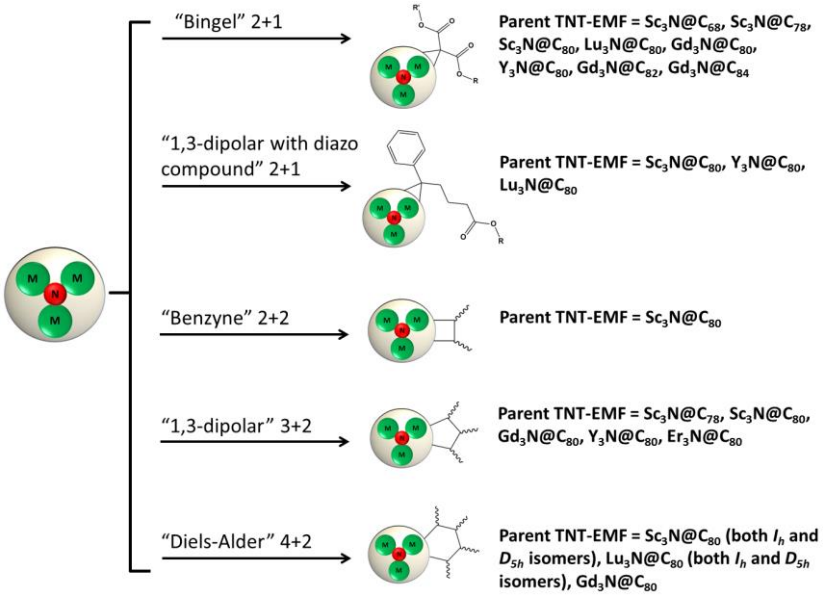

Figure 11. major types of cycloaddition reactions developed on TNT EMFs.

Trifluromethylation reactions of TNT EMFs via a radical mechanism have been conducted on $Sc_3N@C_{80}$ (both I_h and D_{5h} isomers) yielding $Sc_3N@C_{80}(CF_3)_{2n}$ (n=1-6) products.[74] Another UV-initiated radical reaction between benzyl bromide and $Sc_3N@I_h$-C_{80} yields exclusively $Sc_3N@C_{80}(C_7H_8)_2$.[75] In both trifluromethylation and benzyl radical reactions, the functional groups are added pairwise with 1,4-addition across the hexagon rings (para addition) on the fullerene surface. The TNT EMFs have also been functionalized by multi-addition hydroxylation and carboxylation reactions for MRI contrast agents,[76] and electrochemical approaches.[77,78]

Furthermore, several other examples of TNT EMF functionalization have been covered in recent reviews.[14,79]

1.4.5 Applications of TNT EMFs

Since their discovery in 1999, several potential applications for TNT EMFs were recognized. For biomedical applications, the TNT EMF cage has the inherent advantages of high stability and characteristic resistance to any potential biological metabolic cage-opening process(es), which enables the application of toxic lanthanide ions without the risk of release to surrounding tissue, serum, and other biological components. On the other hand, the lower chemical reactivity of the $A_3N@C_{2n}$ families is still sufficient for functionalization by a variety of reactions to convert the hydrophobic fullerene surface to a hydrophilic water/biological fluid compatible surface for drug delivery.

A seminal studies by Shinohara group demonstrated that the hydroxlyated metallofullerene $Gd@C_{82}(OH)_n$ exhibits excellent relaxivity at several different magnetic field strengths (r_1 up to 81 $mM^{-1}s^{-1}$, 10-20 times higher than conventional MRI contrast agent Magnevist).[80] Since 2006, several *in vitro* and *in vivo* MRI relaxivity studies of TNT EMF $Gd_3N@C_{80}$ derivatives have been reported and reviewed. For example, water soluble poly(ethylene glycol) functionalized and hydroxylated TNT EMF derivatives, $Gd_3N@C_{80}[DiPEG(OH)_x]$,[81] were found to have the highest reported relaxivities with values of 237 $mM^{-1}s^{-1}$ for r_1 and 460 $mM^{-1}s^{-1}$ for r_2 (79 $mM^{-1}s^{-1}$ and 153 $mM^{-1}s^{-1}$ based on Gd^{3+} ion) at a clinical-range magnetic field of 2.4 T.[82]

During the last several years the Dorn laboratory started the development of TNT EMF based multi-modal biomedical agents. In collaboration with a team at Virginia Commonwealth University, we have reported an EMF nanoplatform with ^{177}Lu brachytherapy in a murine

glioblastoma multiforme (GBM) model that increases median survival from 21 to 52 days with long-term diagnostic MR imaging.[83] More recently, we reported even longer median survival to over 120 days with this multimodal "theranostic" radiolabeled ^{177}Lu-DOTA-f-$Gd_3N@C_{80}$ EMF platform (Figure 12).[84] In both of these studies, the approach involves external functionalization chemistry and subsequent treatment with a radiolabeled $^{177}LuCl_3$ sample. In contrast to exohedral radiolanthanide EMFs, the encapsulation of radionuclide atoms or clusters inside fullerene cages provides a nearly ideal platform since the radioactive metal ion is completely isolated from the bio-system. We described the preparation of $^{177}Lu_xLu_{(3-x)}N@C_{80}$-TAMRA-IL-13 peptide[85] using a remotely-controlled K-H generator to prepare the ^{177}Lu in a TNT EMF cage and demonstrate that for a period of at least one half-life (6.7 days) the encapsulated $^{177}Lu^{3+}$ ions are not released. This ^{177}Lu radiolabelled EMF agent was subsequently conjugated with a fluorescent tag (TAMRA) and interleukin-13, which is a cytokine peptide designed to target overexpressed receptor cells in GBM. Of critical importance, the cytotoxicity study by Ehrich and colleagues found no notable cytotoxicity for primary mouse brain neuronal cells and human neuroblastoma cells treated with functionalized TNT EMFs and empty-cage fullerenes in concentrations up to 10 μM.[86]

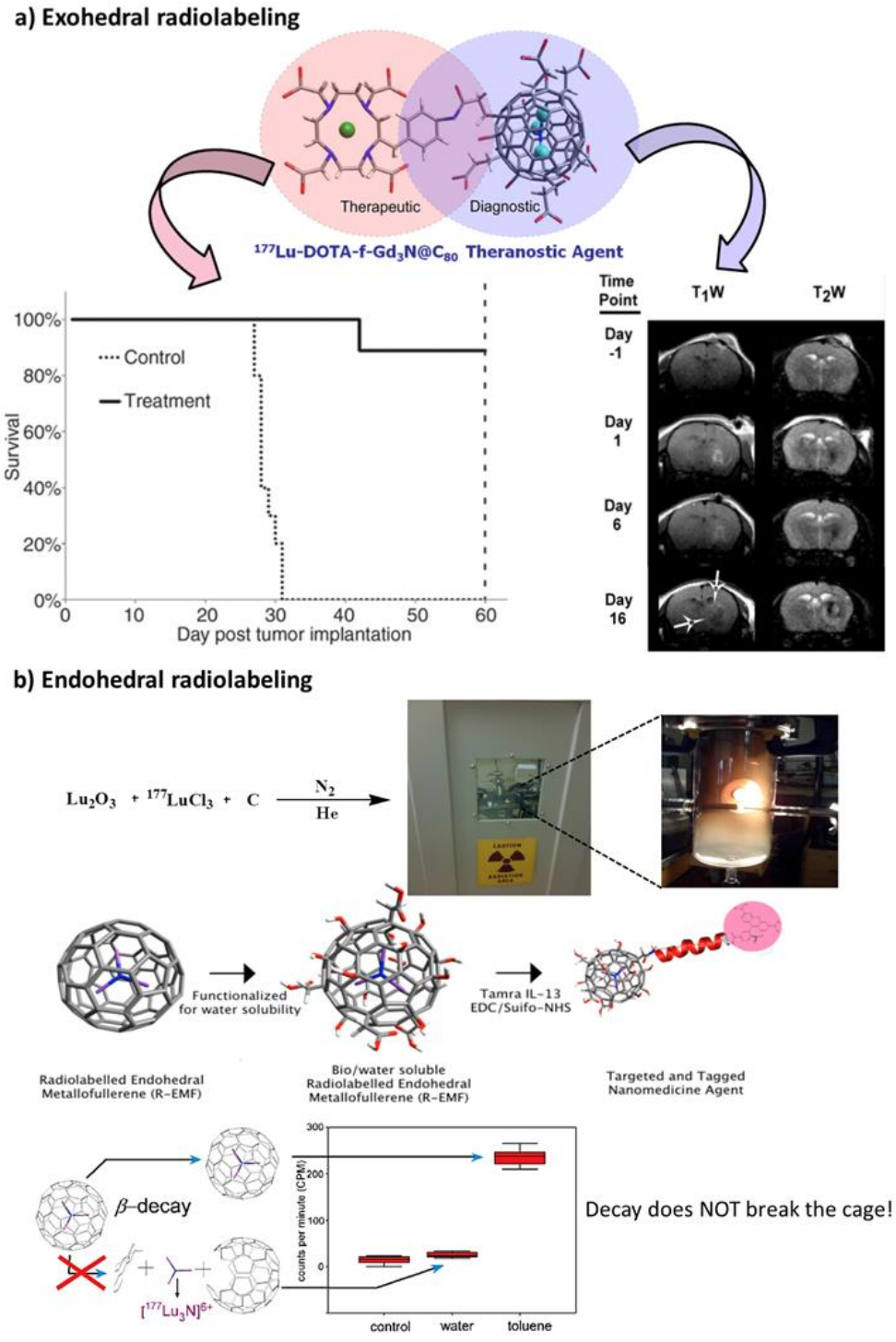

Figure 12. Exohedral and endohedral radiolabeling of TNT EMF derivatives.

TNT EMFs have also emerged as promising building blocks for various semiconductor,

optoelectronic, and light electron/energy conversion systems. As one example, with metallofullerenes as leading candidates for electron acceptors in organic photovoltaic devices, in 2009 Ross and colleagues demonstrated the importance of TNT EMFs in this field with one of the highest open circuit voltages (V_{OC}=810 mv) reported to date for the derivative, Phenyl-$Lu_3N@C_{81}$ butyric hexyl ester (also known as $Lu_3N@C_{80}$-PCBH) and an improved efficiency (4.2%) directly compared with the corresponding C_{60}PCBM derivative under same condition (V_{OC}= 630 mv, 3.4% efficiency).[64 64] On the other hand, the short circuit current of this system was lower than the C_{60}PCBM and the reason was recently investigated.[87] In a paradigm shift, the TNT EMFs was shown to not only exhibit electron acceptor properties, but electron-donation in a covalently linked $Lu_3N@C_{80}$−perylenediimide (PDI) conjugate, in which PDI acts as the light harvester and the electron acceptor.[88] Also of note, Novotny has coupled single $Y_3N@C_{80}$ molecules to single gold nanoparticles as optical antennas to drastically enhance light absorption and emission from poor emitters like rare-earth ions.[89] Although it has been over 13 years since the discovery of the TNT EMFs, their applications (especially as MRI contrast agents and photovoltaic electron acceptors) are only starting to mature. However, recent commercial availability of TNT EMFs has convinced me that these materials have a bright future ahead.

1.5 The carbide clusterfullerenes.

The synthesis, isolation and structural characterization procedures of carbide clusterfullerenes are highly similar to those of the TNT EMFs. One major difference is that mass spectral data cannot confirm the identity of CCFs. Although the CCFs are produced under the same conditions of traditional EMFs since the graphite would provide the nonmetal atoms in the cluster, their existence was not realized until after the discovery of TNT EMFs. This is because many of their mass-spectral peaks were mistakenly assigned as traditionally EMFs (also sometimes they

coexist and contribute to the same mass spectral peak). After the discovery of the $Sc_2C_2@C_{84}$, many of these compounds were revisited and assigned as CCFs. For example, Shinohara and coworkers found a group of compounds assigned as "$Y_2@C_{84}$" were actually three isomers of $Y_2C_2@C_{82}$ with respective cage of C_s(6)-C_{82}, C_{3v}(8)-C_{82} and C_{2v}(9)-C_{82}.[90] The $Ti_2C_2@C_{78}$ was originally thought to be $Ti_2@C_{80}$ and its ^{13}C NMR spectrum was explained as a result of the mixture of I_h-C_{80} and D_{5h}-C_{80} isomers in 2000, but 5 years later it was found that $Ti_2C_2@C_{78}$ better fits the ^{13}C NMR result and is more stable as suggested by DFT computation.[91] Finally in 2006 the carbide cluster was confirmed by high-resolution tunneling electric microscope (HRTEM).[92] A more famous example is that $Sc_3@C_{82}$[93] was re-assigned as $Sc_3C_2@C_{80}$ by single crystal study.[94]

On the other hand, it is also possible that traditional EMFs be assigned as CCFs. Wang et al. proposed the first non-IPR CCF $Sc_2C_2@C_{2v}$(6073)-C_{68} with the evidence ^{13}C NMR result (Figure 13); however a counter argument based on DFT calculation suggested the $Sc_2@C_{2v}$(7854)-C_{70} is more energetically stable.[95] In my own observation, the original ^{13}C NMR spectrum (*vide infra* Figure 13)[96] shows a total of 21 peaks with 14*4 and 7*2 pattern, suggesting a C_{2v}-C_{70} cage rather than a C_{2v}-C_{68} cage.

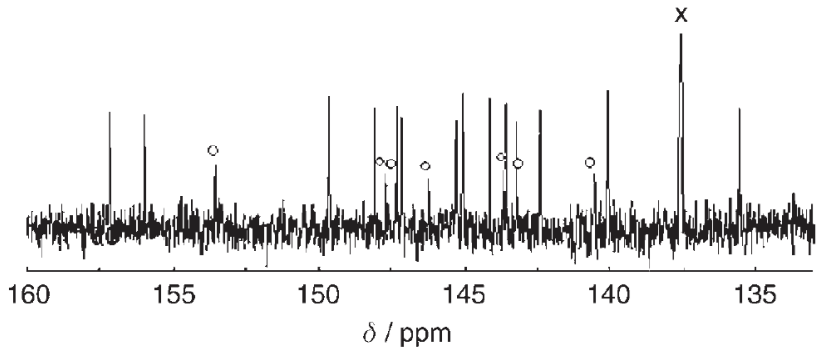

Figure 13. ^{13}C NMR spectrum of the Sc_2C_{70}. The peak with "x" was attributed to impurity.

The two "gold standards", ^{13}C NMR and X-ray single crystal analysis are often employed to judge whether an EMF is traditional metallofullerene or a CCF. The HRTEM mentioned above is not widely used because with higher instrumental cost it does not give any structural information (cage symmetry etc.) at the same time.

As seen in the example above, ^{13}C NMR results could be ambiguous between traditional EMFs and CCFs; however, it can be definitive if the ^{13}C NMR signals from the cluster carbide are seen. The observation of the NMR signal from the carbide was tricky. In the first report of CCF,[15] a small artificial spike at 92 ppm (alternatively it could be due to impurity) in the ^{13}C NMR spectrum was mistakenly assigned for the carbide in $Sc_2C_2@D_{2d}$-C_{84}. In 2008, with 15% ^{13}C enriched samples Akasaka and coworkers were able to perform an INADEQUATE NMR experiment on $Sc_2C_2@C_{3v}(8)$-C_{82} in a very wide scan window.[97] They found the connections among the signals between 134 ppm and 154 ppm defining a C_{3v}-C_{82} structure, with a highly deshielded and isolated signal at 253.2 ppm not coupled to any other ^{13}C signals (Figure 14). The integration of the signal represented two carbon atoms. In addition, DFT simulated ^{13}C NMR spectrum based on optimized structure also suggested the endohedral carbide should show resonance in highly deshielded region. Therefore, they were able to conclude the position of the carbide signals for the first time, followed by the observation of the signal for the endohedral carbide in $Sc_2C_2@D_{2d}$-C_{84} and $(Sc_3C_2@I_h$-$C_{80})^-$ anion in both 1D ^{13}C and 2D INADEQUATE NMR.[97] The carbide signal for the $Sc_2C_2@D_{2d}$-C_{84} had been found to be at 249.2 ppm, which corrects the first CCF report. The unexpected downfield shift could partially explain the signal was not seen in the original CCF discovery work. The carbide resonates at 328.3 ppm for the $[Sc_3C_2@I_h$-$C_{80}]^-$ anion. These three data points seemed to suggest the carbide signal moves

downfield when the space is more stringent in the cage, which provides inspiration for my work described in Chapter 3.

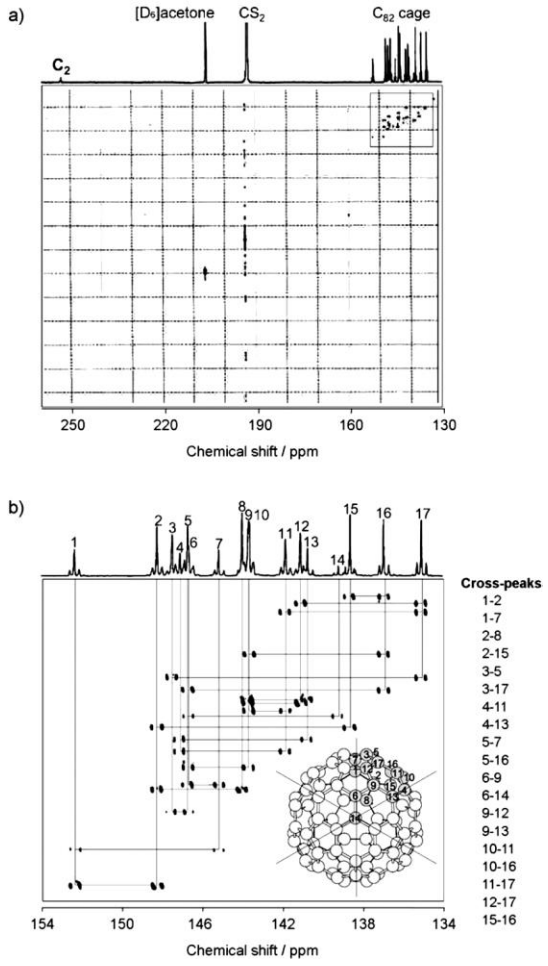

Figure 14. a) INADEQUATE NMR (125 MHz) spectrum of ^{13}C-enriched $Sc_2C_2@C_{3v}(8)$-C_{82} in CS_2 at 298 K and b) the expanded spectrum between d=134 and 154 ppm.

The most unambiguous characterization method for CCFs is X-ray single crystal analysis. In 2007, the X-ray single-crystal analysis was performed by Akasaka and coworkers on the carbene derivative of the $Sc_2C_2@C_{3v}(8)$-C_{82},[98] which revealed the geometry of the carbide cluster for the first time. The structural elucidation of the $Sc_2C_2@C_{3v}(8)$-C_{82} enabled a reliable DFT structural optimization of the CCF that led to the prediction of the ^{13}C NMR shift of the carbide, which was

reported in 2008[97] as abovementioned. The single crystal structure of a larger CCF, $Gd_2C_2@D_3(85)$-C_{92} was also obtained by Balch and coworkers in 2008.[99] The first unambiguous non-IPR CCF characterizations are reported in Chapter 3 in this dissertation.

1.6 Important milestones for EMFs

The important milestones in the EMF area are summarized in Table 1 in chronological order.

Table 1. Milestone publications in the EMF area in chronological order.

Work	Year	Journal	Group
Detection of metallofullerene by mass spectrometry[2]	1985	Nature	Smalley
Krätschmer-Huffman reactor for fullerenes and EMFs[8]	1990	Nature	Krätschmer
Confirmation of the endohedral nature of EMFs by the X-ray diffraction of $Y@C_{82}$[100] incontestably ending the debate whether the metal ions are inside the fullerene cage.	1995	Nature	Shinohara
First derivative of EMF[101]	1995	Nature	Akasaka & Nagase
First NMR study of EMF revealing the structure of $La_2@C_{80}$.[102]	1997	"Angew"	Akasaka & Nagase
Discovery of TNT EMF and clusterfullerenes[6]	1999	Nature	Dorn
Radioactive EMF derivative $^{166}Ho_x@C_{82}$-$(OH)_y$[103]	1999	"PNAS"	Cagle & Wilson
EMFs with fused pentagons ($Sc_3N@C_{68}$)[11]	2000	Nature	Dorn
EMFs with fused pentagons ($Sc_2@C_{66}$)[25]	2000	Nature	Shinohara
Functionalized $Gd@C_{82}$ showing superior ^1H relaxivity[80]	2001	"Bioconjugate"	Shinohara
Discovery of carbide clusterfullerene[15]	2001	"Angew"	Shinohara
First derivative of clusterfullerene[54]	2002	"JACS"	Dorn
Chemical separation of EMFs from empty-cage fullerenes	2005	"JACS"	Gibson & Dorn
First endohedral heterofullerenes, $Y_2@C_{79}N$ and $Tb_2@C_{79}N$[104]	2007	"JACS"	Dorn
Discovery of the oxide clusterfullerenes[16]	2008	"JACS"	Stevenson
Observation of the ^{13}C NMR signal for carbide in carbide clusterfullerenes[97]	2008	"Angew"	Akasaka & Nagase
Using EMF derivative as the electron acceptor in photovoltaic devices for enhanced open-circuit voltage[64]	2009	Nature Materials	Dress
Discovery of the sulfide clusterfullerenes[19]	2010	"JACS"	Dunsch

REFERENCE

(1) Kroto, H. W.; Heath, J. R.; Obrien, S. C.; Curl, R. F.; Smalley, R. E.: C_{60} - Buckminsterfullerene. *Nature* **1985**, *318*, 162-163.

(2) Heath, J. R.; O'Brien, S. C.; Zhang, Q.; Liu, Y.; Curl, R. F.; Tittel, F. K.; Smalley, R. E.: Lanthanum Complexes of Spheroidal Carbon Shells. *J. Am. Chem. Soc.* **1985**, *107*, 7779-7780.

(3) Chaur, M. N.; Melin, F.; Ortiz, A. L.; Echegoyen, L.: Chemical, Electrochemical, and Structural Properties of Endohedral Metallofullerenes. *Angew. Chem. Int. Ed.* **2009**, *48*, 7514-7538.

(4) Shinohara, H.: Endohedral Metallofullerenes. *Rep. Prog. Phys.* **2000**, *63*, 843-892.

(5) Fowler, P. W.; Manolopoulos, D. E.: *An Atlas of Fullerenes*; Dover: Mineola, NY, 2006.

(6) Stevenson, S.; Rice, G.; Glass, T.; Harich, K.; Cromer, F.; Jordan, M. R.; Craft, J.; Hadju, E.; Bible, R.; Olmstead, M. M.; Maitra, K.; Fisher, A. J.; Balch, A. L.; Dorn, H. C.: Small-Bandgap Endohedral Metallofullerenes in High Yield and Purity. *Nature* **1999**, *401*, 55-57.

(7) Stevenson, S.; Dorn, H. C.; Burbank, P.; Harich, K.; Haynes, J.; Kiang, C. H.; Salem, J. R.; Devries, M. S.; Vanloosdrecht, P. H. M.; Johnson, R. D.; Yannoni, C. S.; Bethune, D. S.: Automated Hplc Separation of Endohedral Metallofullerene $Sc@C_{2n}$ And $Y@C_{2n}$ Fractions. *Anal. Chem.* **1994**, *66*, 2675-2679.

(8) Kratschmer, W.; Lamb, L. D.; Fostiropoulos, K.; Huffman, D. R.: Solid C_{60} - A New Form of Carbon. *Nature* **1990**, *347*, 354-358.

(9) Duchamp, J. C.; Demortier, A.; Fletcher, K. R.; Dorn, D.; Iezzi, E. B.; Glass, T.; Dorn, H. C.: An Isomer of the Endohedral Metallofullerene $Sc_3N@C_{80}$ with D_{5h} Symmetry. *Chem. Phys. Lett.* **2003**, *375*, 655-659.

(10) Olmstead, M. H.; de Bettencourt-Dias, A.; Duchamp, J. C.; Stevenson, S.; Marciu, D.; Dorn, H. C.; Balch, A. L.: Isolation and Structural Characterization of the Endohedral Fullerene $Sc_3N@C_{78}$. *Angew. Chem. Int. Ed.* **2001**, *40*, 1223-1224.

(11) Stevenson, S.; Fowler, P. W.; Heine, T.; Duchamp, J. C.; Rice, G.; Glass, T.; Harich, K.; Hajdu, E.; Bible, R.; Dorn, H. C.: Materials Science - A Stable Non-classical Metallofullerene Family. *Nature* **2000**, *408*, 427-428.

(12) Dunsch, L.; Yang, S.: Metal Nitride Cluster Fullerenes: Their Current State and Future Prospects. *Small* **2007**, *3*, 1298-1320.

(13) Rodriguez-Fortea, A.; Balch, A. L.; Poblet, J. M.: Endohedral Metallofullerenes: A Unique Host-guest Association. *Chem. Soc. Rev.* **2011**, *40*, 3551-3563.

(14) Lu, X.; Feng, L.; Akasaka, T.; Nagase, S.: Current Status and Future Developments of Endohedral Metallofullerenes. *Chem. Soc. Rev.* **2012**, *41*, 7723-7760.

(15) Wang, C. R.; Kai, T.; Tomiyama, T.; Yoshida, T.; Kobayashi, Y.; Nishibori, E.; Takata, M.; Sakata, M.; Shinohara, H.: A Scandium Carbide Endohedral Metallofullerene: $(Sc_2C_2)@C_{84}$. *Angew. Chem. Int. Ed.* **2001**, *40*, 397-399.

(16) Stevenson, S.; Mackey, M. A.; Stuart, M. A.; Phillips, J. P.; Easterling, M. L.; Chancellor, C. J.; Olmstead, M. M.; Balch, A. L.: A Distorted Tetrahedral Metal Oxide Cluster inside an Icosahedral Carbon Cage. Synthesis, Isolation, and Structural Characterization of $Sc_4(\mu_3\text{-}O)_2@I_h\text{-}C_{80}$. *J. Am. Chem. Soc.* **2008**, *130*, 11844-11845.

(17) Mercado, B. Q.; Olmstead, M. M.; Beavers, C. M.; Easterling, M. L.; Stevenson, S.; Mackey, M. A.; Coumbe, C. E.; Phillips, J. D.; Phillips, J. P.; Poblet, J. M.; Balch, A. L.: A Seven Atom Cluster in a Carbon Cage, the Crystallographically Determined Structure of $Sc_4(\mu_3\text{-}O)_3@I_h\text{-}C_{80}$. *Chem. Commun.* **2010**, *46*, 279-281.

(18) Mercado, B. Q.; Stuart, M. A.; Mackey, M. A.; Pickens, J. E.; Confait, B. S.; Stevenson, S.; Easterling, M. L.; Valencia, R.; Rodríguez-Fortea, A.; Poblet, J. M.; Olmstead, M. M.; Balch, A. L.: $Sc_2(\mu 2\text{-}O)$ Trapped in a Fullerene Cage: The Isolation and Structural Characterization of $Sc_2(\mu_2\text{-}O)@C_s(6)\text{-}C_{82}$ and the Relevance of the Thermal and Entropic Effects in Fullerene Isomer Selection. *J. Am. Chem. Soc.* **2010**, *132*, 12098-12105.

(19) Dunsch, L.; Yang, S.; Zhang, L.; Svitova, A.; Oswald, S.; Popov, A. A.: Metal Sulfide in a C_{82} Fullerene Cage: A New Form of Endohedral Clusterfullerenes. *J. Am. Chem. Soc.* **2010**, *132*, 5413-5421.

(20) Chen, N.; Chaur, M. N.; Moore, C.; Pinzon, J. R.; Valencia, R.; Rodriguez-Fortea, A.; Poblet, J. M.; Echegoyen, L.: Synthesis of a New Endohedral Fullerene Family, $Sc_2S@C_{2n}$ (n = 40-50) by the Introduction of SO_2. *Chem. Commun.* **2010**, *46*, 4818-4820.

(21) Mercado, B. Q.; Chen, N.; Rodríguez-Fortea, A.; Mackey, M. A.; Stevenson, S.; Echegoyen, L.; Poblet, J. M.; Olmstead, M. M.; Balch, A. L.: The Shape of the $Sc_2(\mu_2\text{-}S)$ Unit Trapped in C_{82}: Crystallographic, Computational, and Electrochemical Studies of the Isomers, $Sc_2(\mu_2\text{-}S)@C_s(6)\text{-}C_{82}$ and $Sc_2(\mu_2\text{-}S)@C_{3v}(8)\text{-}C_{82}$. *J. Am. Chem. Soc.* **2011**, *133*, 6752-6760.

(22) Chen, N.; Beavers, C. M.; Mulet-Gas, M.; Rodriguez-Fortea, A.; Munoz, E. J.; Li, Y. Y.; Olmstead, M. M.; Balch, A. L.; Poblet, J. M.; Echegoyen, L.: $Sc_2S@C_s(10528)\text{-}C_{72}$: A Dimetallic Sulfide Endohedral Fullerene with a Non Isolated Pentagon Rule Cage. *J. Am. Chem. Soc.* **2012**, *134*, 7851-7860.

(23) Chen, N.; Mulet-Gas, M.; Li, Y.-Y.; Stene, R. E.; Atherton, C. W.; Rodriguez-Fortea, A.; Poblet, J. M.; Echegoyen, L.: $Sc_2S@C_2(7892)\text{-}C_{70}$: A Metallic Sulfide Cluster inside a Non-IPR C_{70} Cage. *Chem. Sci.* **2013**, *4*, 180-186.

(24) Kroto, H. W.: The Stability of the Fullerenes C_n, with n = 24, 28, 32, 36, 50, 60 and 70. *Nature* **1987**, *329*, 529-531.

(25) Wang, C. R.; Kai, T.; Tomiyama, T.; Yoshida, T.; Kobayashi, Y.; Nishibori, E.; Takata, M.; Sakata, M.; Shinohara, H.: Materials Science - C_{66} Fullerene Encaging a Scandium Dimer. *Nature* **2000**, *408*, 426-427.

(26) Tan, Y.-Z.; Xie, S.-Y.; Huang, R.-B.; Zheng, L.-S.: The Stabilization of Fused-Pentagon Fullerene Molecules. *Nature Chem.* **2009**, *1*, 450-460.

(27) Dunsch, L.; Krause, M.; Noack, J.; Georgi, P.: Endohedral Nitride Cluster Fullerenes - Formation and Spectroscopic Analysis of $L_{3-x}M_xN@C_{2n}$ (0 <= x <= 3; N=39,40). *J. Phys. Chem. Solids* **2004**, *65*, 309-315.

(28) Stevenson, S.; Thompson, M. C.; Coumbe, H. L.; Mackey, M. A.; Coumbe, C. E.; Phillips, J. P.: Chemically Adjusting Plasma Temperature, Energy, and Reactivity (CAPTEAR) Method Using Nox and Combustion for Selective Synthesis of $Sc_3N@C_{80}$ Metallic Nitride Fullerenes. *J. Am. Chem. Soc.* **2007**, *129*, 16257-16262.

(29) Stevenson, S.; Mackey, M. A.; Thompson, M. C.; Coumbe, H. L.; Madasu, P. K.; Coumbe, C. E.; Phillips, J. P.: Effect of Copper Metal on the Yield of $Sc_3N@C_{80}$ Metallofullerenes. *Chem. Commun.* **2007**, 4263-4265.

(30) Elliott, B.; Yu, L.; Echegoyen, L.: A Simple Isomeric Separation of D_{5h} and I_h $Sc_3N@C_{80}$ by Selective Chemical Oxidation. *J. Am. Chem. Soc.* **2005**, *127*, 10885-10888.

(31) Ge, Z. X.; Duchamp, J. C.; Cai, T.; Gibson, H. W.; Dorn, H. C.: Purification of Endohedral Trimetallic Nitride Fullerenes in a Single, Facile Step. *J. Am. Chem. Soc.* **2005**, *127*, 16292-16298.

(32) Stevenson, S.; Harich, K.; Yu, H.; Stephen, R. R.; Heaps, D.; Coumbe, C.; Phillips, J. P.: Nonchromatographic "Stir and Filter Approach" (SAFA) for Isolating $Sc_3N@C_{80}$ Metallofullerenes. *J. Am. Chem. Soc.* **2006**, *128*, 8829-8835.

(33) Stevenson, S.; Mackey, M. A.; Coumbe, C. E.; Phillips, J. P.; Elliott, B.; Echegoyen, L.: Rapid Removal of D_{5h} Isomer Using the "Stir And Filter Approach" And Isolation of Large Quantities of Isomerically Pure $Sc_3N@C_{80}$ Metallic Nitride Fullerenes. *J. Am. Chem. Soc.* **2007**, *129*, 6072-6073.

(34) Angeli, C. D.; Cai, T.; Duchamp, J. C.; Reid, J. E.; Singer, E. S.; Gibson, H. W.; Dorn, H. C.: Purification of Trimetallic Nitride Templated Endohedral Metallofullerenes by a Chemical Reaction of Congeners with Eutectic 9-Methylanthracene. *Chem. Mater.* **2008**, *20*, 4993-4997.

(35) Stevenson, S.; Mackey, M. A.; Pickens, J. E.; Stuart, M. A.; Confait, B. S.; Phillips, J. P.: Selective Complexation and Reactivity of Metallic Nitride and Oxometallic Fullerenes with Lewis Acids and Use as an Effective Purification Method. *Inorg. Chem.* **2009**, *48*, 11685-11690.

(36) Stevenson, S.; Phillips, J. P.; Reid, J. E.; Olmstead, M. M.; Rath, S. P.; Balch, A. L.: Pyramidalization of Gd_3N inside a C_{80} Cage. The Synthesis and Structure of $Gd_3N@C_{80}$. *Chem. Commun.* **2004**, 2814-2815.

(37) Popov, A. A.; Krause, M.; Yang, S.; Wong, J.; Dunsch, L.: C_{78} Cage Isomerism Defined by Trimetallic Nitride Cluster Size: A Computational and Vibrational Spectroscopic Study. *J. Phys. Chem. B* **2007**, *111*, 3363-3369.

(38) Beavers, C. M.; Chaur, M. N.; Olmstead, M. M.; Echegoyen, L.; Balch, A. L.: Large Metal Ions in a Relatively Small Fullerene Cage: The Structure of $Gd_3N@C_2(22010)$-C_{78} Departs from the Isolated Pentagon Rule. *J. Am. Chem. Soc.* **2009**, *131*, 11519-11524.

(39) Ma, Y.; Wang, T.; Wu, J.; Feng, Y.; Xu, W.; Jiang, L.; Zheng, J.; Shu, C.; Wang, C.: Size Effect of Endohedral Cluster on Fullerene Cage: Preparation and Structural Studies of $Y_3N@C_{78}$-C_2. *Nanoscale* **2011**, *3*, 4955-4957.

(40) Mercado, B. Q.; Beavers, C. M.; Olmstead, M. M.; Chaur, M. N.; Walker, K.; Holloway, B. C.; Echegoyen, L.; Balch, A. L.: Is the Isolated Pentagon Rule Merely a Suggestion for Endohedral Fullerenes? The Structure of a Second Egg-Shaped Endohedral Fullerene-$Gd_3N@C_s(39663)$-C_{82}. *J. Am. Chem. Soc.* **2008**, *130*, 7854-7855.

(41) Fu, W.; Xu, L.; Azurmendi, H.; Ge, J.; Fuhrer, T.; Zuo, T.; Reid, J.; Shu, C.; Harich, K.; Dorn, H. C.: ^{89}Y and ^{13}C NMR Cluster and Carbon Cage Studies of an Yttrium Metallofullerene Family, $Y_3N@C_{2n}$ (n=40-43). *J. Am. Chem. Soc.* **2009**, *131*, 11762-11769.

(42) Beavers, C. M.; Zuo, T.; Duchamp, J. C.; Harich, K.; Dorn, H. C.; Olmstead, M. M.; Balch, A. L.: $Tb_3N@C_{84}$: An Improbable, Egg-Shaped Endohedral Fullerene that Violates the Isolated Pentagon Rule. *J. Am. Chem. Soc.* **2006**, *128*, 11352-11353.

(43) Zuo, T.; Walker, K.; Olmstead, M. M.; Melin, F.; Holloway, B. C.; Echegoyen, L.; Dorn, H. C.; Chaur, M. N.; Chancellor, C. J.; Beavers, C. M.; Balch, A. L.; Athans, A. J.: New Egg-Shaped Fullerenes: Non-Isolated Pentagon Structures of $Tm_3N@C_s(51365)$-C_{84} and $Gd_3N@C_s(51365)$-C_{84}. *Chem. Commun.* **2008**, 1067-1069.

(44) Zuo, T.; Beavers, C. M.; Duchamp, J. C.; Campbell, A.; Dorn, H. C.; Olmstead, M. M.; Balch, A. L.: Isolation and Structural Characterization of a Family of Endohedral Fullerenes Including the Large, Chiral Cage Fullerenes $Tb_3N@C_{88}$ and $Tb_3N@C_{86}$ as well as the I_h and D_{5h} Isomers of $Tb_3N@C_{80}$. *J. Am. Chem. Soc.* **2007**, *129*, 2035-2043.

(45) Chaur, M. N.; Aparicio-Angles, X.; Mercado, B. Q.; Elliott, B.; Rodriguez-Fortea, A.; Clotet, A.; Olmstead, M. M.; Balch, A. L.; Poblet, J. M.; Echegoyen, L.: Structural and Electrochemical Property Correlations of Metallic Nitride Endohedral Metallofullerenes. *J. Phys. Chem. C* **2010**, *114*, 13003-13009.

(46) Fu, W.; Zhang, J.; Champion, H.; Fuhrer, T.; Azuremendi, H.; Zuo, T.; Zhang, J.; Harich, K.; Dorn, H. C.: Electronic Properties and ^{13}C NMR Structural Study of $Y_3N@C_{88}$. *Inorg. Chem.* **2011**, *50*, 4256-4259.

(47) Chaur, M. N.; Melin, F.; Ashby, J.; Elliott, B.; Kumbhar, A.; Rao, A. M.; Echegoyen, L.: Lanthanum Nitride Endohedral Fullerenes $La_3N@C_{2n}$ (43 <= n <= 55): Preferential Formation of $La_3N@C_{96}$. *Chem. Eur. J.* **2008**, *14*, 8213-8219.

(48) Olmstead, M. M.; Lee, H. M.; Duchamp, J. C.; Stevenson, S.; Marciu, D.; Dorn, H. C.; Balch, A. L.: $Sc_3N@C_{68}$: Folded Pentalene Coordination in an Endohedral Fullerene that Does Not Obey the Isolated Pentagon Rule. *Angew. Chem. Int. Ed.* **2003**, *42*, 900-903.

(49) Fu, W.; Wang, X.; Azuremendi, H.; Zhang, J.; Dorn, H. C.: N-14 and Sc-45 NMR Study of Trimetallic Nitride Cluster $(M_3N)^{6+}$ Dynamics inside a Icosahedral C_{80} Cage. *Chem. Commun.* **2011**, *47*, 3858-3860.

(50) Kobayashi, K.; Sano, Y.; Nagase, S.: Theoretical Study of Endohedral Metallofullerenes: Sc_3−nLanN@C_{80} (n=0–3). *J. Comput. Chem.* **2001**, *22*, 1353-1358.

(51) Aihara, J.: Kinetic Stability of Metallofullerenes as Predicted by the Bond Resonance Energy Model. *Phys. Chem. Chem. Phys.* **2001**, *3*, 1427-1431.

(52) Rodriguez-Fortea, A.; Alegret, N.; Balch, A. L.; Poblet, J. M.: The Maximum Pentagon Separation Rule Provides a Guideline for the Structures of Endohedral Metallofullerenes. *Nature Chem.* **2010**, *2*, 955-961.

(53) Popov, A. A.; Dunsch, L.: Structure, Stability, and Cluster-Cage Interactions in Nitride Clusterfullerenes $M_3N@C_{2n}$ (M = Sc, Y; 2n = 68−98): a Density Functional Theory Study. *J. Am. Chem. Soc.* **2007**, *129*, 11835-11849.

(54) Iezzi, E. B.; Duchamp, J. C.; Harich, K.; Glass, T. E.; Lee, H. M.; Olmstead, M. M.; Balch, A. L.; Dorn, H. C.: A Symmetric Derivative of the Trimetallic Nitride Endohedral Metallofullerene, $Sc_3N@C_{80}$. *J. Am. Chem. Soc.* **2002**, *124*, 524-525.

(55) Lee, H. M.; Olmstead, M. M.; Iezzi, E.; Duchamp, J. C.; Dorn, H. C.; Balch, A. L.: Crystallographic Characterization and Structural Analysis of the First Organic Functionalization Product of the Endohedral Fullerene $Sc_3N@C_{80}$. *J. Am. Chem. Soc.* **2002**, *124*, 3494-3495.

(56) Stevenson, S.; Stephen, R. R.; Amos, T. M.; Cadorette, V. R.; Reid, J. E.; Phillips, J. P.: Synthesis and Purification of a Metallic Nitride Fullerene BisAdduct: Exploring the Reactivity of $Gd_3N@C_{80}$. *J. Am. Chem. Soc.* **2005**, *127*, 12776-12777.

(57) Cardona, C. M.; Kitaygorodskiy, A.; Ortiz, A.; Herranz, M. A.; Echegoyen, L.: The First Fulleropyrrolidine Derivative of $Sc_3N@C_{80}$: Pronounced Chemical Shift Differences of the Geminal Protons on the Pyrrolidine Ring. *J. Org. Chem.* **2005**, *70*, 5092-5097.

(58) Cardona, C. M.; Kitaygorodskiy, A.; Echegoyen, L.: Trimetallic Nitride Endohedral Metallofullerenes: Reactivity Dictated by the Encapsulated Metal Cluster. *J. Am. Chem. Soc.* **2005**, *127*, 10448-10453.

(59) Cai, T.; Slebodnick, C.; Xu, L.; Harich, K.; Glass, T. E.; Chancellor, C.; Fettinger, J. C.; Olmstead, M. M.; Balch, A. L.; Gibson, H. W.; Dorn, H. C.: A Pirouette on a Metallofullerene Sphere: Interconversion of Isomers of N-tritylpyrrolidino I_h $Sc_3N@C_{80}$. *J. Am. Chem. Soc.* **2006**, *128*, 6486-6492.

(60) Chen, N.; Zhang, E.-Y.; Tan, K.; Wang, C.-R.; Lu, X.: Size Effect of Encaged Clusters on the Exohedral Chemistry of Endohedral Fullerenes: A Case Study on the Pyrrolidino Reaction of $Sc_xGd_{3-x}N@C_{80}$ (x = 0−3). *Org. Lett.* **2007**, *9*, 2011-2013.

(61) Lukoyanova, O.; Cardona, C. M.; Rivera, J.; Lugo-Morales, L. Z.; Chancellor, C. J.; Olmstead, M. M.; Rodriguez-Fortea, A.; Poblet, J. M.; Balch, A. L.; Echegoyen, L.: "Open Rather Than Closed" Malonate Methano-Fullerene Derivatives. The Formation of Methanofulleroid Adducts of $Y_3N@C_{80}$. *J. Am. Chem. Soc.* **2007**, *129*, 10423-10430.

(62) Shu, C.; Cai, T.; Xu, L.; Zuo, T.; Reid, J.; Harich, K.; Dorn, H. C.; Gibson, H. W.: Manganese(III)-Catalyzed Free Radical Reactions on Trimetallic Nitride Endohedral Metallofullerenes. *J. Am. Chem. Soc.* **2007**, *129*, 15710-15717.

(63) Pinzon, J. R.; Zuo, T.; Echegoyen, L.: Synthesis and Electrochemical Studies of Bingel-Hirsch Derivatives of $M_3N@I_h$-C_{80} (M = Sc, Lu). *Chem. Eur. J.* **2010**, *16*, 4864-4869.

(64) Ross, R. B.; Cardona, C. M.; Guldi, D. M.; Sankaranarayanan, S. G.; Reese, M. O.; Kopidakis, N.; Peet, J.; Walker, B.; Bazan, G. C.; Van Keuren, E.; Holloway, B. C.; Drees, M.: Endohedral Fullerenes for Organic Photovoltaic Devices. *Nature Materials* **2009**, *8*, 208-212.

(65) Shu, C.; Xu, W.; Slebodnick, C.; Champion, H.; Fu, W.; Reid, J. E.; Azurmendi, H.; Wang, C.; Harich, K.; Dorn, H. C.; Gibson, H. W.: Syntheses and Structures of Phenyl-C_{81}-Butyric Acid Methyl Esters (PCBMs) from $M_3N@C_{80}$. *Org. Lett.* **2009**, *11*, 1753-1756.

(66) Li, F.-F.; Pinzon, J. R.; Mercado, B. Q.; Olmstead, M. M.; Balch, A. L.; Echegoyen, L.: 2+2 Cycloaddition Reaction to $Sc_3N@I_h$-C_{80}. The Formation of Very Stable 5,6 - and 6,6 -Adducts. *J. Am. Chem. Soc.* **2011**, *133*, 1563-1571.

(67) Cai, T.; Xu, L.; Anderson, M. R.; Ge, Z.; Zuo, T.; Wang, X.; Olmstead, M. M.; Balch, A. L.; Gibson, H. W.; Dorn, H. C.: Structure and Enhanced Reactivity Rates of the D_{5h} $Sc_3N@C_{80}$ and $Lu_3N@C_{80}$ Metallofullerene Isomers: The Importance of the Pyracylene Motif. *J. Am. Chem. Soc.* **2006**, *128*, 8581-8589.

(68) Osuna, S.; Rodriguez-Fortea, A.; Poblet, J. M.; Sola, M.; Swart, M.: Product Formation in the Prato Reaction on $Sc_3N@D_{5h}$-C_{80}: Preference for [5,6]-Bonds, and not Pyracylenic Bonds. *Chem. Commun.* **2012**, *48*, 2486-2488.

(69) Cai, T.; Xu, L.; Gibson, H. W.; Dorn, H. C.; Chancellor, C. J.; Olmstead, M. M.; Balch, A. L.: $SC_3N@C_{78}$: Encapsulated Cluster Regiocontrol of Adduct Docking on an Ellipsoidal Metallofullerene Sphere. *J. Am. Chem. Soc.* **2007**, *129*, 10795-10800.

(70) Cai, T.; Xu, L.; Shu, C.; Champion, H. A.; Reid, J. E.; Anklin, C.; Anderson, M. R.; Gibson, H. W.; Dorn, H. C.: Selective Formation of a Symmetric $Sc_3N@C_{78}$ Bisadduct: Adduct Docking Controlled by an Internal Trimetallic Nitride Cluster. *J. Am. Chem. Soc.* **2008**, *130*, 2136-2137.

(71) Cai, T.; Xu, L.; Shu, C.; Reid, J. E.; Gibson, H. W.; Dorn, H. C.: Synthesis and Characterization of a Non-IPR Fullerene Derivative: $Sc_3N@C_{68}$ $C(COOC_2H_5)_2$. *J. Phys. Chem. C* **2008**, *112*, 19203-19208.

(72) Chaur, M. N.; Melin, F.; Athans, A. J.; Elliott, B.; Walker, K.; Holloway, B. C.; Echegoyen, L.: The Influence of Cage Size on the Reactivity of Trimetallic Nitride Metallofullerenes: A Mono- and Bis-Methanoadduct of $Gd_3N@C_{80}$ and a Monoadduct of $Gd_3N@C_{84}$. *Chem. Commun.* **2008**, 2665-2667.

(73) Alegret, N.; Chaur, M. N.; Santos, E.; Rodriguez-Fortea, A.; Echegoyen, L.; Poblet, J. M.: Bingel-Hirsch Reactions on Non-IPR $Gd_3N@C_{2n}$ (2n=82 and 84). *J. Org. Chem.* **2010**, *75*, 8299-8302.

(74) Shustova, N. B.; Popov, A. A.; Mackey, M. A.; Coumbe, C. E.; Phillips, J. P.; Stevenson, S.; Strauss, S. H.; Boltalina, O. V.: Radical Trifluoromethylation of $Sc_3N@C_{80}$. *J. Am. Chem. Soc.* **2007**, *129*, 11676-11677.

(75) Shu, C.; Slebodnick, C.; Xu, L.; Champion, H.; Fuhrer, T.; Cai, T.; Reid, J. E.; Fu, W.; Harich, K.; Dorn, H. C.; Gibson, H. W.: Highly Regioselective Derivatization of Trimetallic Nitride Templated Endohedral Metallofullerenes via a Facile Photochemical Reaction. *J. Am. Chem. Soc.* **2008**, *130*, 17755-17760.

(76) Shu, C.; Corwin, F. D.; Zhang, J.; Chen, Z.; Reid, J. E.; Sun, M.; Xu, W.; Sim, J. H.; Wang, C.; Fatouros, P. P.; Esker, A. R.; Gibson, H. W.; Dorn, H. C.: Facile Preparation of a New Gadofullerene-Based Magnetic Resonance Imaging Contrast Agent with High ^{1}H Relaxivity. *Bioconjugate Chem.* **2009**, *20*, 1186-1193.

(77) Li, F.-F.; Rodríguez-Fortea, A.; Poblet, J. M.; Echegoyen, L.: Reactivity of Metallic Nitride Endohedral Metallofullerene Anions: Electrochemical Synthesis of a $Lu_3N@I_h$-C_{80} Derivative. *J. Am. Chem. Soc.* **2011**, *133*, 2760-2765.

(78) Li, F.-F.; Rodríguez-Fortea, A.; Peng, P.; Campos Chavez, G. A.; Poblet, J. M.; Echegoyen, L.: Electrosynthesis of a $Sc_3N@I_h$-C_{80} Methano Derivative from Trianionic $Sc_3N@I_h$-C_{80}. *J. Am. Chem. Soc.* **2012**, *134*, 7480-7487.

(79) Lu, X.; Akasaka, T.; Nagase, S.: Chemistry of Endohedral Metallofullerenes: the Role of Metals. *Chem. Commun.* **2011**, *47*, 5942-5957.

(80) Mikawa, M.; Kato, H.; Okumura, M.; Narazaki, M.; Kanazawa, Y.; Miwa, N.; Shinohara, H.: Paramagnetic Water-soluble Metallofullerenes Having the Highest Relaxivity for MRI Contrast Agents. *Bioconjugate Chem.* **2001**, *12*, 510-514.

(81) Fatouros, P. P.; Corwin, F. D.; Chen, Z.-J.; Broaddus, W. C.; Tatum, J. L.; Kettenmann, B.; Ge, Z.; Gibson, H. W.; Russ, J. L.; Leonard, A. P.; Duchamp, J. C.; Dorn, H. C.: *In vitro* and *in vivo* Imaging Studies of a New Endohedral Metallofullerene Nanoparticle. *Radiology* **2006**, *240*, 756-764.

(82) Zhang, J.; Fatouros, P. P.; Shu, C.; Reid, J.; Owens, L. S.; Cai, T.; Gibson, H. W.; Long, G. L.; Corwin, F. D.; Chen, Z.-J.; Dorn, H. C.: High Relaxivity Trimetallic Nitride (Gd_3N) Metallofullerene MRI Contrast Agents with Optimized Functionality. *Bioconjugate Chem.* **2010**, *21*, 610-615.

(83) Fillmore, H. L.; Shultz, M. D.; Henderson, S. C.; Cooper, P.; Broaddus, W. C.; Chen, Z. J.; Shu, C. Y.; Zhang, J. F.; Ge, J. C.; Dorn, H. C.; Corwin, F.; Hirsch, J. I.; Wilson, J.; Fatouros, P. P.: Conjugation of Functionalized Gadolinium Metallofullerenes with IL-13 Peptides for Targeting and Imaging Glial Tumors. *Nanomedicine* **2011**, *6*, 449-458.

(84) Shultz, M. D.; Wilson, J. D.; Fuller, C. E.; Zhang, J.; Dorn, H. C.; Fatouros, P. P.: Metallofullerene-based Nanoplatform for Brain Tumor Brachytherapy and Longitudinal Imaging in a Murine Orthotopic Xenograft Model. *Radiology* **2011**, *261*, 136-143.

(85) Shultz, M. D.; Duchamp, J. C.; Wilson, J. D.; Shu, C.-Y.; Ge, J.; Zhang, J.; Gibson, H. W.; Fillmore, H. L.; Hirsch, J. I.; Dorn, H. C.; Fatouros, P. P.: Encapsulation of a Radiolabeled Cluster Inside a Fullerene Cage, $^{177}Lu_xLu_{(3-x)}N@C_{80}$: An Interleukin-13-Conjugated Radiolabeled Metallofullerene Platform. *J. Am. Chem. Soc.* **2010**, *132*, 4980-4981.

(86) Ehrich, M.; Van Tassell, R.; Li, Y. B.; Zhou, Z. G.; Kepley, C. L.: Fullerene Antioxidants Decrease Organophosphate-induced Acetylcholinesterase Inhibition *in vitro*. *Toxicol. Vitro* **2011**, *25*, 301-307.

(87) Liedtke, M.; Sperlich, A.; Kraus, H.; Baumann, A.; Deibel, C.; Wirix, M. J. M.; Loos, J.; Cardona, C. M.; Dyakonov, V.: Triplet Exciton Generation in Bulk-Heterojunction Solar Cells Based on Endohedral Fullerenes. *J. Am. Chem. Soc.* **2011**, *133*, 9088-9094.

(88) Feng, L.; Rudolf, M.; Wolfrum, S.; Troeger, A.; Slanina, Z.; Akasaka, T.; Nagase, S.; Martin, N.; Ameri, T.; Brabec, C. J.; Guldi, D. M.: A Paradigmatic Change: Linking Fullerenes to Electron Acceptors. *J. Am. Chem. Soc.* **2012**, *134*, 12190-12197.

(89) Bharadwaj, P.; Novotny, L.: Plasmon-Enhanced Photoemission from a Single $Y_3N@C_{80}$ Fullerene. *J. Phys. Chem. C* **2010**, *114*, 7444-7447.

(90) Inoue, T.; Tomiyama, T.; Sugai, T.; Okazaki, T.; Suematsu, T.; Fujii, N.; Utsumi, H.; Nojima, K.; Shinohara, H.: Trapping a C_2 Radical in Endohedral Metallofullerenes: Synthesis and Structures of $(Y_2C_2)@C_{82}$ (Isomers I, II, and III). *J. Phys. Chem. B* **2004**, *108*, 7573-7579.

(91) Tan, K.; Lu, X.: Ti_2C_{80} Is More Likely a Titanium Carbide Endohedral Metallofullerene $Ti_2C_2@C_{78}$. *Chem. Commun.* **2005**, *0*, 4444-4446.

(92) Sato, Y.; Yumura, T.; Suenaga, K.; Moribe, H.; Nishide, D.; Ishida, M.; Shinohara, H.; Iijima, S.: Direct Imaging of Intracage Structure in Titanium-Carbide Endohedral Metallofullerene. *Phys. Rev. B* **2006**, *73*, 193401.

(93) Shinohara, H.; Sato, H.; Ohkohchi, M.; Ando, Y.; Kodama, T.; Shida, T.; Kato, T.; Saito, Y.: Encapsulation of a Scandium Trimer in C_{82}. *Nature* **1992**, *357*, 52-54.

(94) Iiduka, Y.; Wakahara, T.; Nakahodo, T.; Tsuchiya, T.; Sakuraba, A.; Maeda, Y.; Akasaka, T.; Yoza, K.; Horn, E.; Kato, T.; Liu, M. T. H.; Mizorogi, N.; Kobayashi, K.; Nagase, S.: Structural Determination of Metallofullerene Sc_3C_{82} Revisited: A Surprising Finding. *J. Am. Chem. Soc.* **2005**, *127*, 12500-12501.

(95) Zheng, H.; Zhao, X.; Wang, W.-W.; Yang, T.; Nagase, S.: $Sc_2@C_{70}$ Rather Than $Sc_2C_2@C_{68}$: Density Functional Theory Characterization of Metallofullerene Sc_2C_{70}. *J. Chem. Phys.* **2012**, *137*.

(96) Shi, Z. Q.; Wu, X.; Wang, C. R.; Lu, X.; Shinohara, H.: Isolation and Characterization of $Sc_2C_2@C_{68}$: A Metal-Carbide Endofullerene with a Non-IPR Carbon Cage. *Angew. Chem. Int. Ed.* **2006**, *45*, 2107-2111.

(97) Yamazaki, Y.; Nakajima, K.; Wakahara, T.; Tsuchiya, T.; Ishitsuka, M. O.; Maeda, Y.; Akasaka, T.; Waelchli, M.; Mizorogi, N.; Nagase, S.: Observation of C-13 NMR Chemical Shifts of Metal Carbides Encapsulated in Fullerenes: $Sc_2C_2@C_{82}$, $Sc_2C_2@C_{84}$, and $Sc_3C_2@C_{80}$. *Angew. Chem. Int. Ed.* **2008**, *47*, 7905-7908.

(98) Iiduka, Y.; Wakahara, T.; Nakajima, K.; Nakahodo, T.; Tsuchiya, T.; Maeda, Y.; Akasaka, T.; Yoza, K.; Liu, M. T. H.; Mizorogi, N.; Nagase, S.: Experimental and Theoretical Studies of the Scandium Carbide Endohedral Metallofullerene $Sc_2C_2@C_{82}$ and Its Carbene Derivative. *Angew. Chem. Int. Ed.* **2007**, *46*, 5562-5564.

(99) Yang, H.; Lu, C.; Liu, Z.; Jin, H.; Che, Y.; Olmstead, M. M.; Balch, A. L.: Detection of a Family of Gadolinium-Containing Endohedral Fullerenes and the Isolation and Crystallographic Characterization of One Member as a Metal-Carbide Encapsulated inside a Large Fullerene Cage. *J. Am. Chem. Soc.* **2008**, *130*, 17296-17300.

(100) Takata, M.; Umeda, B.; Nishibori, E.; Sakata, M.; Saito, Y.; Ohno, M.; Shinohara, H.: Confirmation by X-Ray-Diffraction of the Endohedral Nature of the Metallofullerene $Y@C_{82}$. *Nature* **1995**, *377*, 46-49.

(101) Akasaka, T.; Kato, T.; Kobayashi, K.; Nagase, S.; Yamamoto, K.; Funasaka, H.; Takahashi, T.: Exohedral Adducts of $La@C_{82}$. *Nature* **1995**, *374*, 600-601.

(102) Akasaka, T.; Nagase, S.; Kobayashi, K.; Wälchli, M.; Yamamoto, K.; Funasaka, H.; Kako, M.; Hoshino, T.; Erata, T.: ^{13}C and ^{139}La NMR Studies of $La_2@C_{80}$: First Evidence for Circular Motion of Metal Atoms in Endohedral Dimetallofullerenes. *Angew. Chem. Int. Ed. in English* **1997**, *36*, 1643-1645.

(103) Cagle, D. W.; Kennel, S. J.; Mirzadeh, S.; Alford, J. M.; Wilson, L. J.: *In vivo* Studies of Fullerene-Based Materials Using Endohedral Metallofullerene Radiotracers. *Proc. Natl. Acad. Sci. U. S. A.* **1999**, *96*, 5182-5187.

(104) Zuo, T.; Xu, L.; Beavers, C. M.; Olmstead, M. M.; Fu, W.; Crawford, T. D.; Balch, A. L.; Dorn, H. C.: $M_2@C_{79}N$ (M = Y, Tb): Isolation and Characterization of Stable Endohedral Metallofullerenes

Exhibiting M-M Bonding Interactions inside Aza[80]fullerene Cages. *J. Am. Chem. Soc.* **2008**, *130*, 12992-12997.

Chapter 2 Introduction of Special Isotopes to Endohedral Metallofullerenes

2.1 Introduction

Endohedral metallofullerenes (EMFs) can be modified with special isotopes. Based on the identity of the isotopes, the modification can be assorted to radioactive modification and non-radioactive modification. The radioactive modification could introduce radioactive metallic isotope into the cage which leads to EMF-based radiopharmaceuticals. For example, in 1999 the $^{166}Ho_x@C_{82}$-$(OH)_y$ was synthesized as a water soluble EMF-based medicine.[1] In 2010 Fatouros, Dorn and coworkers reported the first radioactive clusterfullerene for therapeutics agents.[2] The non-radioactive modification normally relates to NMR study. A direct thought would be enrich the fullerene cage surface with ^{13}C for enhanced ^{13}C NMR signals. This idea was successfully fulfilled by Akasaka and coworkers who achieved the first observation of the NMR signal from the endohedral carbide cluster with ^{13}C enriched samples.[3] Moreover, other nuclei including ^{15}N and ^{17}O can be potentially introduced to EMFs for NMR purposes, although a previous attempt to observe the ^{15}N NMR signal for $Sc_3{}^{15}N@C_{80}$ by our group was not fruitful.

Based on the synthetic protocols, the introduction of special isotopes can be classified as pre-synthesis modification, which use desired isotope in the starting materials to produce EMFs, and post-synthesis modification, which introduce the desired isotope via exchange or activation reactions with already produced EMFs. For ^{13}C enrichment, using ^{13}C labeled graphite as part of the starting material is the most and only practical way. For radioactive metal isotopes, both methods could be used.

2.2 ^{13}C enrichment of yttrium EMFs

2.2.1 The choice of metal

^{13}C enrichment in EMF can not only significantly increase the signal to noise ratio in 1D ^{13}C NMR, but also open the possibility of INADEQUATE 2D NMR studies. Since any paramagnetic metal ions will impede NMR studies, only Sc^{3+}, Lu^{3+}, Y^{3+}, which are diamagnetic ions, are feasible candidates (the studies of EMFs encapsulating divalent-ions, such as Sm^{2+} and Yb^{2+} emerged in recent 2 years, but by the time we tried to make ^{13}C enriched samples we did not have the knowledge about them). We weighed the advantages and disadvantages of these three metals as listed in the table below.

Table 1. Advantages and disadvantages for Sc^{3+}, Lu^{3+} and Y^{3+} for ^{13}C enriched EMFs.

Metal ion	Advantage	Disadvantage
Sc^{3+}	1) Very-high yield. 2) Known to form both TNT-EMFs and CCFs. 3) ^{45}Sc-^{13}C interaction may be observed.	1) Do not form large TNT-EMFs beyond C_{80}. 2) ^{13}C enriched CCFs have been reported.[3]
Lu^{3+}	1) High-yield. 2) Known to form TNT-EMFs.	1) Low yield for large TNT-EMFs beyond C_{80}. 2) Formation of CCFs is uncertain.
Y^{3+}	1) Known to form both TNT-EMFs and CCFs. 2) Higher yield for large EMFs beyond C_{80}. 3) ^{89}Y-^{13}C coupling has been confirmed in earlier experiment.	1) Lower yield overall. 2) ^{13}C NMR of the TNT-EMF family has been extensively studied by our group.[4]

Considering the potential of observation of ^{89}Y-^{13}C coupling and that overall yield would not be a major problem for ^{13}C NMR study on ^{13}C enriched samples, we finally decided to investigate ^{13}C labeled graphite on yttrium metal.

2.2.2 Optimization of graphite rod composition

As mentioned above, ^{13}C enrichment can be achieved by adding ^{13}C labeled graphite as the starting material, which is commercially available for $200-350 per gram in powder form. Therefore, the ^{13}C graphite needs to be packed into the rod together with the metal oxide and catalysts. As shown in Figure 1, a 1-inch-diameter graphite rod was truncated into about 6 inch length, and drilled to 5-inch depth with a 3/8 inch drill. The butt of the rod is about 1-inch long and does not participate in the reaction. The mass of the "graphite wall" that does participate in the reaction can be calculated by 7/9 multiplied by the mass difference before and after the drilling because the cavity accounts for 3/4 of the rod diameter and thereby 9/16 of the total volume (mass) of the top 5 inches of the graphite rod. Therefore, the ^{13}C graphite ratio was estimated by the following equation:

$$^{13}C \text{ ratio} = m_{packed} / [(7/9)\,(m_0-m_1)+m_{packed}]$$

where m_{packed} is the mass of graphite in the rod with copper and yttrium oxide, m_0 and m_1 are the mass of the graphite rod before and after drill, respectively. In the trial runs normal graphite was used while in actual runs the graphite packed inside was 99% ^{13}C labeled graphite.

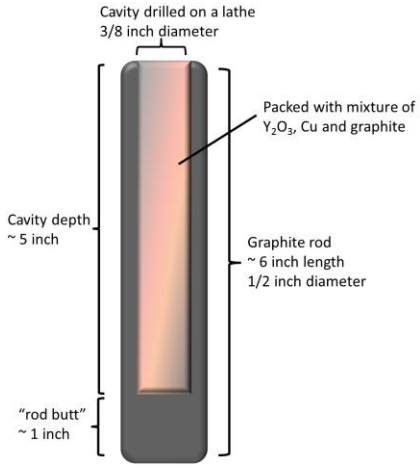

Figure 1. A packed graphite rod for the synthesis of ^{13}C enriched yttrium EMFs

A standard packing composition for yttrium EMF synthesis had been established to be ~13 g Y_2O_3 with ~12 g Cu, but packing graphite into the rod requires the amount of Y_2O_3 or Cu to be reduced. Our goal was to keep the Y_2O_3 amount relatively high while compromise Cu amount for the space of graphite, because it had been anticipated replacing Y_2O_3 with graphite too much would lead to significantly reduced yields of EMFs, but the effect of copper was not certain. To optimize the balance over cost, yield and percentage of enrichment, trial runs were performed for the following packing compositions, which were based on previous data and trial packing:

1) 13.1 g Y_2O_3, 12.2 g Cu (control group)

2) 8.9 g Y_2O_3, 7.2 g Cu, 2.9 g graphite (trial run for 20% ^{13}C ratio)

3) 9.3 g Y_2O_3, 2.1 g Cu, 3.6 g graphite (trial run for 26% ^{13}C ratio)

All mass values above were obtained from the actual packing, based on the average value of 5 rods in each trial run. Comparing recipe 2 to the control group, to accommodate the 2.9 g graphite, both the mass of Y_2O_3 and Cu were reduced. From recipe 2 to recipe 3, the Y_2O_3 amount was kept constant and only the amount of Cu was reduced.

The soot was extracted in a Soxhlet-extractor in refluxing xylene for 48 hours and the resulting solution was concentrated and then mildly treated with cyclopentadiene-functionalized silica[5] in a "stir and filter approach".[6] The HPLC traces on a 5-pentabromobenzyloxypropylsilyl (5-PBB) column for are shown below. The peaks were assigned based on mass spectral data and previous studies on yttrium based TNT EMFs.[4] The chromatogram for the products from recipe 2 and recipe 3 were almost identical, but both showed lower EMF abundance compared to the empty-cages. The total yields of $Y_3N@C_{80}$ were 3.9 mg, 2.2 mg and 1.9 mg, respectively.

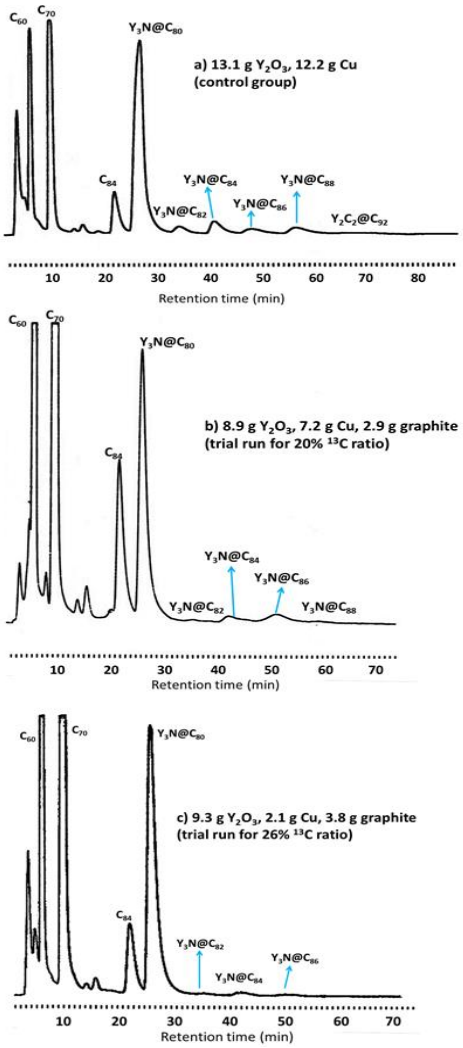

Figure 2 HPLC traces for the EMF products for a) recipe 1 without graphite packed inside the rod. b) recipe 2 with 20% of total reacting graphite packed inside the rod c) recipe 3 with 26% of total reacting graphite packed inside the rod after mild cyclopentadiene treatment.

From the data I was able to conclude that the amount of Y_2O_3 has more significant influence than the amount of Cu. The yield only slightly decreased when the amount of Cu was significantly reduced, and the product distributions over different EMFs were about identical.

2.2.3 Synthesis and mass-spectral identification of the ^{13}C enriched yttrium EMFs

Based on the trials runs, in the actual ^{13}C enriched synthesis we used 20% ^{13}C for one run and 25% ^{13}C in another run, both with maximum amount of Y_2O_3 but minimum amount of Cu. The ^{13}C enriched EMF synthesis was commissioned to *LUNA Innovations* with 1-inch-diamater graphite rod. The ratio of enrichment was evaluated based on the isotopic distributions of C_{60} and $Y_3N@C_{80}$ mass-spectral peaks as shown in Figure 3. From both the C_{60} peak and the $Y_3N@C_{80}$ peak, I was able to conclude that the 20% packed ^{13}C graphite had led to 6%-7% ^{13}C enrichment and the 25% packed ^{13}C graphite had led to 9%-10% ^{13}C enrichment. From an NMR point of view, the latter is a better choice as 25% more packed ^{13}C graphite led to ~50% more ^{13}C ratio in the products.

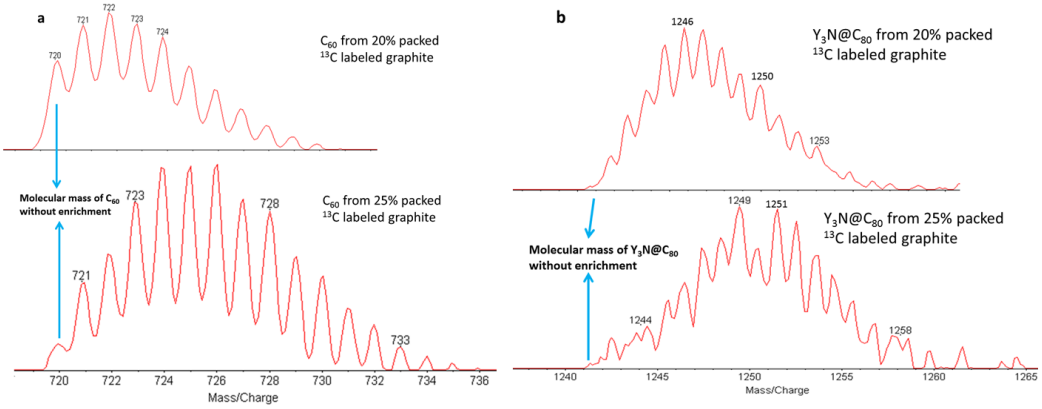

Figure 3. Isotopic distribution of ^{13}C enriched C_{60} and $Y_3N@C_{80}$ mass-spectral peaks. a) 20% ^{13}C graphite batch. b) 25% ^{13}C graphite batch.

To keep the most useful metallofullerenes, I only applied a very mild cyclopentadiene-functionalized silica treatment. Then, the resulting solution from the batch with 25% ^{13}C graphite was further separated with a large automated HPLC unit. Each cycle took slightly over 3 hours. As shown in Figure 4, the cut-off time between peaks was arbitrarily decided based mainly on

TNT-EMF components as reported before[4] and also seen above in Figure 2a as fractions Y-1 to Y-7. An eighth fraction Y-8 was added to collect unknown large EMFs.

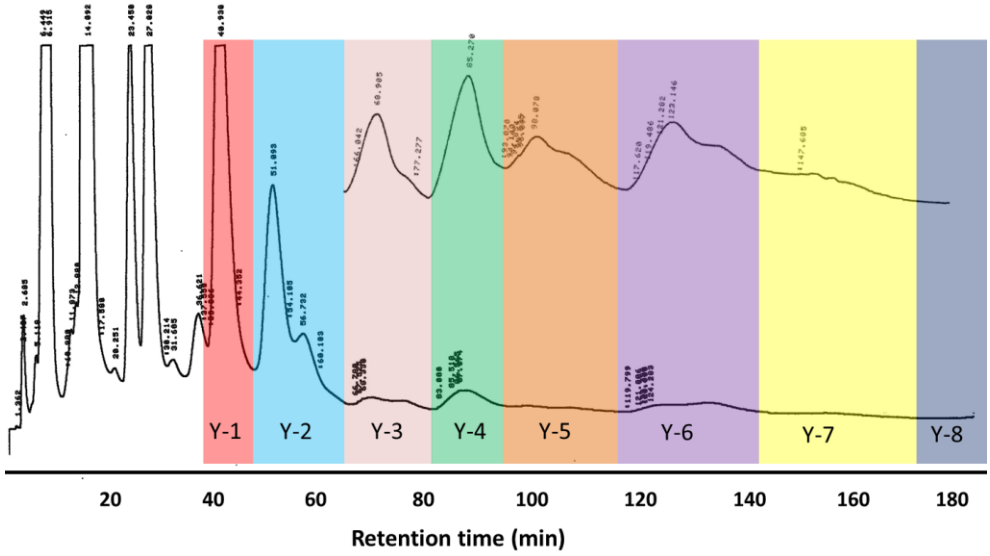

Figure 4. HPLC separation of ^{13}C enriched EMFs. The fractions from Y-1 to Y-8 are shown in different colors. The inset shows the expansion from Y-3 to Y-8 obtained from an independent injection with larger attenuation setting.

Due to the milder cyclopentadiene treatment than before (smaller amount silica and shorter reaction time), more empty-cage fullerenes were kept. For example, the Y-1 fraction which represents both $Y_2@C_{79}N$[7] and empty cage C_{84} is normally smaller than the Y-2 fraction ($Y_3N@C_{80}$) in terms of peak area, but in this case it was the largest fraction due to the large retained amount of C_{84} survived after the chemical treatment. What is more interesting to note is milder treatment led to the survival of more yttrium based EMFs, as can be clearly seen as minor peaks in the inset of Figure 4. All 8 fractions were collected and characterized by mass spectrometry, and the results are shown in Figure 5. Meanwhile a parallel HPLC separation was performed for the trial synthesis without ^{13}C enrichment to provide standard mass values.

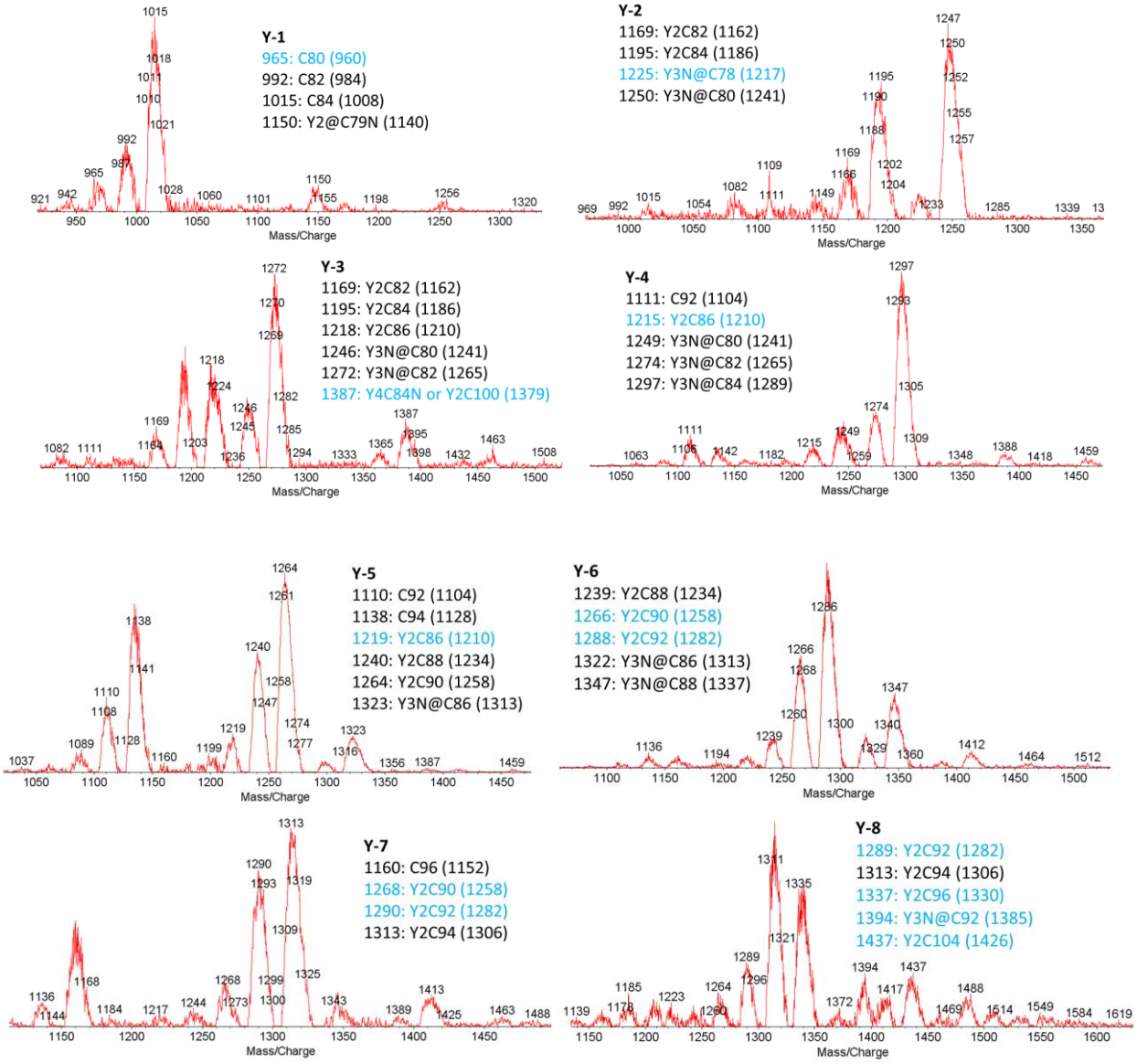

Figure 5. Mass spectrometry of the collected fractions of 9%-10% ^{13}C enriched samples with identification of the peaks. The numbers in parentheses are obtained from a counterpart fraction without ^{13}C enrichment as standard for the molecular mass values to better assign a molecular formula. TNT-EMFs are written in the form of $Y_3N@C_{2n}$ while dimetallic fullerenes are written as Y_2C_{2n} since they could be either a traditional EMF or a CCF. Highlighted in blue are the molecular formulas that were not known before.

I performed further separation and detailed study for the Y-2, Y-3, Y-6 and Y-7 fractions as discussed in the following chapters. To date the large family of yttrium EMFs has only been partially exploited and there is no doubt that future investigations of these fractions will lead to other exciting discoveries of new molecules.

2.3 Metal exchange reaction for radioactive EMFs

After we developed the peroxide reaction that to modify $Gd_3N@C_{80}$ with hydrophilic groups for application as magnetic resonance imaging (MRI) contrast agents,[8] the reaction was applied to a radiolabeled TNT-EMF, $^{177}Lu_xLu_{3-x}N@C_{80}$, to produce a therapeutic biomedicine for tumors.[2] I performed the functionalization reaction in the latter work. The $^{177}Lu_xLu_{3-x}N@C_{80}$ was produced by adding ^{177}Lu labeled $LuCl_3$ into the rod mixed with Lu_2O_3 in the EMF synthesis in a modified K-H reactor that allowed extraction of the soot without opening the sealed chamber to protect the operating personnel from the radioactive materials. However, in this process the radioactivity yield was very low. We started with 10 mCi of radioactive materials packed in the rod but in three different trials our best yield was 0.2 μCi in the toluene extraction, corresponding to a 0.02% yield.

The low yield was due to the intrinsic low yield of metallofullerenes, which was improving over the last decades but still much lower compared to most chemical reactions. Therefore, it is critical to develop a post-synthesis protocol using metallofullerenes as starting material. Considering fullerene cages could open and close back at high temperatures,[9] we tried a bold idea of exchanging element metal with the metal ion inside the fullerene cage. The reaction scheme is shown in Figure 6a. The reaction is thermodynamically favored and the question is the

kinetic feasibility. If the reaction had worked any better than 0.02% yield we could then use ^{89}Y or ^{177}Lu to exchange the metals in TNT-EMFs.

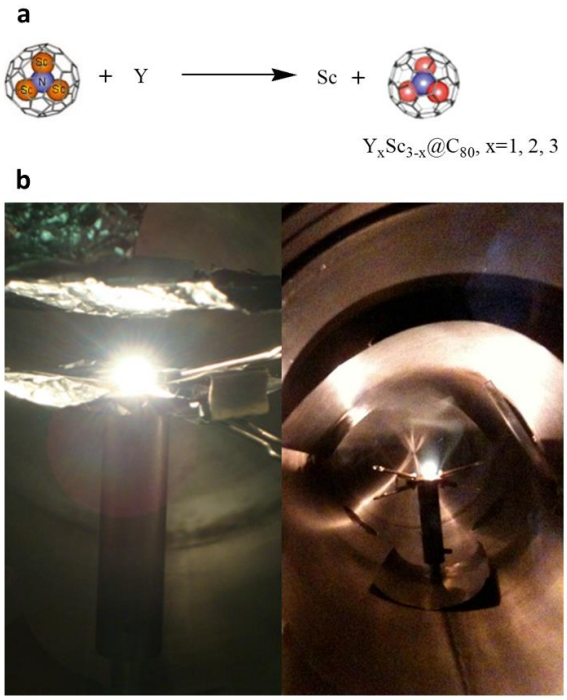

Figure 6. The exchange reaction between Y metal and $Sc_3N@C_{80}$. a) the reaction scheme. b) setup for the laser apparatus.

The reaction setup is shown in Figure 6b. The two figures are the same idea conveyed in slightly different setups. $Sc_3N@C_{80}$ and Y metal were pressed into a small pellet and put on top of a tungsten base. Aluminum foils (Figure 6b left) or plates (Figure 6b right) were placed both over and underneath the setup to collect the product. The pellet was irradiated by a CO_2 laser under inert atmosphere (vacuum or different pressure of N_2) for 5-10 minutes, during which glow and plume was observed. After the glow and plume stopped the laser beam was turned off and the system was let cool. The aluminum collectors were washed with toluene and the resulting solution was characterized by mass spectrometry. Unfortunately only the trial with

aluminum foil (left setup in Figure 6b) in 50 torr of N_2 could have resulted a new peak in the mass-spectrum (Figure 7), and the change was not visible in HPLC. A peak with molecular weight of 1152 seemed to be emerging in the experiment group of Figure 7c. Since the purity of the starting material was checked (Figure 7a), empty cage C_{96} should not exist in the product. Therefore, if the peak was real, it could be due to trace amount (marginal for mass-spec sensitivity of nanogram scale) of $Sc_2YN@C_{80}$.

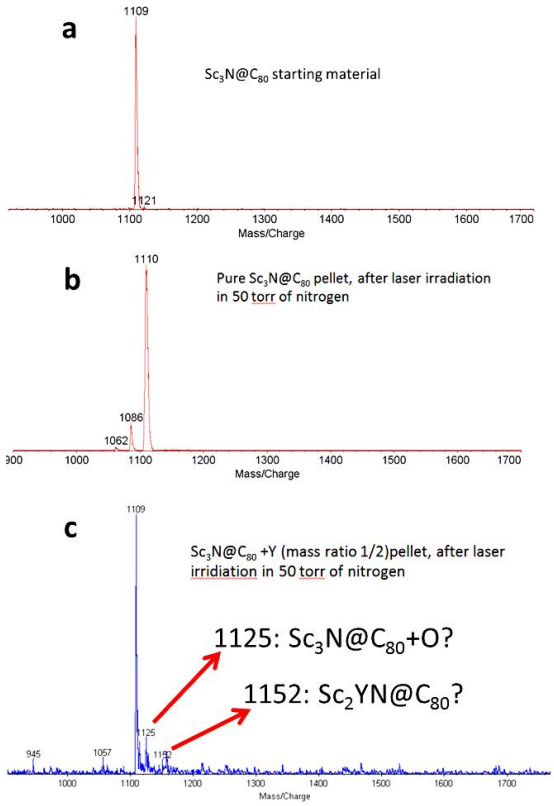

Figure 7. Mass-spectra of the a) starting material b) control group and c) experiment group for the laser experiment of $Sc_3N@C_{80}$ and Y metal mixture.

After several other attempts no mass spectral peaks other than the starting material showed again, and we realized this reaction was not practical for our purpose. Then we shifted to other post-synthesis modifications. For example, an on-going project is to make $^{177}Lu_xLu_{3-x}N@C_{80}$ by

neutron activation of $Lu_3N@C_{80}$. However, the laser experiment had left two questions waiting to be answered by future work:

1) In the control group, two mass-spectral peaks corresponding to $Sc_3C_{78}N$ and $Sc_3C_{76}N$ appeared. Are they due to fragmentation (which is rare for fullerenes and EMFs) or some new molecules formed in the process?

2) Was the 1152 peak real? Did $Sc_2YN@C_{80}$ form in trace amount?

2.4 Synthesis of ^{177}Lu-Gd bifunctional radiolanthanides

The TNT-EMF based nanoplatform f-$Gd_3N@C_{80}$-Lu-DOTA which functioned as both therapeutic and diagnostic agent ("theranostic agent")[10] led to the challenge to put both the therapeutic ^{177}Lu and diagnostic Gd^{3+} inside the same cage. An attempt was made by me and coworkers to synthesize mixed-metal EMFs with Gd_2O_3, Lu_2O_3 and $^{177}Lu_xLu_{2-x}O_3$. We started with 10 mCi radioactivity and got 0.05-0.1 μCi in the product. The radioactivity yield was even lower than the pure Lu case, which forced us to abandon this method.

REFERENCE

(1) Cagle, D. W.; Kennel, S. J.; Mirzadeh, S.; Alford, J. M.; Wilson, L. J.: *In vivo* Studies of Fullerene-based Materials Using Endohedral Metallofullerene Radiotracers. *Proc. Natl. Acad. Sci. U. S. A.* **1999**, *96*, 5182-5187.

(2) Shultz, M. D.; Duchamp, J. C.; Wilson, J. D.; Shu, C.-Y.; Ge, J.; Zhang, J.; Gibson, H. W.; Fillmore, H. L.; Hirsch, J. I.; Dorn, H. C.; Fatouros, P. P.: Encapsulation of a Radiolabeled Cluster Inside a Fullerene Cage, $^{177}Lu_xLu_{(3-x)}N@C_{80}$: An Interleukin-13-Conjugated Radiolabeled Metallofullerene Platform. *J. Am. Chem. Soc.* **2010**, *132*, 4980-4981.

(3) Yamazaki, Y.; Nakajima, K.; Wakahara, T.; Tsuchiya, T.; Ishitsuka, M. O.; Maeda, Y.; Akasaka, T.; Waelchli, M.; Mizorogi, N.; Nagase, S.: Observation of C-13 NMR Chemical Shifts of Metal Carbides Encapsulated in Fullerenes: $Sc_2C_2@C_{82}$, $Sc_2C_2@C_{84}$, and $Sc_3C_2@C_{80}$. *Angew. Chem. Int. Ed.* **2008**, *47*, 7905-7908.

(4) Fu, W.; Xu, L.; Azurmendi, H.; Ge, J.; Fuhrer, T.; Zuo, T.; Reid, J.; Shu, C.; Harich, K.; Dorn, H. C.: ^{89}Y and ^{13}C NMR Cluster and Carbon Cage Studies of an Yttrium Metallofullerene Family, $Y_3N@C_{2n}$ (n=40-43). *J. Am. Chem. Soc.* **2009**, *131*, 11762-11769.

(5) Ge, Z. X.; Duchamp, J. C.; Cai, T.; Gibson, H. W.; Dorn, H. C.: Purification of Endohedral Trimetallic Nitride Fullerenes in a Single, Facile Step. *J. Am. Chem. Soc.* **2005**, *127*, 16292-16298.

(6) Stevenson, S.; Harich, K.; Yu, H.; Stephen, R. R.; Heaps, D.; Coumbe, C.; Phillips, J. P.: Nonchromatographic "Stir And Filter Approach" (SAFA) for Isolating $Sc_3N@C_{80}$ Metallofullerenes. *J. Am. Chem. Soc.* **2006**, *128*, 8829-8835.

(7) Zuo, T.; Xu, L.; Beavers, C. M.; Olmstead, M. M.; Fu, W.; Crawford, T. D.; Balch, A. L.; Dorn, H. C.: $M_2@C_{79}N$ (M = Y, Tb): Isolation and Characterization of Stable Endohedral Metallofullerenes Exhibiting M-M Bonding Interactions inside Aza[80]fullerene Cages. *J. Am. Chem. Soc.* **2008**, *130*, 12992-12997.

(8) Shu, C.; Corwin, F. D.; Zhang, J.; Chen, Z.; Reid, J. E.; Sun, M.; Xu, W.; Sim, J. H.; Wang, C.; Fatouros, P. P.; Esker, A. R.; Gibson, H. W.; Dorn, H. C.: Facile Preparation of a New Gadofullerene-Based Magnetic Resonance Imaging Contrast Agent with High ^1H Relaxivity. *Bioconjugate Chem.* **2009**, *20*, 1186-1193.

(9) Troshin, P. A.; Avent, A. G.; Darwish, A. D.; Martsinovich, N.; Abdul-Sada, A. K.; Street, J. M.; Taylor, R.: Isolation of Two Seven-membered Ring C_{58} Fullerene Derivatives: $C_{58}F_{17}CF_3$ and $C_{58}F_{18}$. *Science* **2005**, *309*, 278-281.

(10) Shultz, M. D.; Wilson, J. D.; Fuller, C. E.; Zhang, J.; Dorn, H. C.; Fatouros, P. P.: Metallofullerene-based Nanoplatform for Brain Tumor Brachytherapy and Longitudinal Imaging in a Murine Orthotopic Xenograft Model. *Radiology* **2011**, *261*, 136-143.

Chapter 3 Nanoscale Fullerene Compression of an Yttrium Carbide Cluster

This chapter is adopted from the manuscript published on *Journal of the American Chemical Society* with appropriate modifications under the permission of the American Chemical Society. Full text of the published manuscript entitled "*Nanoscale fullerene compression of an yttrium carbide cluster*" by Jianyuan Zhang, Tim Fuhrer, Wujun Fu, Jiechao Ge, Daniel W. Bearden, Jerry Dallas, James Duchamp, Kenneth Walker, Hunter Champion, Hugo Azurmendi, Kim Harich, and Harry C. Dorn can be obtained at http://pubs.acs.org/doi/pdf/10.1021/ja300134x.

3.1 Introduction

Isolation of metal clusters from adjacent lattice units frees them from their usual intramolecular interactions, and provides a paradigm of understanding their size and shape within constrained models. A recent seminal example of this approach is the encapsulation of a single water molecule in the fullerene C_{60} which isolates it from other water molecules preventing intramolecular hydrogen bonding.[1] For metal clusters, fullerene carbon cages also provide ideal environments for the isolation purpose to study the size and shape of metal lattice and other important nanoscale parameters, thereby tuning their physical properties.

Our hypothesis is that decreasing the fullerene cage size of endohedral metallofullerenes (EMFs) will dramatically change the size and shape of the encapsulated metal clusters. Furthermore, nanoscale fullerene compression (NFC) of the metal clusters by decreasing fullerene cage size can be directly compared with macroscopic pressure compression (MPC) of the same metal carbide lattice, yttrium carbide. In this chapter I present a detailed structural investigation of the yttrium carbide clusters in progressing from large (~C_{100}) to smaller fullerene cages (C_{82}). The results from the isolated model can be related to the metal

lattice in other systems, for example, in superconducting metal carbide systems. We also compare crystal structural parameters of a previously reported metal carbide, Y_2C_3 to the $(Y_2C_2)^{4+}$ cluster in the current metallofullerene study, illustrating the influence of nanoscale FC when compared with the effects of macroscopic external pressure compression.[2,3] In the Y_2C_3 superconducting system, the superconducting transition temperature (T_c) of Y_2C_3 is strongly dependent on the external pressure.[4]

To date, metal clusters encapsulated in the fullerene cages have included: metal atoms,[5-9] metal clusters,[10-14] metal nitride clusters[15,16] and metal carbide clusters.[17-25] Encapsulated metal carbide clusters reported to date have fullerene cages ranging from C_{68} to C_{92}, but the attempts to detect the ^{13}C chemical shift of the endohedral carbide cluster were not successful until Nagase et al. utilized isotopically enriched ^{13}C samples.[23] Single crystal structures of $Gd_2C_2@C_{92}$[22] and two $Sc_2C_2@C_{82}$ isomers[26,27] have been studied, and a very recent X-ray crystal study of $Sc_2C_2@C_{2n}$ (n=40-42) shows that the change in carbon cage size can result in different carbide cluster shapes.[25] For a clear understanding of the structural changes of the metal carbide clusters as a function of cage size, we have performed a detailed ^{13}C NMR study of the yttrium-carbide dimetallofullerene, $Y_2C_2@D_3$-C_{92}, ^{13}C enriched $Y_2C_2@C_{3v}$-C_{82}, and $Y_2C_2@C_s$-C_{82}[18] as well as an isomer of $Y_2C_2@C_{84}$. For the first time, we have observed the important scalar $^1J_{Y\text{-}C}$ coupling for all samples. In addition, the experimental results are supported by DFT calculations of the $(Y_2C_2)^{4+}$ cluster in various environments, including the cluster (Y_2C_2),[4+] $Y_2C_2@D_5$-C_{100}, $Y_2C_2@D_3$-C_{92}, and $Y_2C_2@C_{3v}$-C_{82}.

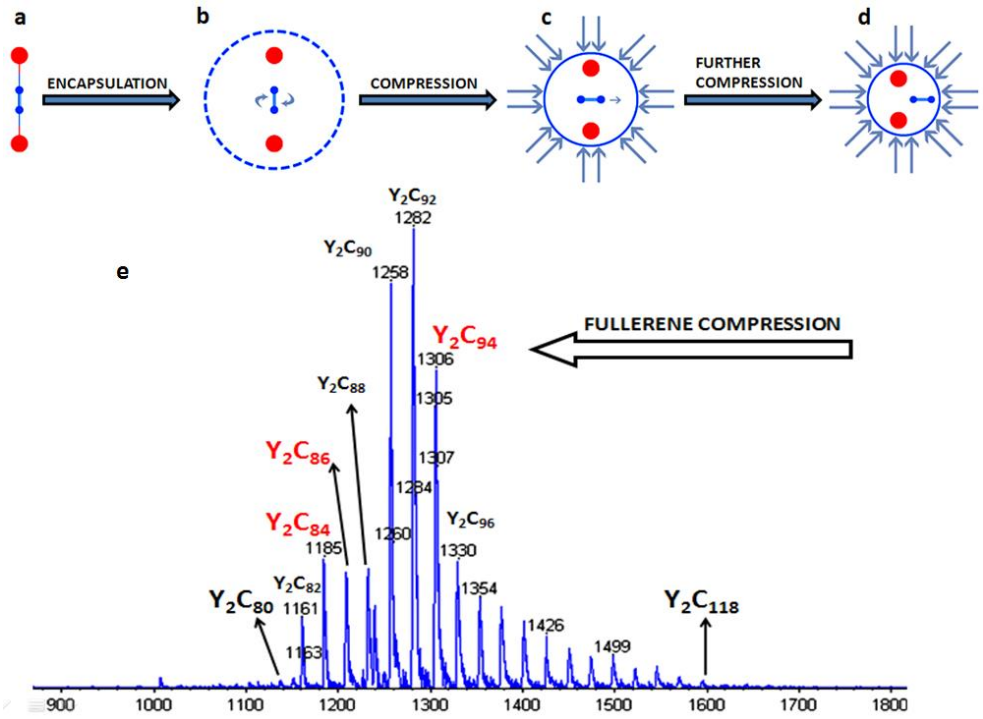

Figure 1. Nanoscale fullerene compression of yttrium carbide clusters. (a) $Y_2C_2^{4+}$ cluster without a cage. (b) linear $Y_2C_2^{4+}$ cluster inside a large fullerene cage. (c) $Y_2C_2^{4+}$ cluster with carbide bond vector orthogonal to the yttrium-yttrium vector in a compressed fullerene cage. (d) $Y_2C_2^{4+}$ cluster with carbide bond vector orthogonal to and deviated from yttrium-yttrium vector. (e) mass spectrometry showing a family of endohedral metallofullerenes with formula Y_2C_{2n}.

A previous DFT computational study of the Y_2C_2 neutral molecular cluster supports a stable linear structural arrangement as illustrated (upper Figure 1a) although a square planar structure is only slightly less stable.[28] For the charged $(Y_2C_2)^{4+}$ cluster, the DFT results of our current study also suggest a stable linear structure *vide supra* (Figure 1b). However, the study on metallofullerenes encapsulating other metals (Gd and Sc) also established that the $(M_2C_2)^{4+}$ metal-carbide clusters inside mid-sized fullerene cages can have the carbide bond

vector orthogonal to the metal-metal bond adopt an "idealized butterfly shape" (as in $Gd_2C_2@C_{92}$, Figure 1c)[22] and further compression of the $(M_2C_2)^{4+}$ cluster by a small cage leads to a butterfly shape in which the carbide is orthogonal to but displaced from the metal-metal bond axis (as in $Sc_2C_2@C_{82}$, Figure 1d).[26] We propose that this structural difference is due to the cage size rather than the metal, and a certain encapsulated $(M_2C_2)^{4+}$ cluster in a progressively smaller cage changes the most stable cluster conformation from a linear to butterfly shape.

In the soot of an independent endohedral metallofullerene (EMF) synthesis by arcing Y_2O_3 filled graphite rods in helium, a family of EMFs with the formula Y_2C_{2n} (n=40-59) dominated mass-spectrometry after selective removal of empty caged fullerenes (Figure 1e). Although some of the peaks in Figure 1e could result from classic dimetallic EMFs $Y_2@C_{2n}$, we have isolated four yttrium carbide members of this family, $Y_2C_2@C_{3v}$-C_{82}, $Y_2C_2@C_s$-C_{82}, and $Y_2C_2@C_{84}$ and the larger cage $Y_2C_2@D_3$-C_{92} for our experimental study.

3.2 Experimental Section

3.2.1 Synthesis and isolation of $Y_2C_2@D_3$-C_{92}.

$Y_2C_2@D_3$-C_{92} was synthesized in a Krätschmer-Huffman generator by vaporizing composite graphite carbon rods filled with a mixture Y_2O_3, graphite powder and metallic Cu with a weight ratio of 1.1/1.0/2.1 in a dynamic flow of He and N_2 (flow rate ratio of N_2/He=3/100). The resulting soot was then extracted with refluxing toluene in a Soxhlet extractor and soluble extract was applied to a cyclopentadiene-functionalized Merrifield peptide resin column. The eluent from the column was separated by multi-stage HPLC. The

purity of $Y_2C_2@C_{92}$ was confirmed by HPLC chromatogram, laser-desorption time-of-light (LD-TOF MS) mass spectrometry (Figure 2). A Raman spectroscopic study of this sample describing the carbide tunneling has been reported.[29]

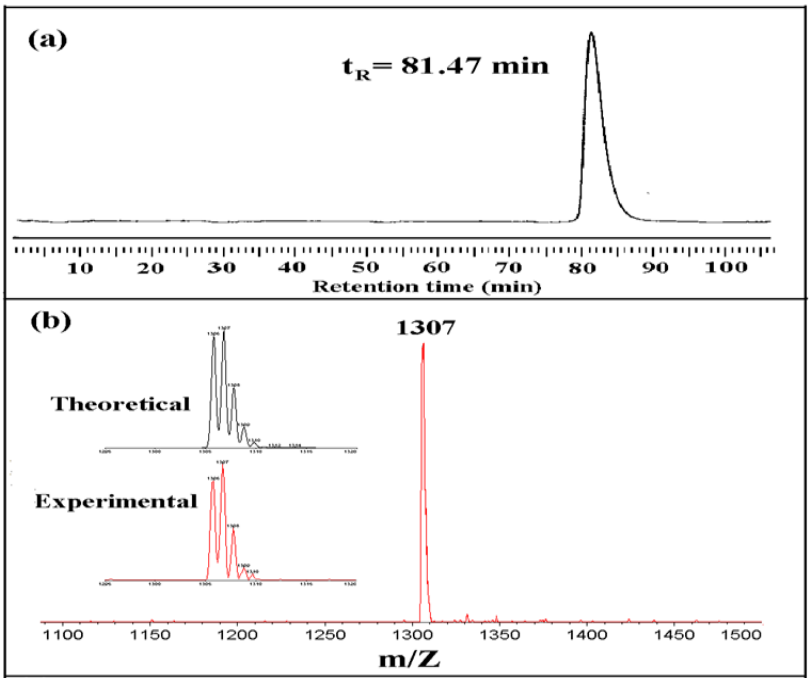

Figure. 2. (a) HPLC of $Y_2C_2@D_3$-C_{92} (a 10 x 250 mm 5PYE column; λ=390 nm; flow rate 2.0 mL/min; toluene as eluent; 25 ℃); (b) LD-TOF mass spectrum of $Y_2C_2@D_3$-C_{92} with positive ionization.

3.2.2 Synthesis and isolation of $Y_2C_2@C_{3v}$-C_{82}, $Y_2C_2@C_s$-C_{82}, and $Y_2C_2@C_{84}$.

The ^{13}C labeled yttrium carbide EMFs were produced in a similar process with a Krätschmer -Huffman generator, with the graphite electrode filled with Y_2O_3 and ^{13}C labeled amorphous carbon powder (99% Cambridge Isotopes). The mass ratio between ^{13}C packed amorphous carbon powder and the graphite rod wall was 1/3. After solvent extraction, the soluble portion of the soot was subject to a mild "stir and filter approach" with

cyclopentadiene-functionalized silica to remove the majority of the empty-cage fullerenes while maintaining a significant portion of the yttrium carbide EMFs.[30] The resulting solution was loaded onto a 5-PBB column for chromatographic separation. The $Y_2C_2@C_s$-C_{82} and $Y_2C_2@C_{3v}$-C_{82} were co-eluted with the $Y_3N@C_{80}$, and the $Y_2C_2@C_{84}$ was co-eluted with $Y_3N@C_{82}$. With further multi-stage isolation on a 5-PYE HPLC column, the $Y_2C_2@C_{3v}$-C_{82}, $Y_2C_2@C_s$-C_{82}, and $Y_2C_2@C_{84}$ were obtained and the corresponding chromatograms of the purified products are shown in Figure 3 (a, c, e). These EMFs are also characterized by LD-TOF mass-spectrometry (b, d, f). To ensure the accuracy of the molecular mass of the ^{13}C enriched peaks in the mass spectra, the well-characterized EMF $Sc_3N@C_{80}$ (m/z=1109) was used as an internal mass calibrator in $Y_2C_2@C_s$-C_{82}, as shown in Figure 3d. The molecular peak in the mass spectrum is broadened and shifted to higher mass by 7-8 mass units (1193 rather than 1186 for Y_2C_{84} and 1218 instead of 1210 for Y_2C_{86}), suggesting a ~9% ^{13}C enrichment.

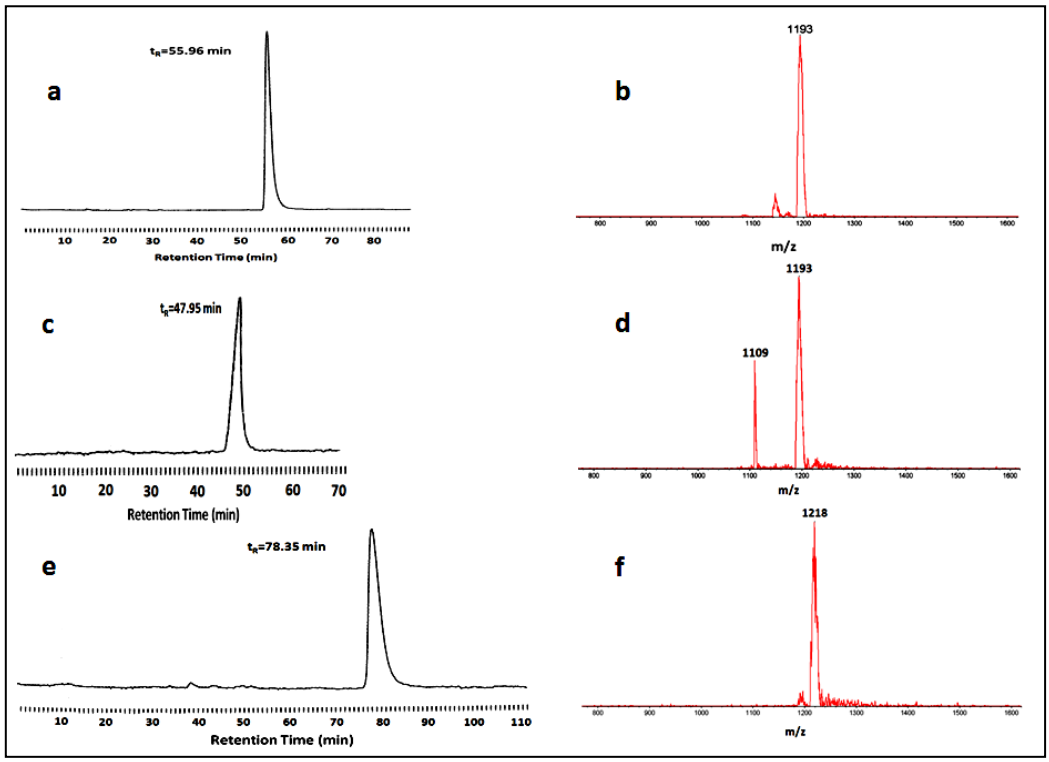

Figure. 3. (a) HPLC of $Y_2C_2@C_{3v}$-C_{82} (a 10 x 250 mm 5PYE column; λ=390 nm; flow rate 2.0 mL/min; toluene as eluent; 25 ℃). (b) LD-TOF mass spectra of ^{13}C enriched $Y_2C_2@C_{3v}$-C_{82} with positive ionization. The two smaller peaks are M-24 and M-48, respectively, resulted from the loss of C_2 units in the ionization process. (c) HPLC of $Y_2C_2@C_s$-C_{82}. (d) LD-TOF mass spectra of ^{13}C enriched $Y_2C_2@C_{3v}$-C_{82} with positive ionization. $Sc_3N@C_{80}$ (m/z=1109) is an internal standard calibrator. (e) HPLC Chromatogram of $Y_2C_2@C_{84}$. (f) LD-TOF mass spectra of ^{13}C enriched $Y_2C_2@C_{84}$ with positive ionization. The smaller peak M-24 is resulted from the loss of a C_2 unit.

3.2.3 ^{13}C NMR sample preparation and spectroscopy.

EMF samples were dissolved in 90% CS_2/10% CD_3COCD_3 (v/v) and approximately 8-10 mg $Cr(acac)_2$ was added as a relaxation agents. The ^{13}C NMR spectra were obtained utilizing a Bruker 800 MHz (Hollings Marine Laboratory facility) at 298K with 4s delay time between

pulses, by Dr Daniel Bearden from the Hollings Marines Laboratory. Because of very limited sample quantity of 0.1-1 mg, each spectrum required 2 to 5 days scan time.

3.3 ^{13}C NMR Studies of $Y_2C_2@D_3(85)$-C_{92}, $Y_2C_2@C_{3v}$-C_{82}, $Y_2C_2@C_s$-C_{82}, and $Y_2C_2@C_{84}$.

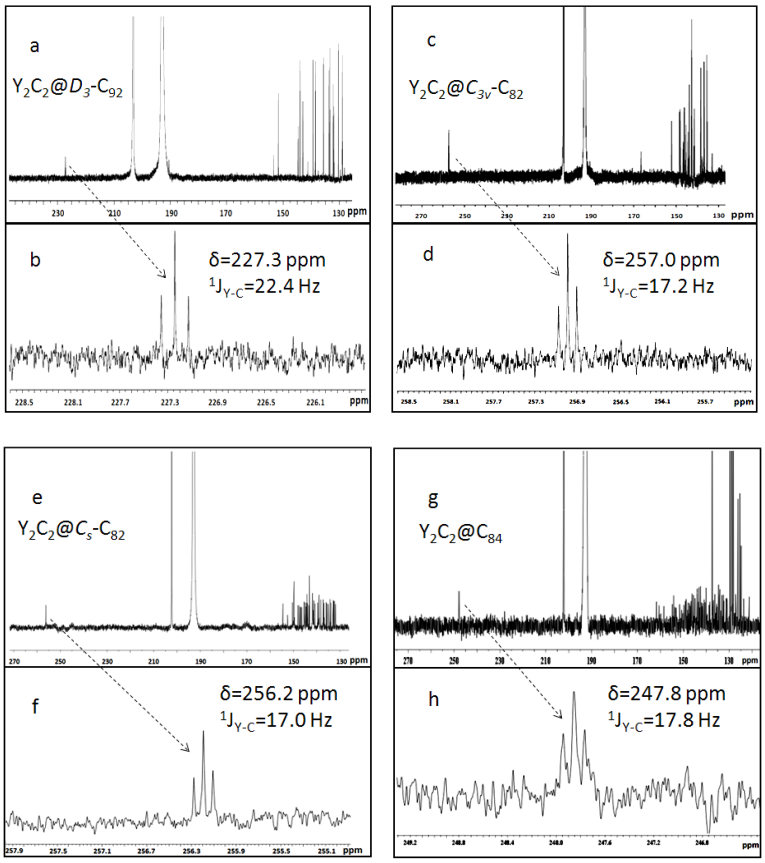

Figure 4. (a) 200 MHz ^{13}C NMR spectrum of $Y_2C_2@D_3$-C_{92}. (b) Expanded region of (a) from 225.8 to 228.6 ppm showing the signal from the cluster. (c) 200 MHz ^{13}C NMR spectrum of $Y_2C_2@C_{3v}$-C_{82}. (d) Expanded region of (c) from 255.4 to 258.6 ppm showing the signal from the cluster. (e) 200 MHz ^{13}C NMR spectrum of $Y_2C_2@C_s$-C_{82}. (f) Expanded region of (e) from 255.1 to 257.9 ppm showing the signal from the cluster. (g) 200 MHz ^{13}C NMR spectrum of $Y_2C_2@C_{84}$. The tall peaks in the aromatic region are the result of residual solvents (toluene and o-xylene). (h) Expanded region of (g) from 246.4 to 249.2 ppm showing the signal from the cluster.

The 200 MHz ^{13}C NMR spectrum of $Y_2C_2@C_{92}$ (Figure 4a, aromatic region expanded in Figure 5) consists of a series of 15 distinct lines between δ =128 to 152 ppm. There are 1 double intensity, 13 full intensity and one 1/3 intensity signals, indicating a 15x6, 1x2 (number of NMR lines x relative intensity) pattern which is consistent with the C_{92} cage with D_3 symmetry of $Y_2C_2@D_3(85)$-C_{92}, an analogue to the previously reported $Gd_2C_2@D_3(85)$-C_{92} structure.[22] The DFT computational ^{13}C NMR chemical shift range, 129.47 to 153.15 ppm, is also in good agreement with the range of the experimental spectrum, 128.97 to 151.69 ppm *vide infra*. One deshielded triplet signal was detected at a chemical shift of δ = 227.3 ppm which originates from the carbide in $Y_2C_2@D_3(85)$-C_{92}. Of special interest is the observed sharp triplet (1:2:1 pattern) signals which is consistent with an yttrium-carbide scalar coupling ($^1J_{YC}$= 22.4 Hz) between a carbide atom and two chemically equivalent yttrium atoms. To our best knowledge, this is the first observation of a resolved scalar coupling between encapsulated cluster atoms within an EMF cage.

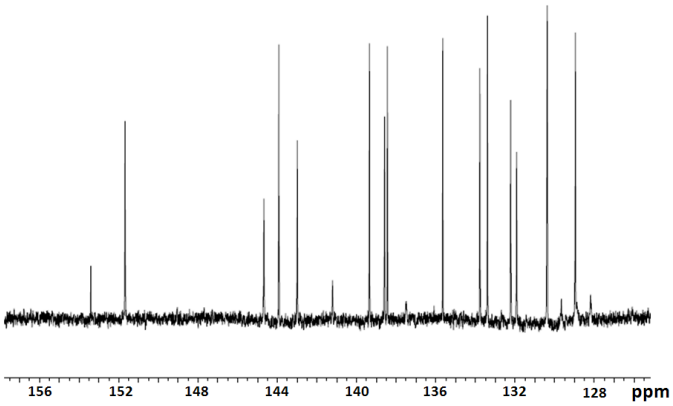

Figure 5. Expansion of the *sp*^{2} Region (127-157 ppm) of the 200 MHz ^{13} C NMR spectrum of $Y_2C_2@D_3(85)$-C_{92}. The chemical shifts are: 151.7, 144. 7, 143.9, 143.0, 141.2 (1/3 intensity), 139.4, 138.6, 138.4, 135.7, 133.8, 133.4, 132.2, 132.0, 130.4 (double intensity), 129.0 ppm.

The ^{13}C NMR spectrum of $Y_2C_2@C_{3v}$-C_{82} exhibits 17 signals in the aromatic region (Figure 4c, aromatic region expanded in Figure 6) and also one highly deshielded signal. The 17 lines consist of 11 full intensity lines (6 carbons), 5 half intensity lines (3 carbons) and 1 one sixth intensity line (1 carbon), confirming the C_{3v} symmetry of the cage.[18] With ^{13}C isotopic labeling, the ^{13}C NMR deshielded triplet signal was observed at a chemical shift of δ = 257.0 ppm confirming that this signal originates from the carbide in $Y_2C_2@C_{3v}$-C_{82}. This shift is only slightly more deshielded than those reported for $Sc_2C_2@C_{3v}$-C_{82} (δ = 253.2 ppm) and $Sc_2C_2@D_{2d}$-C_{84} (δ = 249.0 ppm) with similar fullerene cages.[23] In similar fashion to $Y_2C_2@D_3$-C_{92}, a sharp triplet (1:2:1 pattern) signal is observed. Significantly, the $J_{Y\text{-}C}$ coupling of the cluster in $Y_2C_2@C_{3v}$-C_{82} is 17.2 Hz, which is reduced from the 22.4 Hz of $Y_2C_2@C_{3v}$-C_{92}, suggesting a more compressed cluster conformation of the former yttrium carbide EMF in a smaller cage.

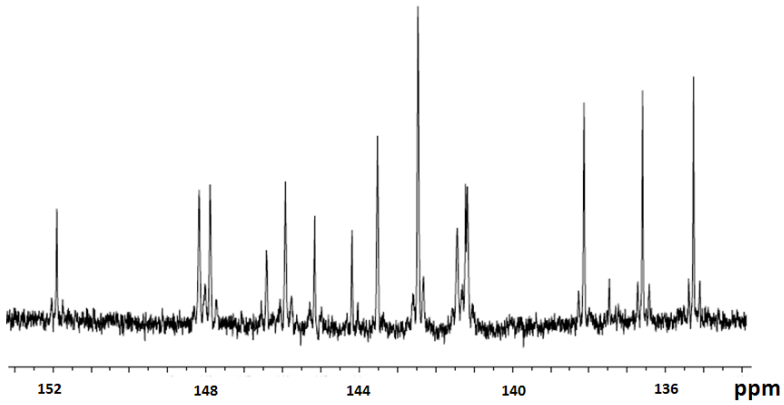

Figure 6. Expansion of the *sp*^{2} Region (134-152 ppm) of the 200 MHz ^{13}C NMR spectrum of $Y_2C_2@C_{3v}(8)$-C_{82}. The chemical shifts are: 151.8, 148.1, 147.8, 146.4, 145.9, 145.1, 144.1, 143.5, 142.4, 141.4, 141.2, 141.1, 138.1, 137.4, 136.5, 135.2 ppm. The smaller peaks are both sides of above listed peaks are ^{13}C satellite peaks.

The ^{13}C NMR spectrum of $Y_2C_2@C_s$-C_{82} shows 44 lines in aromatic region (expanded as Figure 7), which confirms the identity of the molecule in comparison with previously reported results,[18] and one deshielded signal with a chemical shift of 256.2 ppm. The carbide signal shows the same 1:2:1 fashion resulted from the coupling between ^{89}Y and ^{13}C of the cluster (Figure 4f), with $J_{Y\text{-}C}$ coupling being 17.0 Hz. It is important to note that despite the major differences between the cage symmetry of the C_s-C_{82} and C_{3v}-C_{82} cages, the carbide signals from the $(Y_2C_2)^{4+}$ clusters have almost identical chemical shifts and $J_{Y\text{-}C}$ coupling constants (Figure 4d and 4f). This suggests a very similar electronic environment of the $(Y_2C_2)^{4+}$ cluster in these C_{82} cages with very different symmetries.

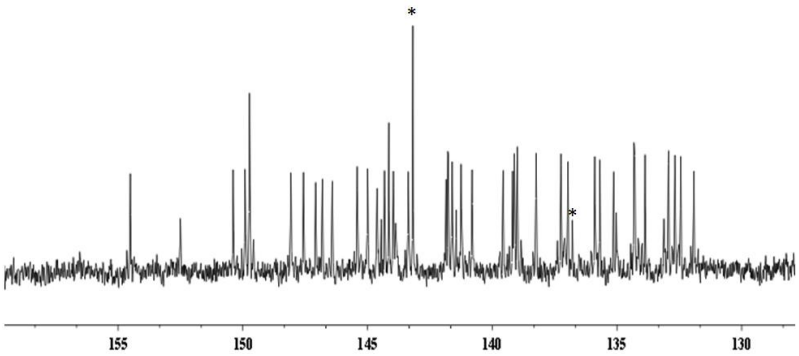

Figure 7. Expansion of the sp^2 Region (130-158 ppm) of the 200 MHz ^{13} C NMR spectrum of $Y_2C_2@C_s(6)$-C_{82}. The chemical shifts are: 154.5, 152.5, 150.4, 149.9, 149.7, 148.1, 147.6, 147.1, 146.8, 146.4, 145.4, 145.0, 144.6, 144.4, 144.3, 144.1, 144.0, 143.9, 143.4, 141.8, 141.8, 141.6, 141.4, 141.2, 140.8, 139.6, 139.2, 139.1, 139.0, 138.2, 137.2, 137.0, 135.9, 135.7, 135.1, 135.0, 134.3, 134.3, 133.9, 133.1, 132.9, 132.7, 132.4, 131.9 ppm. The smaller peaks are both sides of above listed peaks are ^{13}C satellite peaks. The peaks with stars are from $Sc_3N@I_h$-C_{80} which was used as internal standard in mass spectrometry.

The ^{13}C NMR spectrum of $Y_2C_2@C_{84}$ also shows a highly deshielded carbide signal with the coupling between ^{89}Y and ^{13}C resulting in a 1:2:1 pattern (Figure 4h). The chemical shift of this signal is 247.8 ppm, which is slightly more shielded than the signals in both $Y_2C_2@C_{82}$ isomers (256-257 ppm) and much more deshielded than the carbide signal in $Y_2C_2@C_{92}$ (227.3 ppm). In addition, the triplet 1:2:1 pattern is significantly broader in this case and could even possibly suggest a slight inequivalence of the two Y atoms. The $J_{Y\text{-}C}$ coupling of the signal is estimated at ~17.8 Hz, which is higher than those of both $Y_2C_2@C_{82}$ isomers but lower than that of the $Y_2C_2@C_{92}$. The poor signal-to-noise ratio in the aromatic region makes it difficult to assign the symmetry of this C_{84} cage. However, we can estimate at least ~70 separate spectral lines in the aromatic region (expanded as Figure 8). In addition, other lines could overlap the toluene solvent impurities in this spectrum. Moreover, the two relatively deshielded peaks at 161.7 ppm and 160.6 ppm are characteristic of fused pentalene carbons,[31] suggesting this C_{84} cage is most likely an isolated pentagon rule (IPR)-violating cage. In future additional studies will be necessary to identify the actual symmetry of this C_{84} cage.

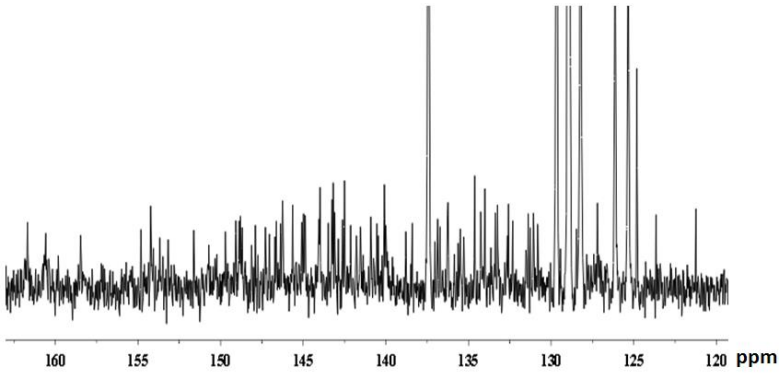

Figure 8. Expansion of the *Sp*^{2} Region (120-162 ppm) of the 200 MHz ^{13} C NMR spectrum of $Y_2C_2@C_{84}$. Due to extensive scan numbers, the residual solvent peaks from

toluene and o-xylene are picked up as the off-scale peaks here. The tall spike at 124.9 ppm was an artificial projection caused by the CS_2 peak. At current signal to noise level it is difficult to assign the cage symmetry.

3.4 DFT Computational Studies

The computational studies were performed by Tim Fuhrer from our group, and this section is written based on my interpretation of the results after discussion with Tim and our advisor, Professor Dorn.

3.4.1 Computational Studies of the $(Y_2C_2)^{4+}$ cluster.

As indicated above, DFT computational studies for the neutral Y_2C_2 molecular cluster support a stable linear structure as illustrated (upper Figure 1A).[28] However, encapsulation of the yttrium carbide cluster involves a charged cluster with transfer of electrons to the fullerene cage. For the charged $(Y_2C_2)^{4+}$ cluster, DFT results also predict a linear structure stable when not encapsulated in a fullerene cage. The DFT computational results predict a carbide ^{13}C NMR chemical shift of 150 ppm and a scalar coupling of $^1J_{YC}$=55.5 Hz. These values compare favorably with the experimental values reported for the organometallic compound $(Cp)_2YC{\equiv}CPh{\bullet}OEt_2$ (147 ppm and 70.9 Hz) and other similar systems in which the yttrium atom is also collinear with the carbide moiety (YC≡C).[32]

3.4.2 Computational Studies of $Y_2C_2@D_5$ *(450)*-C_{100}, $Y_2C_2@D_3$*(85)*-C_{92}, And $Y_2C_2@C_{3v}$*(8)*-C_{82}.

Based on the optimized geometry of the $(Y_2C_2)^{4+}$, large cages should lead to linear clusters

as found above for simpler yttrium carbides. To test this hypothesis, we carried out DFT computations on the $(Y_2C_2)^{4+}$ cluster encapsulated in a *D_5(450)*-C_{100} cage (Y_2C_2@*D_5(450)*-C_{100}). The *D_5(450)*-C_{100} cage can be viewed as an icosahedral C_{80} cage cut in half and a nanotube segment (hexagonal carbons) consisting of 20 carbons added in the middle and it was chosen due to its good stability found in other fullerene and metallofullerene studies.[27] The DFT computational study leads to the optimized stable structure illustrated in Figure 9a. The Y atoms in this structure are not exactly linear with the carbide C_2 vector, but are only slightly displaced from the predicted linear YC≡CY structure (Y-C-C angle is 22 degree). In addition, the computed carbide ^{13}C NMR chemical shift of 142.0 ppm and the scalar coupling of $^1J_{YC}$=57.1 Hz are in good agreement with the prediction for the linear $(Y_2C_2)^{4+}$ cluster *vide supra.* Although Y_2C_2 clusters have not been experimentally studied in cages greater that C_{92}, the current computational study predicts linear Y_2C_2 cluster structures are feasible if the fullerene cage is a relatively large cage of at least 100 carbons or has an unusual shape.

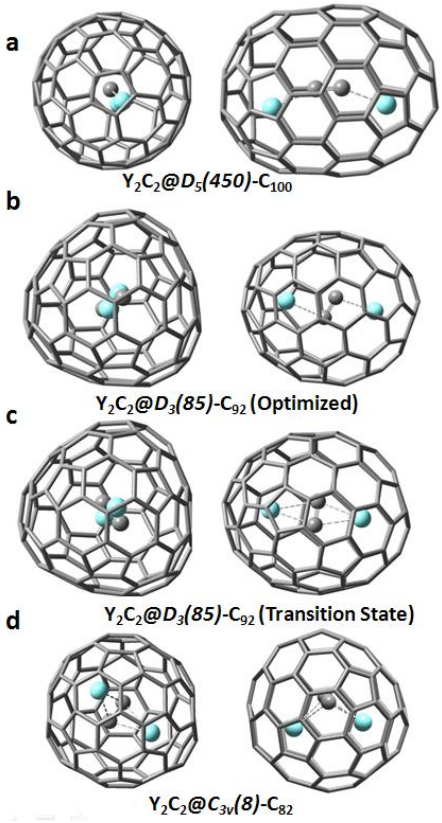

Figure 9. simulated structure of (a) optimized $Y_2C_2@D_5(8)$-C_{100}. (b) Optimized $Y_2C_2@D_3(85)$-C_{92}. (c) Transition state of $Y_2C_2@D_3(85)$-C_{92}. (d) Optimized $Y_2C_2@C_{3v}(450)$-C_{100}.

The DFT calculations for $Y_2C_2@D_3(85)$-C_{92} suggest an optimized stable structure in which the two yttrium atoms are slightly displaced from the C_3 symmetry axis and the carbide vector is nearly orthogonal, but with inequivalent distances from each carbide atom to each yttrium atom (Figure 9b). The transition state (TS) structure of $Y_2C_2@D_3(85)$-C_{92} exhibits an "idealized butterfly shape", where in the C_2 carbide unit is perpendicular to a line between the two metal atoms (Figure 9c). The energy difference between the most stable structure and this butterfly structure is only ~12 kJ/mol, which is consistent with the observed ^{13}C NMR sharp triplet (1:2:1 pattern) for a small $(Y_2C_2)^{4+}$ cluster rotational barrier between these two states

suggesting rapid motional averaging of the carbide atoms about the overall C_3 axis (Figure 10a) on the NMR time scale. However, the total electron surface map (Figure 10b) defines a belt motif reflecting a significant repulsive interaction with the rotational carbide $(C_2)^{-2}$ at the three-fold symmetry 6,6,5 junction site of the two pentagons in this belt motif. This suggests rapid carousel rotational motion of the encapsulated C_2 carbide unit about the overall C_3 axis of the $Y_2C_2@D_3(85)$-C_{92} molecule at ambient temperatures.

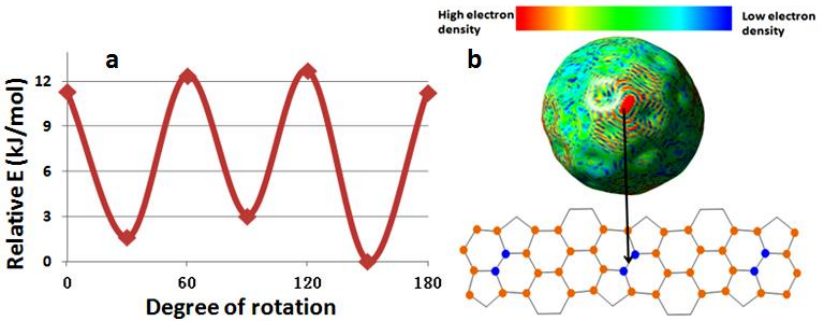

Figure 10. Cluster motion study with DFT computation. (a) Relative energy of different states of the molecule with rotating $(Y_2C_2)^{4+}$ cluster. The energy values are referenced to the most stable structure. (b) Commutated total electron density map of $Y_2C_2@D_3(85)$-C_{92} defining a belt motif with a repulsive interaction between the 5,6,6 junction sites on the cage (blue) and the encapsulated carbide.

In the optimized structure of $Y_2C_2@C_{3v}(8)$-C_{82} (Figure 9d), with two yttrium atoms lying along the C_3 axis, the carbide bond is orthogonal to and considerably displaced from the C_3 axis to form a "butterfly", or bent geometry which is suggested by independent computational study of $M_2C_2@C_{3v}(8)$-C_{82} system[33] and experimental study of $Y_2C_2@C_{3v}(8)$-C_{82}.[34]

3.5 Summary and Discussion of Results

The experimental and computational results are summarized in Figure 11. It is clear that

the $(Y_2C_2)^{4+}$ cluster prefers a linear configuration in the absence of a fullerene cage. However, even in relatively large cages like C_{100} the cluster adopts a cage only slightly distorted from a linear configuration. For an intermediate cage size, $Y_2C_2@D_3$-C_{92}, the cluster is compressed to make the carbide bond nearly orthogonal to the yttrium bond vector and with only a slightly less stable transition state having an "idealized butterfly" shaped cluster. For a small cage as in the $Y_2C_2@C_{3v}$-C_{82} system, even greater compression is present and the $(Y_2C_2)^{4+}$ cluster adopts a definitive butterfly shape.

Molecule	Optimized cluster structure	Average atomic distance in the cluster Y-C/Y-Y/C-C (Å)	C_2 ^{13}C NMR chemical shift (ppm)	$^1J_{Y\text{-}C}$ (Hz)
$(Y_2C_2)^{4+}$		2.92/5.83/1.27	147* (150)	70.9* (55.5)
$Y_2C_2@D_5$-C_{100}		2.89/5.51/1.26	(156)	(57.1)
$Y_2C_2@D_3$-C_{92} (opt)	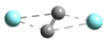	2.53/4.92/1.27	227.3 (229)	22.4 (22.5**)
$Y_2C_2@D_3$-C_{92} (TS)		2.48/4.81/1.27	(288)	(21.6)
$Y_2C_2@C_{84}$	--	--	247.8	17.8
$Y_2C_2@C_{3v}$-C_{82}		2.43/3.74/1.27	257.0 (288)	17.2 (18.3)
$Y_2C_2@C_s$-C_{82}	--	--	256.2	17.0

Numbers in parentheses are computational results.

* These values represent the experimental result of $(Cp)_2YC{\equiv}CPh{\bullet}OEt_2$
**This number represents average value of the scalar coupling constants between Y atom and carbon 1 (40.6 Hz) and carbon 2 (4.4 Hz)

Figure 11 Key results from NMR experiments and DFT calculations.

It is also clear that the ^{13}C NMR chemical shift and scalar $^1J_{YC}$ coupling parameters provide a very sensitive probe of the degree of NF compression of $(Y_2C_2)^{4+}$ cluster, as illustrated in the right two columns in Figure 11. The ^{13}C NMR results for the carbide signal exhibit a significant deshielding, which increases even more upon NF compression, as the chemical shift increases by over 100 ppm from about 150 ppm for the stretched (nearly linear) clusters (no cage or in D_5-C_{100}) to over 250 ppm for the compressed clusters (C_{3v}-C_{82} and C_s-C_{82}). At

the same time, the scalar $^{1}J_{YC}$ decreases upon NF compression from over 50 Hz for the nearly linear clusters to about 17 Hz found in the compressed clusters in smaller cages (C_{3v}-C_{82} and C_s-C_{82}).

In addition, it can be concluded that the cage size plays a decisive role in determining the shape of the cluster structure. For example, $Y_2C_2@C_{3v}$-C_{82} represents a highly symmetry case with only 17 NMR signals for 82 aromatic carbon atoms, while $Y_2C_2@C_s$-C_{82} represents the low-symmetry case with 44 NMR signals for the 82 aromatic carbon atoms. Despite these major differences in cage symmetry (C_{3v} versus C_s), they have very similar chemical shifts (257.0 ppm vs 256.2 ppm) and $^{1}J_{YC}$ couplings (17.2 ppm vs 17.0 ppm). Also, the $Y_2C_2@C_{84}$ shows a carbide signal with 247.8 ppm chemical shift and $^{1}J_{YC}$ =18.0 Hz which both agree with the NF compression trend very well, indicating the unique pentalene motif only has a limited influence on the cluster structure and NMR parameters. These results suggest that cage symmetry for a given cage size (C_{82}) plays only a minor role in influencing the ^{13}C NMR spectral parameters and corresponding shape of the $(Y_2C_2)^{4+}$ cluster. In summary, the more important factor in dictating the structure of the encapsulated $(Y_2C_2)^{4+}$ cluster is the carbon cage size. However, it is possible that for significantly larger EMFs the cage structure may play a more important role.

Also summarized in Figure 11, the atomic distances within the $(Y_2C_2)^{4+}$ cluster provided by DFT computation suggests that the cluster atoms are forced closer with increasing compression, as indicated by the decrease of both Y-C distance (average of Y-C1 and Y-C2) and Y-Y distance. It should be noted that the C-C distance remains almost almost unchanged

within the bond length uncertainty limits. It is also interesting to note that the alteration in cluster atomic distances under NF compression exhibits the same trend as the lattice atomic distances for the yttrium carbide Y_2C_3 system under MP compression,[3] as shown in Figure 12. In both systems, the Y-C and Y-Y distances decrease with increasing compression, either from smaller fullerene cage or a higher external pressure. Moreover, the C-C distances remain nearly constant in both cases. Qualitatively, decreasing cage size by ~18 carbons within the investigated region (~C_{82}-C_{100}) in NF compression is nearly equivalent to increasing the external pressure from 0 to 50 Gpa in MP compression based on the changes in Y-C interatomic distance. The Y-C distance under upper limit of pressure ~50 GPa is also reflective of the experimental limit to date for the smallest cages (~C_{80}, see Figure 1) that can potentially be isolated. It is worth mentioning that such contraction upon MP compression is not limited to the yttrium carbide (Y_2C_3), but has also been observed in lanthanum carbide systems as well.[35]

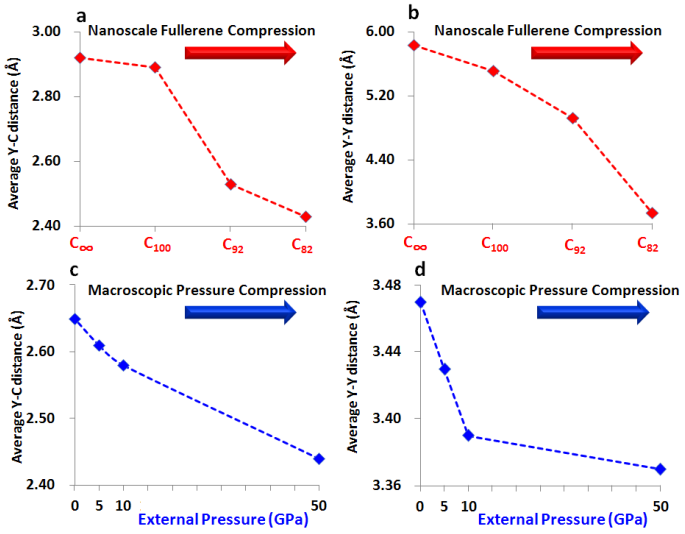

Figure 12. The change of interatomic distances upon on compression. Red lines and points denote the data obtained from NFC (data source Figure 7, C_∞ represents the calculated interatomic distances for $[Y_2C_2]^{4+}$ cluster), and blue lines and points denote the data obtained from MPC (data source Ref. 3 and transferred as in Figure S13 in SI). Y-C distances are average values of corresponding Y-C1, Y-C2 and Y-C3 distance in the lattice. Y-Y distances are average values of corresponding Y-Y1 and Y-Y2 distance in the lattice). (a) Y-C distances in fullerene cages. (b) Y-Y distances in fullerene cages. (c) Y-C distances in superconducting materials. (d) Y-Y distances in superconducting materials.

3.6 Conclusion

In this chapter, I described the synthesis, purification and characterization of a di-yttrium metallofullerene family, four yttrium carbide endohedral metallofullerenes (EMFs), $Y_2C_2@D_3(85)$-C_{92}, $Y_2C_2@C_{3v}$-C_{82}, $Y_2C_2@C_s$-C_{82}, and $Y_2C_2@C_{84}$. We have investigated the $(Y_2C_2)^{4+}$ cluster structural features in this EMF family by ^{13}C NMR and DFT computational approaches. With the chemical shift and first-time observation of metal-carbide $^1J_{YC}$ coupling of the $(Y_2C_2)^{4+}$ cluster, we have probed the structural change of the endohedral clusters under

the influence of NF compression. The ^{13}C NMR chemical shift and scalar $^{1}J_{YC}$ coupling parameters provide a very sensitive measure of the structural changes of the $(Y_2C_2)^{4+}$ cluster with respect to changes in the size of the carbon cage size (C_{82}-C_{100}). In contrast with changes in the size of the cage, the results suggest only a minor role for changes in cage symmetry for a given cage size (C_{82}) as reflected by influences on the ^{13}C NMR spectral parameters. These results confirm the hypothesis that influence of nanoscale fullerene compression (NFC) on interatomic distances on yttrium carbide clusters is consistent with the influence of macroscopic pressure compression (MPC). With the support of DFT calculation results, one can conclude that upon NFC the cluster changed from a stretched linear shape to a compressed "butterfly shape", with increasing chemical shift values, decreasing $^{1}J_{Y\text{-}C}$ coupling constants and interatomic distances found for the clusters. The crystal structural parameters of a previously reported metal carbide Y_2C_3 are directly compared to the $(Y_2C_2)^{4+}$ cluster in the current metallofullerene study illustrating the influence of nanoscale FC when compared with the effects of macroscopic PC. In the future, the possibility of using EMFs as isolated ideal model clusters to mimic other metal lattice clusters under ultra-high pressure could be important metal carbide materials research.

REFERENCE

(1) Kurotobi, K.; Murata, Y.: A Single Molecule of Water Encapsulated in Fullerene C_{60}. *Science* **2011**, *333*, 613-616.

(2) Nakane, T.; Naka, T.; Kito, H.; Wada, T.; Matsushita, A.; Kumakura, H.; Mochiku, T.: The Effect of Pressure on the T_c Value of Y_2C_3 Compounds. *Physica C* **2005**, *426*, 492-496.

(3) Yu, C.; Liu, J. Y.; Lu, H.; Li, P. L.; Fan, R. Z.; Xiao, J. Y.: First-Principles Investigation Of Pressure-Induced Changes in Structural and Electronic Properties of Y_2C_3 Superconductor. *Solid State Commun.* **2007**, *142*, 536-540.

(4) Amano, G.; Akutagawa, S.; Muranaka, T.; Zenitani, Y.; Akimitsu, J.: Superconductivity at 18 K in Yttrium Sesquicarbide System, Y_2C_3. *J. Phys. Soc. Jpn.* **2004**, *73*, 530-532.

(5) Chai, Y.; Guo, T.; Jin, C. M.; Haufler, R. E.; Chibante, L. P. F.; Fure, J.; Wang, L. H.; Alford, J. M.; Smalley, R. E.: Fullerenes with Metals Inside. *J. Phys. Chem-US* **1991**, *95*, 7564-7568.

(6) Shinohara, H.; Sato, H.; Saito, Y.; Ohkohchi, M.; Ando, Y.: Mass Spectroscopic and ESR Characterization of Soluble Yttrium-containing Metallofullerenes YC_{82} and Y_2C_{82}. *J. Phys. Chem-Us* **1992**, *96*, 3571-3573.

(7) Wakahara, T.; Okubo, S.; Kondo, M.; Maeda, Y.; Akasaka, T.; Waelchli, M.; Kako, M.; Kobayashi, K.; Nagase, S.; Kato, T.; Yamamoto, K.; Gao, X.; Van Caemelbecke, E.; Kadish, K. M.: Ionization And Structural Determination of The Major Isomer of $Pr@C_{82}$. *Chem. Phys. Lett.* **2002**, *360*, 235-239.

(8) Wakahara, T.; Kobayashi, J.; Yamada, M.; Maeda, Y.; Tsuchiya, T.; Okamura, M.; Akasaka, T.; Waelchli, M.; Kobayashi, K.; Nagase, S.; Kato, T.; Kako, M.; Yamamoto, K.; Kadish, K. M.: Characterization of $Ce@C_{82}$ and Its Anion. *J. Am. Chem. Soc.* **2004**, *126*, 4883-4887.

(9) Akasaka, T.; Kono, T.; Takematsu, Y.; Nikawa, H.; Nakahodo, T.; Wakahara, T.; Ishitsuka, M. O.; Tsuchiya, T.; Maeda, Y.; Liu, M. T. H.; Yoza, K.; Kato, T.; Yamamoto, K.; Mizorogi, N.; Slanina, Z.; Nagase, S.: Does $Gd@C_{82}$ Have an Anomalous Endohedral Structure? Synthesis and Single Crystal X-Ray Structure of the Carbene Adduct. *J. Am. Chem. Soc.* **2008**, *130*, 12840-12841.

(10) Wang, C. R.; Kai, T.; Tomiyama, T.; Yoshida, T.; Kobayashi, Y.; Nishibori, E.; Takata, M.; Sakata, M.; Shinohara, H.: Materials science - C_{66} Fullerene Encaging a Scandium Dimer. *Nature* **2000**, *408*, 426-427.

(11) Kato, H.; Taninaka, A.; Sugai, T.; Shinohara, H.: Structure of a Missing-caged Metallofullerene: $La_2@C_{72}$. *J. Am. Chem. Soc.* **2003**, *125*, 7782-7783.

(12) Lu, X.; Nikawa, H.; Nakahodo, T.; Tsuchiya, T.; Ishitsuka, M. O.; Maeda, Y.; Akasaka, T.; Toki, M.; Sawa, H.; Slanina, Z.; Mizorogi, N.; Nagase, S.: Chemical Understanding of a Non-IPR Metallofullerene: Stabilization Of Encaged Metals on Fused-pentagon Bonds in $La_2@C_{72}$. *J. Am. Chem. Soc.* **2008**, *130*, 9129-9136.

(13) Cao, B.; Nikawa, H.; Nakahodo, T.; Tsuchiya, T.; Maeda, Y.; Akasaka, T.; Sawa, H.; Slanina, Z.; Mizorogi, N.; Nagase, S.: Addition of adamantylidene to $La_2@C_{78}$: Isolation and single-crystal X-ray structural determination of the monoadducts. *J. Am. Chem. Soc.* **2008**, *130*, 983-989.

(14) Yamada, M.; Wakahara, T.; Tsuchiya, T.; Maeda, Y.; Akasaka, T.; Mizorogi, N.; Nagase, S.: Spectroscopic and theoretical study of endohedral dimetallofullerene having a Non-IPR fullerene cage: $Ce_2@C_{72}$. *J. Phys. Chem. A* **2008**, *112*, 7627-7631.

(15) Stevenson, S.; Rice, G.; Glass, T.; Harich, K.; Cromer, F.; Jordan, M. R.; Craft, J.; Hadju, E.; Bible, R.; Olmstead, M. M.; Maitra, K.; Fisher, A. J.; Balch, A. L.; Dorn, H. C.: Small-bandgap Endohedral Metallofullerenes In High Yield And Purity. *Nature* **1999**, *401*, 55-57.

(16) Dunsch, L.; Yang, S.: Metal Nitride Cluster Fullerenes: Their Current State And Future Prospects. *Small* **2007**, *3*, 1298-1320.

(17) Wang, C. R.; Kai, T.; Tomiyama, T.; Yoshida, T.; Kobayashi, Y.; Nishibori, E.; Takata, M.; Sakata, M.; Shinohara, H.: A Scandium Carbide Endohedral Metallofullerene: $Sc_2C_2@C_{84}$. *Angew. Chem. Int. Ed.* **2001**, *40*, 397-399.

(18) Inoue, T.; Tomiyama, T.; Sugai, T.; Okazaki, T.; Suematsu, T.; Fujii, N.; Utsumi, H.; Nojima, K.; Shinohara, H.: Trapping a C_2 Radical in Endohedral Metallofullerenes: Synthesis and Structures of $(Y_2C_2)@C_{82}$ (Isomers I, II, and III). *J. Phys. Chem. B* **2004**, *108*, 7573-7579.

(19) Tan, K.; Lu, X.: Ti_2C_{80} is More Likely a Titanium Carbide Endohedral Metallofullerene $Ti_2C_2@C_{78}$. *Chem. Comm.* **2005**, 4444-4446.

(20) Liduka, Y.; Wakahara, T.; Nakahodo, T.; Tsuchiya, T.; Sakuraba, A.; Maeda, Y.; Akasaka, T.; Yoza, K.; Horn, E.; Kato, T.; Liu, M. T. H.; Mizorogi, N.; Kobayashi, K.; Nagase, S.: Structural Determination of Metallofuilerene Sc_3C_{82} Revisited: A Surprising Finding. *J. Am. Chem. Soc.***2005**, *127*, 12500-12501.

(21) Shi, Z. Q.; Wu, X.; Wang, C. R.; Lu, X.; Shinohara, H.: Isolation and Characterization of $Sc_2C_2@C_{68}$: A Metal-Carbide Endofullerene with a Non-IPR Carbon Cage. *Angew.Chem. Int. Ed.* **2006**, *45*, 2107-2111.

(22) Yang, H.; Lu, C.; Liu, Z.; Jin, H.; Che, Y.; Olmstead, M. M.; Balch, A. L.: Detection of a Family of Gadolinium-Containing Endohedral Fullerenes and the Isolation and Crystallographic Characterization of One Member as a Metal-Carbide Encapsulated inside a Large Fullerene Cage. *J. Am. Chem. Soc.* **2008**, *130*, 17296-17300.

(23) Yamazaki, Y.; Nakajima, K.; Wakahara, T.; Tsuchiya, T.; Ishitsuka, M. O.; Maeda, Y.; Akasaka, T.; Waelchli, M.; Mizorogi, N.; Nagase, S.: Observation of ^{13}C NMR Chemical Shifts of Metal Carbides Encapsulated in Fullerenes: $Sc_2C_2@C_{82}$, $Sc_2C_2@C_{84}$, and $Sc_3C_2@C_{80}$. *Angew. Chem. Int. Ed.* **2008**, *47*, 7905-7908.

(24) Kurihara, H.; Lu, X.; Iiduka, Y.; Mizorogi, N.; Slanina, Z.; Tsuchiya, T.; Akasaka, T.; Nagase, S.: $Sc_2C_2@C_{80}$ Rather than $Sc_2@C_{82}$: Templated Formation of Unexpected $C_{2v}(5)$-C_{80} and Temperature-Dependent Dynamic Motion of Internal Sc_2C_2 Cluster. *J. Am. Chem. Soc.* **2011**, *133*, 2382-2385.

(25) Kurihara, H.; Lu, X.; Iiduka, Y.; Nikawa, H.; Hachiya, M.; Mizorogi, N.; Slanina, Z.; Tsuchiya, T.; Nagase, S.; Akasaka, T.: X-ray Structures of $Sc_2C_2@C_{2n}$ (n = 40–42): In-Depth Understanding of the Core–Shell Interplay in Carbide Cluster Metallofullerenes. *Inorg. Chem.* **2011**, *51*, 746-750.

(26) Iiduka, Y.; Wakahara, T.; Nakajima, K.; Nakahodo, T.; Tsuchiya, T.; Maeda, Y.; Akasaka, T.; Yoza, K.; Liu, M. T. H.; Mizorogi, N.; Nagase, S.: Experimental and Theoretical Studies Of The Scandium Carbide Endohedral Metallofullerene $Sc_2C_2@C_{82}$ and Its Carbene Derivative. *Angew. Chem. Int. Ed.* **2007**, *46*, 5562-5564.

(27) Yang, T.; Zhao, X.; Nagase, S.: Di-Lanthanide Encapsulated Into Large Fullerene C_{100}: a DFT Survey. *Phys. Chem. Chem. Phys.* **2011**, *13*, 5034-5037.

(28) Roszak, S.; Balasubramanian, K.: Structural and Thermodynamic Properties of Diyttrium Carbides Y_2C_n (n=2-8): A theoretical study. *J. Phys. Chem. A* **1998**, *102*, 6004-6009.

(29) Burke, B. G.; Chan, J.; Williams, K. A.; Fuhrer, T.; Fu, W.; Dorn, H. C.; Puretzky, A. A.; Geohegan, D. B.: Vibrational Spectrum of the Endohedral $Y_2C_2@C_{92}$ Fullerene by Raman Spectroscopy: Evidence for Tunneling of the Diatomic C_2 Molecule. *Phys. Rev. B* **2011**, *83*.

(30) Stevenson, S.; Harich, K.; Yu, H.; Stephen, R. R.; Heaps, D.; Coumbe, C.; Phillips, J. P.: Nonchromatographic "stir and filter approach" (SAFA) for isolating $Sc_3N@C_{80}$ metallofullerenes. *J. Am. Chem. Soc.* **2006**, *128*, 8829-8835.

(31) Fu, W.; Xu, L.; Azurmendi, H.; Ge, J.; Fuhrer, T.; Zuo, T.; Reid, J.; Shu, C.; Harich, K.; Dorn, H. C.: ^{89}Y and ^{13}C NMR Cluster and Carbon Cage Studies of an Yttrium Metallofullerene Family, $Y_3N@C_{2n}$ (n=40-43). *J. Am. Chem. Soc.* **2009**, *131*, 11762-11769.

(32) Denhaan, K. H.; Wielstra, Y.; Teuben, J. H.: Reactions of Yttrium Carbon Bonds with Active Hydrogen-containing Molecules - a Useful Synthetic Method for Permethylyttrocene Derivatives. *Organometallics* **1987**, *6*, 2053-2060.

(33) Valencia, R.; Rodriguez-Fortea, A.; Poblet, J. M.: Understanding the Stabilization of Metal Carbide Endohedral Fullerenes $M_2C_2@C_{82}$ and Related Systems. *J. Phys. Chem. A* **2008**, *112*, 4550-4555.

(34) Nishibori, E.; Ishihara, M.; Takata, M.; Sakata, M.; Ito, Y.; Inoue, T.; Shinohara, H.: Bent $(Metal)_2C_2$ Clusters Encapsulated in $(Sc_2C_2)@C_{82}$(III) and $(Y_2C_2)@C_{82}$(III) metallofullerenes. *Chem. Phys. Lett.* **2006**, *433*, 120-124.

(35) Wang, X.; Loa, I.; Syassen, K.; Kremer, R. K.; Simon, A.; Hanfland, M.; Ahn, K.: Structural Properties of the Sesquicarbide Superconductor La_2C_3 at High Pressure. *Phys. Rev. B* **2005**, *72*.

Chapter 4 Enhanced Dipole Moments in Trimetallic Nitride Template Endohedral Metallofullerenes with the Pentalene Motif

This chapter is adopted from a manuscript published on *Journal of the American Chemical Society* with appropriate modifications under the permission of the American Chemical Society. Full text of the published manuscript, entitled "*Enhanced dipole moments in trimetallic nitride template endehedral metallofullerenes with the pentalene motif*", by Jianyuan Zhang, Daniel W. Bearden, Tim Fuhrer, Liaosa Xu, Wujun Fu, Tianming Zuo and Harry C. Dorn, can be obtained at http://pubs.acs.org/doi/pdf/10.1021/ja312045t.

4.1 Introduction

As advanced by Kroto, the isolated pentagon rule (IPR) states that there is a significant energy penalty for pentagons fused together on fullerene cages.[1] Although this seminal predictive tool was intended for "pristine" empty-cage fullerenes, the rule has been ostensibly extended to endohedral metallofullerenes (EMFs). The first EMFs with fused pentagons (pentalenes) were independently reported by Shinohara et al.[2] and Dorn et al.[3] for the molecules $Sc_2@C_{66}$ and $Sc_3N@C_{68}$, respectively, in 2000. Since then, the pentalene group has been found in almost all major families of EMFs, including monometallic EMFs,[4,5] dimetallic EMFs,[2,4,6] metal carbide fullerenes,[7] metal sulfide fullerenes,[8,9] and trimetallic nitride template (TNT) EMFs (metal nitride fullerenes),[3,10-18] which contribute most to pentalene-containing EMFs. To date, the structurally investigated TNT EMFs have adopted fullerene cages of D_3(6140)-C_{68},[3] C_{2v}(7854)-C_{70},[12] C_s(17490)-C_{76},[19] D_{3h}(5)-C_{78},[20] C_2(22010)-C_{78},[17] I_h(7)-C_{80},[21] D_{5h}(6)-C_{80},[22] C_s(39663)-C_{82},[15] C_s(51365)-C_{84},[10] D_3(19)-C_{86},[22] and D_2(35)-C_{88}.[22] On this list, the D_3-C_{68}, C_{2v}-C_{70}, C_s-C_{76}, C_2-C_{78}, C_s-C_{82}, and C_s-C_{84} isomers contain the pentalene groups.

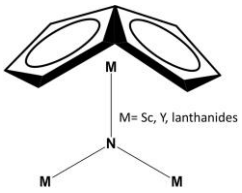

Figure 1. Fused pentagon motif and the trimetallic nitride cluster in pentalene-containing TNT EMFs.

Although there is a significant energy penalty for the anti-aromatic 8 π-electron pentalene motif in empty-cage fullerenes, electron transfer from a metal to the pentalene nearby, creating a localized Hückel-aromatic system, can stabilize EMFs (Figure 1).[23] This reasoning is supported by multiple single crystal x-ray studies where a metal ion is associated with a pentalene site with localized negative charge.[8,10,14,15,17,24] In this chapter, I present evidence for significant dipole moments (~1D) for those members of the $Y_3N@C_{2n}$ (n=39-44) family with the pentalene motif**.** In addition, we predict significant dipole moments for other members of the $M_3N@C_{2n}$ family that contain an M-N bond oriented toward a pentalene motif. We also present the first ^{13}C NMR result for a member of the $M_3N@C_2$-C_{78} system that contains two pentalenes in a relatively small cage (C_{78}).

The yttrium nitride cluster forms a family of TNT EMFs, $Y_3N@C_{2n}$ with n=39-44,[16,25] which is a common range for many other metals, including Gd, Tb and Tm. The C_2-C_{78} cage for $M_3N@C_{78}$ was initially proposed by Dunsch and co-workers.[13] Although limited sample quantities of $Tm_3N@C_{78}$ and $Dy_3N@C_{78}$ hampered this experimental structural study, their remarkable density functional theory (DFT) computations for $Y_3N@C_{78}$ predicted the C_2(22010)-C_{78} cage out of 24109 possibilities as the most stable cage for larger metal $M_3N@C_{78}$ systems. In 2009, the first unambiguous structural study of this family was reported by Balch and coworkers with the single-crystal of $Gd_3N@C_2$(22010)-C_{78}.[17] In this study, the striking

differences between the UV-vis spectra for the $Gd_3N@C_2(22010)$-C_{78} and that for the $Sc_3N@D_{3h}(5)$-C_{78} was also reported to illustrate the importance of UV-vis data for establishing cage isomer features.[18] Wang and coworkers isolated $Y_3N@C_{78}$ and assigned it the $C_2(22010)$ cage based on spectral similarities to $Dy_3N@C_2$-C_{78} and $Gd_3N@C_2$-C_{78}.[18]

4.2 Synthesis and identification of the $Y_3N@C_{78}$ sample

I prepared a ^{13}C-enriched sample of $Y_3N@C_{78}$ as described in Chapter 2 and Chapter 3. The $Y_3N@C_{78}$ was isolated from the fraction 2 as defined in Chapter 2. The final HPLC purification process and the characterization of the purified product are shown in Figure 2.

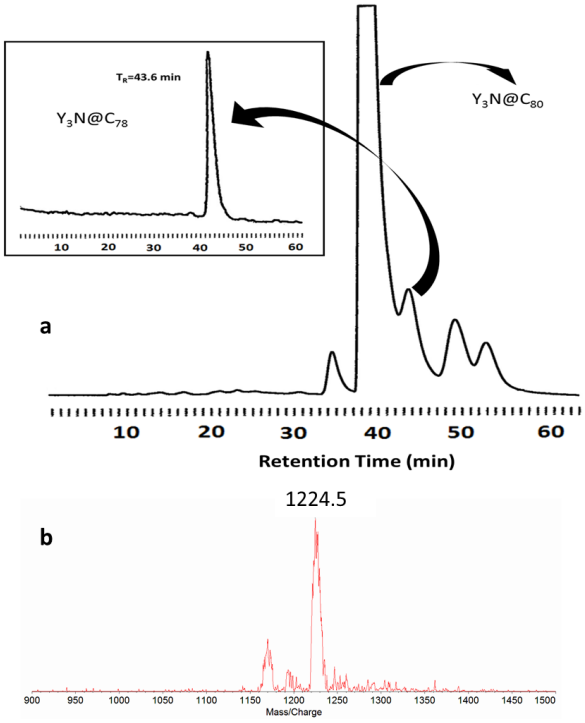

Figure 2. HPLC and mass-spectral characterization of the $Y_3N@C_{78}$. a) HPLC stage leading to the isolation of $Y_3N@C_{78}$ (toluene elution at 2 mL/min, 298K, on 5-PYE column).

Inset: Chromatogram of purified $Y_3N@C_{78}$ solution re-injected to 5-PYE column. b) Laser-desorption time-of-flight (LD-TOF) mass spectrometry of $Y_3N@C_{78}$. Note that the molecular ion peak shifted higher to an m/z of 1224.5 instead of 1217 due to the ~9% ^{13}C enrichment. The small peak coming out of noise at 1170 is due to a very little amount of Y_2C_{82} (original molecular mass 1162, about 1170 after ^{13}C enrichment) that is not detectable by either HPLC or NMR but sensitive to mass spectrometry.

With improved UV-vis peak resolution relative the previous $Y_3N@C_{78}$ report, the UV-vis absorptive features of the $Y_3N@C_{78}$ are almost identical to those previously reported $M_3N@C_2(22010)\text{-}C_{78}$ molecules (M=Dy, Gd, Y) which confirms the same $C_2(22010)\text{-}C_{78}$ cage for $Y_3N@C_{78}$ in the current study.[14,18,19]

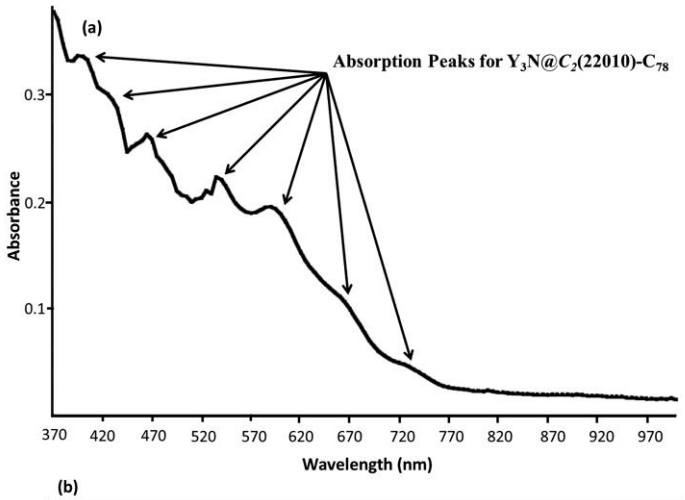

(b)

$M_3N@C_2$ (22010)-C_{78}	UV-vis absorption peaks (nm)
M=Dy[14]	410*, 460*, 560*, 600*, 670*, 730*
M=Gd[17]	410*, 460*, 550*, 590*, 670*, 730*
M=Y[18]	400†, 590†, 670†
M=Y (current study)	400, 420, 460, 540, 590, 670, 730

* These values are careful estimates obtained from corresponding references.[14,17]
† These values are reported by the authors in the corresponding reference.[18]

Figure 3. a) UV-vis spectrum of the $Y_3N@C_2\text{-}C_{78}$ in toluene with absorption peaks pointed. b) absorption peak summary of $M_3N@C_2(22010)\text{-}C_{78}$ (M=Dy, Gd, Y).

4.3 ^{13}C NMR characterization of the $Y_3N@C_{78}$

The ^{13}C NMR spectrum for the ^{13}C-enriched $Y_3N@C_{78}$ is shown in Figure 3a. There are a total of 39 lines with approximately the same height suggesting a 39*2 pattern, with two highly deshielded peaks at 170.0 and 162.9 ppm, corresponding to the four carbon atoms on the [5,5,6] junction found only in pentalene-containing fullerene cages. In addition, there are 26 peaks corresponding to 52 carbon atoms on the [5,6,6] junctions and 11 peaks corresponding to 22 carbon atoms on the [6,6,6] junctions. The ^{13}C NMR spectrum is in agreement with the structural prediction for $Y_3N@C_{78}$[13] as well as the crystal study of $Gd_3N@C_{78}$,[17] suggesting the cage structure of $Y_3N@C_{78}$ is C_2(22010)-C_{78}. The smaller C_{78} cage is distorted by the two pentalene motifs that contribute to the deshielded signals from the four carbon atoms fusing the adjacent pentagons. Since the ^{13}C NMR chemical shift of carbon atoms on fullerene cages is related to several factors (including torsion strain[26]), deshielding of the ^{13}C NMR signals is in agreement with other ^{13}C NMR studies of pentalene-containing cages.[3,16] It is also noted that the peak at 170.0 ppm is the most downfield ^{13}C NMR signal for a fullerene or metallofullerene cage observed to date, indicating that very large strain is associated with the two pentalene motifs on the oblate C_2 cage. This helps to localize the negative charge which is essential to the stabilization of the pentalene unit.

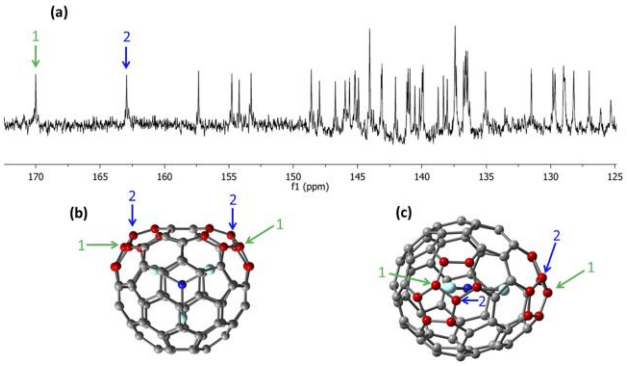

Figure 4. (a) 200 MHz ^{13}C NMR spectrum from an 800 MHz instrument of the $Y_3N@C_{78}$ in carbon disulfide/acetone-d_6 (v/v=9/1) with 8 mg $Cr(acac)_2$ as a relaxation agent; (b) top view; (c) side view optimized structure of $Y_3N@C_2$-C_{78} with the pentalenes highlighted.

In addition, DFT computational structural optimization of $Y_3N@C_{78}$ has been independently performed based on the single crystal structure of $Gd_3N@C_{78}$.[17] In both the view perpendicular (Figure 4b) and parallel (Figure 4c) to the TNT cluster, cage distortion near the pentalene sites (red) is clearly present. The ^{13}C NMR chemical shift values were then calculated based on the optimized structure. The calculated values exhibit good agreement with the experimental results supporting the structural assignment of $Y_3N@C_2$(22010)-C_{78} (Figure 5).

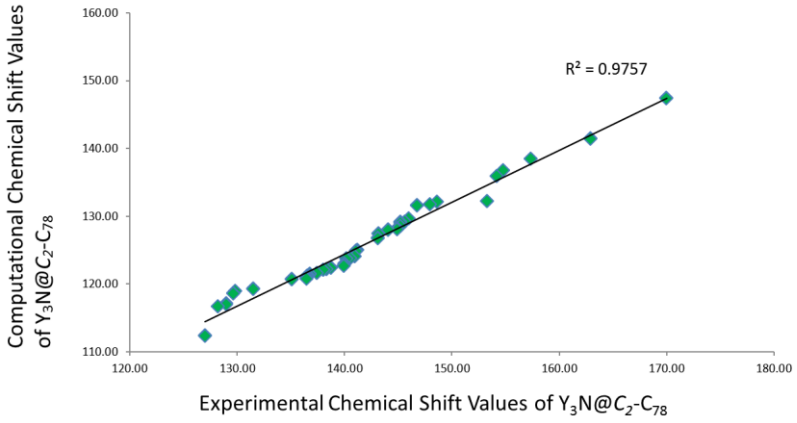

Figure 5. Computational vs experimental chemical shift values of the $Y_3N@C_2$(22010)-C_{78}.

4.4 The HPLC retention behaviors of the $Y_3N@C_{2n}$ (n=39-44) family

The chromatographic retention behaviors of the TNT EMF $Y_3N@C_{2n}$ family are compared with empty-cage fullerenes in Figure 6, utilizing a PYE (pyrenylethyl) column. Fuchs et al. showed that chromatographic data can be used to predict the dipole moments for EMFs.[27] Specifically, it is recognized that the retention mechanism between the solute (EMF) and chromatographic stationary phase (PYE, Figure 6a) consists of both π-π interactions and dispersion forces, and the latter depend on the polarizability of the fullerenes (or EMFs) and the stationary phase. In addition, earlier studies have clearly demonstrated a linear relationship between the chromatographic capacity factor K ($K=(t_R-t_0)/t_0$, in which t_R is the retention time and t_0 is the dead time) and the number of π electrons on empty fullerene cages,[27] as seen in figure 6b (blue). For TNT EMFs (red), the number of π electrons equals the number of carbon atoms plus 6, due to the formal transfer of 6 electrons. In the cases of the IPR-allowed EMFs $Y_3N@I_h$-C_{80}, $Y_3N@D_3$-C_{86}, and $Y_3N@D_2$-C_{88}, the corresponding linearity (with the empty-cages) is still maintained, even for widely different cage symmetries (Figure 6c). In contrast, the pentalene-containing $Y_3N@C_{2n}$ members $Y_3N@C_2$-C_{78}, $Y_3N@C_s$-C_{82}, and $Y_3N@C_s$-C_{84}, all significantly deviate from the correlation with longer retention times, which suggests that those non-IPR members possess significant permanent dipole moments.

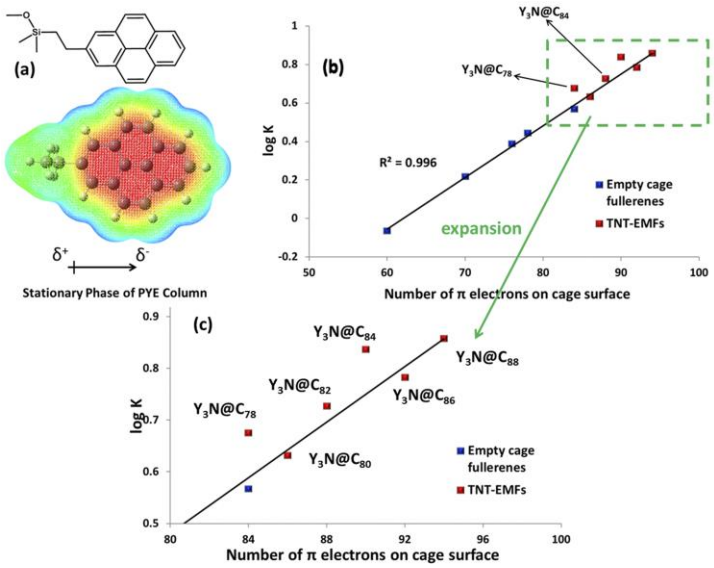

Figure 6. HPLC retention behavior study of the yttrium TNT-EMFs. (a) The structure and electronic property of the stationary phase of PYE column; (b) Retention behaviors of fullerenes (blue) and the $Y_3N@C_{2n}$ family (red) on PYE column; (c) Expansion of the framed area in (b) emphasizing the EMFs.

4.5 Enhanced Dipole Moments in TNT-EMFs $M_3N@C_{78}$, $M_3N@C_{82}$ and $M_3N@C_{84}$.

4.5.1 Calculated dipole moments

The DFT-calculated dipole moment values for the yttrium TNT EMF family (Figure 7) are consistent with the chromatographic retention time data. Namely, there is a clear gap between pentalene-containing species (overall dipole > 1.0 Debye) and species without the pentalene motif (overall dipole < 0.2 Debye). Specifically, the dipole moments of $Y_3N@C_2$-C_{78} and $Y_3N@C_s$-C_{84} are dominated by contributions from the cluster metal atom interaction with the pentalene group, leading to an induced dipole moment along that vector axis. The dipole moment for $Y_3N@C_s$-C_{82} is along two different vector axes, and the larger is along the pentalene-metal axis. As expected, there is no significant dipole moment for the TNT EMFs

without pentalene groups, since there is no significant difference in the local three-fold C_{3v} environment of the $(Y_3N)^{6+}$ cluster.

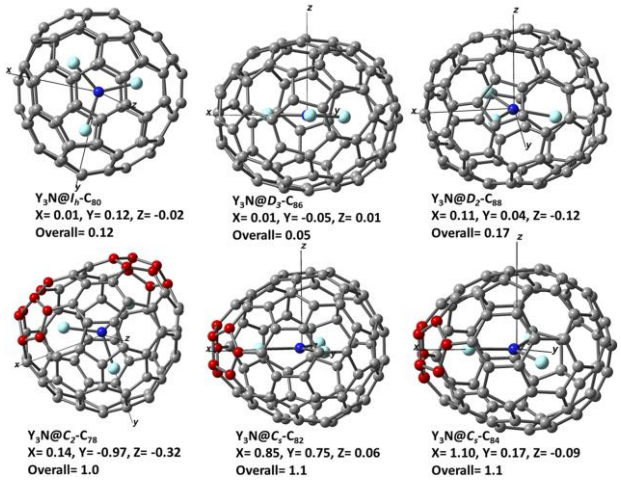

Figure 7. DFT-computed dipole moments of the $Y_3N@C_{2n}$ (n=39-44) family (in Debye). The pentalene groups are highlighted in red.

4.5.2 Lengthening of the M-N bond.

The prediction of a significant dipole moment for the pentalene-containing $Y_3N@C_{2n}$ EMFs also suggests lengthening of the covalent Y-N bond in the $(Y_3N)^{3+}$ cluster. In addition, bond lengthening should be reflected in all TNT EMFs that have significant dipole moments, since the molecular dipole moment strongly depends on the charge multiplying distance for the M-N bond vector (M and N have significantly different electronegativities). The lengthening of the M-N bond will break the symmetry of the M_3N cluster and lead to a non-zero dipole moment. As illustrated in Figure 8, available single-crystal data and DFT calculation results for all reported members of the $M_3N@C_{2n}$ (M=Gd,[14,15,17] Tb,[10] and Y, n=39-44) family that contain at least one pentalene motif show that they exhibit longer M-N bonds oriented toward the pentalene motif. The trend is even more convincing for the $Gd_3N@C_2$-C_{78} and $Y_3N@C_2$-C_{78} examples that

contain two pentalene motifs for both experimental and DFT computational results. This bond lengthening could result from either a strong metal-pentalene interaction or the creation of extra space by the pentalene-caused cage distortion. In either mechanism, enhanced dipole moments for pentalene-containing TNT EMFs would be predicted.

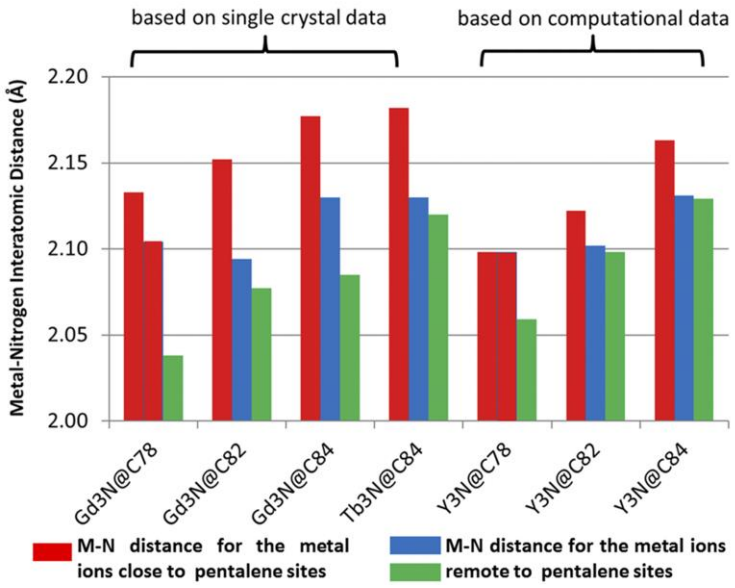

Figure 8 Metal-nitrogen distances in the $(M_3N)^{6+}$ cluster of pentalene-containing TNT EMFs.

4.6 Conclusion

In this chapter, significant dipole moments are predicted for lanthanide members of the $M_3N@C_{2n}$ (n=39-44) family that contain an M-N bond oriented toward a pentalene motif. This prediction could also be extended to other pentalene-containing EMFs, but, for the mono- and dimetallic EMFs, the case could be more complicated due to the non-centroid position of the endohedral ion(s).[27,28] The enhanced dipole moments will lead to improved solubility in polar

solvents and this could be an important consideration for utilizing EMFs in molecular optoelectronic devices and biomedical applications. For comparison, the dipole moment induced by the pentalene groups in TNT EMFs is comparable to that of azulene (1.08 Debye),[29] which has an ionic aromatic model and a solubility in water of 20 mg/L. Although the TNT EMF $Gd_3N@I_h$-C_{80} requires surface functionalization of the fullerene cage surface to impart water solubility for magnetic resonance imaging (MRI) contrast agent applications,[30] the enhanced dipole moments for $Gd_3N@C_2$-C_{78}, $Gd_3N@C_s$-C_{82}, and $Gd_3N@C_s$-C_{84} suggest the possibility that these EMFs could alleviate this requirement, especially for lipid solubility applications. Finally, the finding of significant dipole moments for TNT EMFs containing the pentalene motif could also lead to the possibility of controlling molecular orientation in an external electric field.[28]

REFERENCES

(1) Kroto, H. W. The Stability of the Fullerenes C_{24}, C_{28}, C_{32}, C_{36}, C_{50}, C_{60} and C_{70}. *Nature* **1987**, *329*, 529-531.

(2) Wang, C. R.; Kai, T.; Tomiyama, T.; Yoshida, T.; Kobayashi, Y.; Nishibori, E.; Takata, M.; Sakata, M.; Shinohara, H. C_{66} Fullerene Encaging a Scandium Dimer. *Nature* **2000**, *408*, 426-427.

(3) Stevenson, S.; Fowler, P. W.; Heine, T.; Duchamp, J. C.; Rice, G.; Glass, T.; Harich, K.; Hajdu, E.; Bible, R.; Dorn, H. C. A Stable Non-classical Metallofullerene Family. *Nature* **2000**, *408*, 427-429.

(4) Nikawa, H.; Kikuchi, T.; Wakahara, T.; Nakahodo, T.; Tsuchiya, T.; Rahman, G. M. A.; Akasaka, T.; Maeda, Y.; Yoza, K.; Horn, E.; Yamamoto, K.; Mizorogi, N.; Nagase, S. Missing Metallofullerene La@C_{74}. *J. Am. Chem. Soc.* **2005**, *127*, 9684-9685.

(5) Wakahara, T.; Nikawa, H.; Kikuchi, T.; Nakahodo, T.; Rahman, G. M. A.; Tsuchiya, T.; Maeda, Y.; Akasaka, T.; Yoza, K.; Horn, E.; Yamamoto, K.; Mizorogi, N.; Slanina, Z.; Nagase, S. La@C_{72} Having a Non-IPR Carbon Cage. *J. Am. Chem. Soc.* **2006**, *128*, 14228-14229.

(6) Kato, H.; Taninaka, A.; Sugai, T.; Shinohara, H. Structure of a Missing-Caged Metallofullerene: La_2@C_{72}. *J. Am. Chem. Soc.* **2003**, *125*, 7782-7783.

(7) Yamada, M.; Wakahara, T.; Tsuchiya, T.; Maeda, Y.; Akasaka, T.; Mizorogi, N.; Nagase, S. Spectroscopic and Theoretical Study of Endohedral Dimetallofullerene Having a Non-IPR Fullerene Cage: $Ce_2@C_{72}$. *J. Phys. Chem. A* **2008**, *112*, 7627-7631.

(8) Shi, Z. Q.; Wu, X.; Wang, C. R.; Lu, X.; Shinohara, H. Isolation and Characterization Of $Sc_2C_2@C_{68}$: A Metal-Carbide Endofullerene with a Non-IPR Carbon Cage. *Angew. Chem. Int. Ed.* **2006**, *45*, 2107-2111.

(9) Chen, N.; Beavers, C. M.; Mulet-Gas, M.; Rodriguez-Fortea, A.; Munoz, E. J.; Li, Y. Y.; Olmstead, M. M.; Balch, A. L.; Poblet, J. M.; Echegoyen, L. $Sc_2S@C_s(10528)$-C_{72}: A Dimetallic Sulfide Endohedral Fullerene with a Non Isolated Pentagon Rule Cage. *J. Am. Chem. Soc.* **2012**, *134*, 7851-7860.

(10) Chen, N.; Mulet-Gas, M.; Li, Y.-Y.; Stene, R. E.; Atherton, C. W.; Rodriguez-Fortea, A.; Poblet, J. M.; Echegoyen, L. $Sc_2S@C_2(7892)$-C_{70}: A Metallic Sulfide Cluster inside a Non-IPR C_{70} Cage. *Chem. Sci.* **2013**, *4*, 180-186.

(11) Beavers, C. M.; Zuo, T.; Duchamp, J. C.; Harich, K.; Dorn, H. C.; Olmstead, M. M.; Balch, A. L. An Improbable, Egg-shaped Endohedral Fullerene That Violates the Isolated Pentagon Rule. *J. Am. Chem. Soc.* **2006**, *128*, 11352-11353.

(12) Yang, S.; Popov, A. A.; Dunsch, L. The Role of an Asymmetric Nitride Cluster on a Fullerene Cage: The Non-IPR Endohedral $DySc_2N@C_{76}$ *J. Phys. Chem. B* **2007**, *111*, 13659-13663.

(13) Yang, S.; Popov, A. A.; Dunsch, L. Violating the Isolated Pentagon Rule (IPR): The Endohedral Non-IPR C_{70} Cage of $Sc_3N@C_{70}$. *Angew. Chem. Int. Ed.* **2007**, *46*, 1256-1259.

(14) Popov, A. A.; Krause, M.; Yang, S.; Wong, J.; Dunsch, L. C_{78} Cage Isomerism Defined by Trimetallic Nitride Cluster Size: a Computational and Vibrational Spectroscopic Study. *J. Phys. Chem. B* **2007**, *111*, 3363-3369.

(15) Zuo, T.; Walker, K.; Olmstead, M. M.; Melin, F.; Holloway, B. C.; Echegoyen, L.; Dorn, H. C.; Chaur, M. N.; Chancellor, C. J.; Beavers, C. M.; Balch, A. L.; Athans, A. J. New Egg-shaped Fullerenes: Non-Isolated Pentagon Structures of $Tm_3N@C_s(51365)$-C_{84} and $Gd_3N@C_s(51365)$-C_{84}. *Chem. Comm.* **2008**, 1067-1069.

(16) Mercado, B. Q.; Beavers, C. M.; Olmstead, M. M.; Chaur, M. N.; Walker, K.; Holloway, B. C.; Echegoyen, L.; Balch, A. L. Is the Isolated Pentagon Rule Merely a Suggestion for Endohedral Fullerenes? The Structure of a Second Egg-Shaped Endohedral Fullerene-$Gd_3N@C_s(39663)$-C_{82}. *J. Am. Chem. Soc.* **2008**, *130*, 7854-7855.

(17) Fu, W.; Xu, L.; Azurmendi, H.; Ge, J.; Fuhrer, T.; Zuo, T.; Reid, J.; Shu, C.; Harich, K.; Dorn, H. C ^{89}Y and ^{13}C NMR Cluster and Carbon Cage Studies of an Yttrium Metallofullerene Family, $Y_3N@C_{2n}$ (n=40-43). *J. Am. Chem. Soc.* **2009**, *131*, 11762-11769.

(18) Beavers, C. M.; Chaur, M. N.; Olmstead, M. M.; Echegoyen, L.; Balch, A. L. Large Metal Ions in a Relatively Small Fullerene Cage: The Structure of $Gd_3N@C_2(22010)$-C_{78} Departs from the Isolated Pentagon Rule. *J. Am. Chem. Soc.* **2009**, *131*, 11519-11524.

(19) Ma, Y.; Wang, T.; Wu, J.; Feng, Y.; Xu, W.; Jiang, L.; Zheng, J.; Shu, C.; Wang, C. Size Effect of Endohedral Cluster on Fullerene Cage: Preparation And Structural Studies of $Y_3N@C_{78}$-C_2. *Nanoscale* **2011**, *3*, 4955-4957.

(20) Olmstead, M. H.; de Bettencourt-Dias, A.; Duchamp, J. C.; Stevenson, S.; Marciu, D.; Dorn, H. C.; Balch, A. L. Isolation and Structural Characterization of the Endohedral Fullerene $Sc_3N@C_{78}$. *Angew. Chem. Int. Ed.* **2001**, *40*, 1223-1224.

(21) Stevenson, S.; Rice, G.; Glass, T.; Harich, K.; Cromer, F.; Jordan, M. R.; Craft, J.; Hadju, E.; Bible, R.; Olmstead, M. M.; Maitra, K.; Fisher, A. J.; Balch, A. L.; Dorn, H. C. Small-bandgap Endohedral Metallofullerenes In High Yield and Purity. *Nature* **1999**, *401*, 55-57.

(22) Zuo, T.; Beavers, C. M.; Duchamp, J. C.; Campbell, A.; Dorn, H. C.; Olmstead, M. M.; Balch, A. L. Isolation and Structural Characterization of a Family of Endohedral Fullerenes Including the Large, Chiral Cage Fullerenes $Tb_3N@C_{88}$ and $Tb_3N@C_{86}$ as well as the I_h and D_{5h} Isomers of $Tb_3N@C_{80}$. *J. Am. Chem. Soc.* **2007**, *129*, 2035-2043.

(23) Slanina, Z.; Chen, Z.; Schleyer, P. v. R.; Uhlík, F.; Lu, X.; Nagase, S. $La_2@C_{72}$ and $Sc_2@C_{72}$: Computational Characterizations. *J. Phys. Chem. A* **2006**, *110*, 2231-2234.

(24) Olmstead, M. M.; Lee, H. M.; Duchamp, J. C.; Stevenson, S.; Marciu, D.; Dorn, H. C.; Balch, A. L. $Sc_3N@C_{68}$: Folded Pentalene Coordination in an Endohedral Fullerene that Does Not Obey the Isolated Pentagon Rule. *Angew. Chem. Int. Ed.* **2003**, *42*, 900.

(25) Fu, W.; Zhang, J.; Champion, H.; Fuhrer, T.; Azuremendi, H.; Zuo, T.; Zhang, J.; Harich, K.; Dorn, H. C. Electronic Properties and ^{13}C NMR Structural Study of $Y_3N@C_{88}$. *Inorg. Chem.* **2011**, *50*, 4256-4259.

(26) Taylor, R.; Hare, J. P.; Abdulsada, A. K.; Kroto, H. W. Isolation, Separation and Characterisation of the Fullerenes C_{60} And C_{70}: the Third Form of Carbon. *J. Chem. Soc. Chem. Comm.* **1990**, 1423-1425.

(27) Fuchs, D.; Rietschel, H.; Michel, R. H.; Fischer, A.; Weis, P.; Kappes, M. M. Extraction and Chromatographic Elution Behavior of Endohedral Metallofullerenes: Inferences Regarding Effective Dipole Moments. *J. Phys. Chem.* **1996**, *100*, 725-729.

(28) Yasutake, Y.; Shi, Z. J.; Okazaki, T.; Shinohara, H.; Majima, Y. Single Molecular Orientation Switching of an Endohedral Metallofullerene. *Nano Lett.* **2005**, *5*, 1057.

(29) Anderson, A. G.; Steckler, B. M. Azulene. VIII. A Study of the Visible Absorption Spectra and Dipole Moments of Some 1- and 1,3-Substituted Azulenes[1,2]. *J. Am. Chem. Soc.* **1959**, *81*, 4941-4946.

(30) Zhang, J.; Fatouros, P. P.; Shu, C.; Reid, J.; Owens, L. S.; Cai, T.; Gibson, H. W.; Long, G. L.; Corwin, F. D.; Chen, Z.-J.; Dorn, H. C. High Relaxivity Trimetallic Nitride (Gd_3N) Metallofullerene MRI Contrast Agents with Optimized Functionality. *Bioconjugate Chem.* **2010**, *21*, 610-615.

Chapter 5 A Missing Link in the Transformation from Asymmetric to Symmetric Metallofullerene Cages Implies a Top-Down Fullerene Formation Mechanism

This chapter is adopted from the manuscript published on *Nature Chemistry* with appropriate modifications. Full text of the published manuscript entitled "*A missing link in the transformation from asymmetric to symmetric metallofullerene cages implies a top-down fullerene formation mechanism*", by Jianyuan Zhang, Faye L. Bowles, Daniel W. Bearden, W. Keith Ray, Tim Fuhrer, Youqing Ye, Caitlyn Dixon, Kim Harich, Richard F. Helm, Marilyn M. Olmstead, Alan L. Balch and Harry C. Dorn, can be obtained at http://www.nature.com/nchem/journal/v5/n10/full/nchem.1748.html.

5.1 A missing link in the "top-down" fullerene formation

The discovery of the fullerenes[1] has opened new vistas in nanoscience, and metallofullerenes have shown vast promise in photovoltaic[2] and biomedical[3] applications; however, their formation mechanism remains unclear. Various versions of the "bottom-up mechanism", which suggests fullerenes are formed by consecutively adding C_2 units to small carbon nanoclusters and cages, have been the main pathway advanced for fullerene formation.[4,5] In recent years, with the development of graphene[6] evidence is emerging to suggest a "top-down mechanism", whereby fullerene cages are formed via shrinkage of giant fullerene structures generated from graphene. One piece of direct evidence for the top-down mechanism is the reported laboratory transformation from graphene to fullerene.[7] It had also been illustrated that fullerenes can be pyrolyzed and lose carbon atoms to form smaller fullerenes at high temperature in an argon stream.[8] Another strong supporting argument for the top-down mechanism is that fullerenes are formed in the interstellar medium[9] by a photochemical process in which graphene sheets curve and lose C_2 and other fragments.[10] However, evidence for the top-down mechanism has not been demonstrated at the molecular level. Herein, we present NMR and X-ray crystallographic structural characterization for $M_2C_2@C_1$(51383)-C_{84} (M=Y, Gd) metallofullerenes. These

molecules exhibit a unique asymmetric cage C_1(51383)-C_{84} which represents the first characterized preserved intermediate suggesting top-down formation of fullerenes and metallofullerenes.

The proposed top-down mechanism is illustrated in Fig. 1. Under appropriate conditions, graphene sheets can spontaneously roll and warp to form other nanostructures,[11,12] including randomly formed giant closed carbon networks, the primitive fullerene cages.[7] In an important computational study, a "shrinking hot giant fullerene" mechanism that leads to smaller fullerene structures has been advanced,[13] which suggests a cascade shrinking process (multiple C_2 losses) of giant fullerenes with spontaneous self-assembly to appropriate high-symmetry fullerene cages (HSFCs, e.g. I_h-C_{60}, D_{5h}-C_{70}). Curl attributed the driving force of the shrinking process to C_2 swapping.[14] Possible modes for fullerene cage rearrangements (isomerization and/or shrinkage by loss of C_2) are also suggested in Fig. 1. The "Stone-Wales" transformation (SWT) realizes an orthogonal pentagon shift by rotating the central bond of a pyracylene motif. A second mode involves relieving the high torsional strain in a pentalene motif (fused pentagons) by extrusion of the central C_2 unit to form a hexagon.[15] Another possibility is loss of a C_2 unit by extrusion of the central bond of an indene motif as suggested by Murry and coworkers.[16] This process has been experimentally demonstrated by the capture of heptagon-containing intermediates.[17,18] Kroto was the first to recognize that final fullerene cages prefer high symmetry without direct pentagon-pentagon contact (the isolated pentagon rule, IPR).[19]

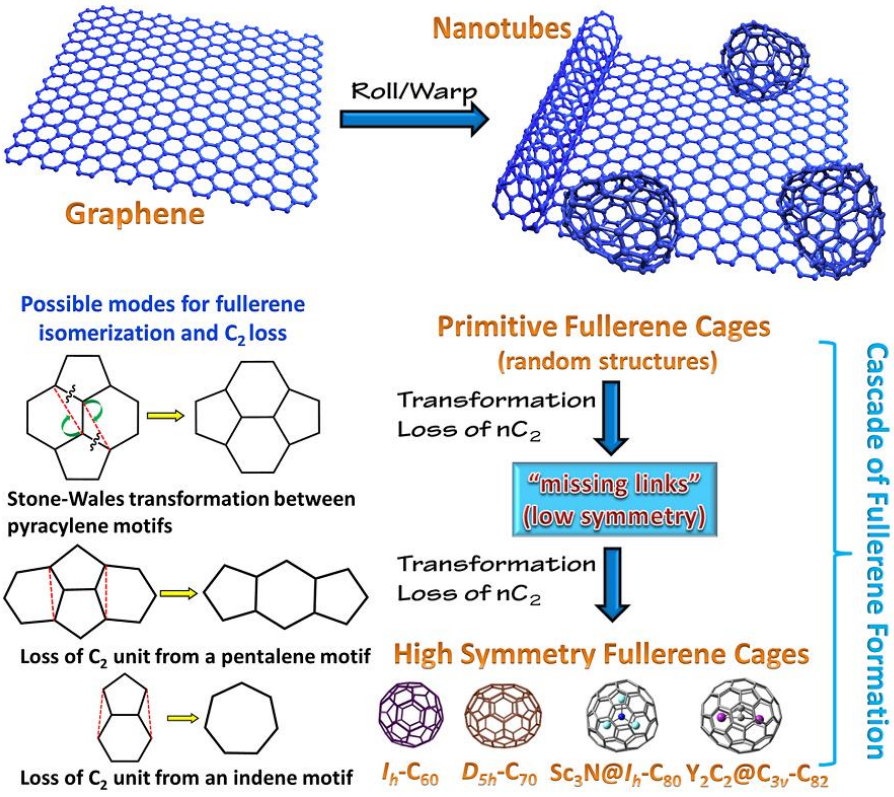

Figure 1 The "Top-down mechanism" for fullerene formation. a) A possible spontaneous transformation of graphene into other nanostructures. b) Cascade shrinkage of fullerenes. In this process random, giant fullerene structures can shrink and rearrange into high-symmetry small fullerene structures. c) Possible modes of fullerene isomerization (Stone-Wales transformation) and C_2 loss (C_2 extrusion from pentalene and indene motif).

The incorporation of a metal source in the reaction path can lead to the formation of endohedral metallofullerenes (EMF), in which particular HSFCs are stabilized by the presence of encapsulated atoms or clusters, such as I_h-C_{80} and C_{3v}-C_{82}. Also, endohedral atoms and clusters may cause the rearrangement to stop early, and preserve intermediate, unstable fullerene cages. For example, some pentalene-containing cages in the formation process were found to survive in EMFs.[20-22] In a cascade to HSFCs, a characteristic feature of an intermediate "missing link" fullerene cage should be a random asymmetric (C_1 symmetry), unstable (containing pentalene

motifs) structure, but capable of a process of rearrangement to high symmetry and IPR-allowed fullerene cages. Although multiple "missing links" are possible as intermediates in different pathways of fullerene formation, no definitive structure has been experimentally isolated or characterized. In this paper we report the first example of a proposed "missing link" in metallofullerene formation, the chiral C_1(51383)-C_{84} fullerene cage, which is stabilized by an encapsulated metal carbide cluster. Although there is an earlier report of a scandium metal carbide metallofullerene $Sc_2C_2@C_{2v}$-C_{68} containing a pentalene motif,[23] the structure of this molecule has been challenged and suggested to be $Sc_2@C_{2v}$-C_{70}.[24] The $M_2C_2@C_1$(51383)-C_{84} molecules reported herein represent the first unambiguous X-ray structural characterization of a pentalene-containing metal carbide metallofullerene, and the first asymmetric fullerene cage with a pentalene motif. More importantly, it is a starting point in the rearrangement cascade to form smaller HSFCs via simple, well-defined mechanistic steps.

5.2 Characterization of $Y_2C_2@C_1$(51383)-C_{84} and $Gd_2C_2@C_1$(51383)-C_{84}

5.2.1 Sample Preparation

The ^{13}C enriched fullerenes and yttrium metallofullerenes were synthesized by electric-arc synthesis with graphite rod packed with 99% ^{13}C amorphous carbon and Y_2O_3 (average 26 w% or 24 mol% ^{13}C in carbon starting material).[25] The gadolinium metallofullerenes were synthesized by normal electric-arc procedure with natural abundance carbon rods.[26] The ^{13}C enriched $Y_2C_2@C_1$(51383)-C_{84} and natural abundance $Gd_2C_2@C_1$(51383)-C_{84} samples were isolated by multistage HPLC (Fig. S1-S6 for details) after selective removal of empty cage fullerenes. Both the $Y_2C_2@C_{84}$ and $Gd_2C_2@C_{84}$ exhibit abnormally long, but equal, retention times on a pyrenylethyl (PYE) HPLC column (Fig. S3, S6). The long retention times for both molecules are consistent with the existence of pentalene motifs.[27] The structure of

$Gd_2C_2@C_1$(51383)-C_{84} was unambiguously elucidated by single-crystal analysis, and the structure of $Y_2C_2@C_1$(51383)-C_{84} was confirmed by equal retention time, identical UV-vis spectra (Fig. S7) and ^{13}C NMR chemical shift correlation (*vide infra* Fig. 2b).

5.2.2 ^{13}C NMR characterization of $Y_2C_2@C_1$*(51383)*-C_{84}

In the ^{13}C NMR spectrum for $Y_2C_2@C_1$(51383)-C_{84} (Fig. 2a for expanded regions, Fig S8 for full spectrum), the aromatic region consists of 84 nearly equal intensity peaks consistent with low C_1 symmetry. The two peaks downfield at 160 ppm confirm the presence of a pentalene motif. The structure for this preliminarily studied[25] low symmetry molecule was proposed to be $Y_2C_2@C_1$(51383)-C_{84}, based on an independent exhaustive DFT theoretical study.[28] The computationally-derived ^{13}C NMR chemical shifts were in excellent agreement with the experimental results (Fig. 2b). The carbide resonance exhibits two different scalar couplings to yttrium ($^1J_{Y\text{-}C}$= 16.6 Hz and $^1J_{Y\text{-}C}$= 18.8 Hz, Fig. S9), indicating that the C_2 unit is asymmetrically positioned between the two non-equivalent yttrium ions with one of them associated with the pentalene motif.[29]

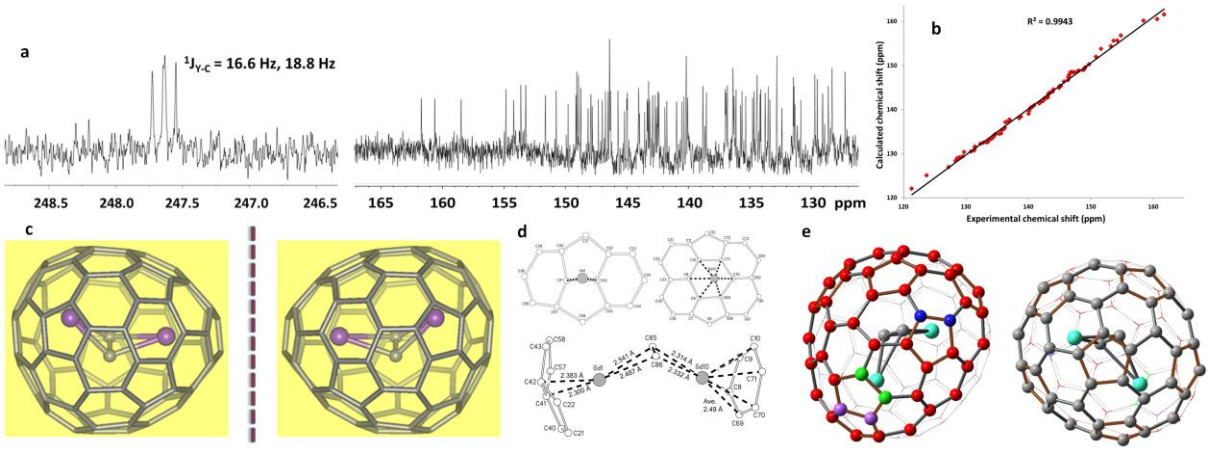

Figure 2. The ^{13}C NMR and single-crystal study of $M_2C_2@C_1(51383)$-C_{84} (M=Y, Gd). a) ^{13}C NMR spectrum of the $Y_2C_2@C_1(51383)$-C_{84}. b) Correlation between the calculated (ref. 28) and experimental chemical shift values. c) X-ray single-crystal results of $Gd_2C_2@C_1(51383)$-C_{84} showing both enantiomers. d) Relative position between the Gd_2C_2 cluster and the C_{84} fullerene cage. e) The "hot half" (left, red) and "cold half" (right, grey) of the $M_2C_2@C_1(51383)$-C_{84} based on the single-crystal structure of $Gd_2C_2@C_1(51383)$-C_{84}. The pentagons are highlighted in tan color. The fragments in green, purple and blue colors in the "hot half" correspond to three C_2 extrusion routes described in Fig. 3.

5.2.3 Single crystal study of $Gd_2C_2@C_1(51383)$-C_{84}

It is well recognized that every fullerene inevitably is comprised of some number of hexagons and exactly twelve pentagons. A fullerene can be imagined to occur as an "orange peel" in which successive hexagons or pentagons are added in a spiral fashion until the cage is closed. If each hexagon and pentagon is numbered in sequence, the ring spiral pattern can be simply represented by the numerical order of the twelve pentagons alone.[15] For a fullerene cage made up of 84 carbon atoms, there are 51,568 pentalene-containing and 24 IPR isomers. Single-crystal X-ray analysis has been performed for the $Gd_2C_2@C_{84}$ and confirmed that the fullerene site contains a

racemic mixture (Fig. 2c) of the chiral pentalene-containing C_1 isomer 51383 with the ring spiral 1 2 11 13 16 19 28 31 33 35 37 44. The crystallographic results are consistent with the computationally proposed structure[28] and ^{13}C NMR study for $Y_2C_2@C_1(51383)$-C_{84}. Both enantiomers occupy a common site (Fig. S10) in the crystal due to disorder. Although there is considerable disorder in the Gd positions, the major location (Gd1, 54% occupancy) is in the unique pentalene region where two pentagons are fused to give a nose-like effect to the cage with high torsional strain. The other prominent Gd location is approximately η^6 to a hexagonal ring (Fig. 2d). The Gd_2C_2 cluster is more compressed in comparison to that in the larger EMF $Gd_2C_2@D_3(85)$-C_{92}[30] and is asymmetrically placed along this span of the asymmetric C_{84} cage. Interatomic distances (Fig. 2d) suggest the pentalene is "dragging" the metal ion closer for stabilization.

The asymmetry in the Gd_2C_2 cluster is consistent with the observation of two different $^1J_{Y\text{-}C}$ values for $Y_2C_2@C_1(51383)$-C_{84}. The bisection of the $C_1(51383)$-C_{84} fullerene cage yields two halves that are uniquely different in terms of their relative stability and chemical reactivity. The half close to Gd1 is the "hot half" (Fig. 2e left), with six pentagons forming pentalene and pyracylene motifs which, according to the "maximum pentagon separation" theory,[31] are unstable and subject to further rearrangements. The other half close to Gd10 is the "cold half" (Fig. 2e right), in which six pentagons are well separated from each other.

5.3 Rearranging cascade of $C_1(51383)$-C_{84} fullerene cage

We propose that $C_1(51383)$-C_{84} cage can rearrange to more stable structures at high temperature by elimination of the destabilizing pentalene and pyracylene motifs. At elevated temperatures, even stable fullerenes readily lose C_2 units.[17,18] The presence of an electrophilic metal ion near the pentalene portion of the cage may mechanistically facilitate C_2 extrusion. A

mass-spectral study has confirmed the $Gd_2C_2@C_1(51383)$-C_{84} is capable of C_2 loss by laser ablation (Fig. S11). A series of rearrangements of the "hot half" via well-defined mechanistic steps (*vide supra* in Fig. 1c) is shown in Fig. 3. A direct C_2 loss from the pentalene unit (purple route) converts the $C_1(51383)$-C_{84} cage to the $C_s(6)$-C_{82} structure. Subsequently, the $C_s(6)$-C_{82} cage can undergo an SWT to form the more symmetric $C_{2v}(9)$-C_{82} cage with elimination of pyracylene motifs. In addition, the $C_{2v}(9)$-C_{82} cage can convert to the $C_{3v}(8)$-C_{82} cage via a separate SWT step. An alternative way for $C_1(51383)$-C_{84} to relieve the pentalene torsional strain is extrusion of a C_2 unit from an indene unit sharing a pentalene pentagon (green route). This process would form a heptagon-containing intermediate, which quickly converts to $C_{3v}(8)$-C_{82}. The C_2 loss could also occur from another indene motif (blue route), which leads to a heptagon-containing precursor of $C_s(39663)$-C_{82}, the cage found in trimetallic nitride template (TNT) EMF $M_3N@C_{82}$.[32] Furthermore, the $C_{3v}(8)$-C_{82} cage can convert to the well-known $I_h(7)$-C_{80} cage via another heptagon-containing intermediate. An important but minor isomer of C_{80}, the D_{5h}-C_{80} cage can form by loss of C_2 from the pentalene unit in $C_s(39663)$-C_{82}. We also note that the $C_1(51383)$-C_{84} cage can convert to the pentalene-containing $C_s(51365)$-C_{84} cage via a one-step SWT (Fig. S12). The pentalene-containing $C_s(51365)$-C_{84} is the only C_{84} cage found for TNT EMF $M_3N@C_{84}$,[33] and loss of C_2 from its pentalene will give the $C_{2v}(9)$-C_{82} isomer. In these routes the "missing link" $C_1(51383)$-C_{84} cage is the point for metallofullerene cage to lose chirality and gain symmetry.

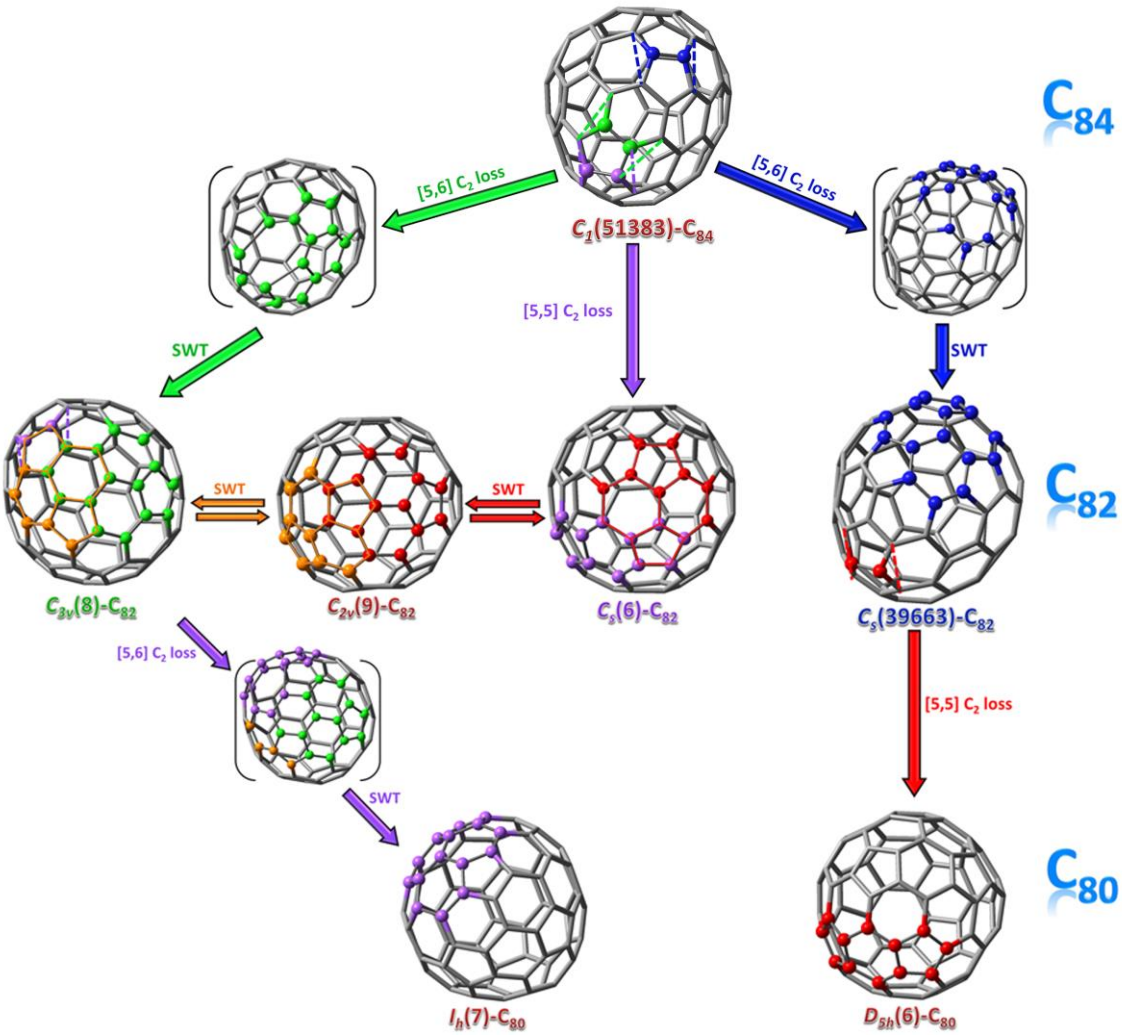

Figure 3. The fullerene structural rearrangement map starting from the missing link *C*$_1$(51383)-C$_{84}$ cage. Many well-known metallofulerene cages are involved in this process. Depending on the size and charge of the encapsulated atom(s) or clusters, the cage may prefer a certain sequence of the transformation map. The colors are used for visual aid of the motifs involved in respective steps matching the color of the arrows.

5.4 Mass spectral investigation of the ^{13}C isotopic distribution in fullerenes and metallofullerenes

High resolution mass-spectrometry is a powerful tool to investigate the formation process of fullerenes and metallofullerenes.[5,34] Isotopic distribution of ^{13}C enriched fullerenes and

metallofullerenes was studied in respective chromatographic fractions (Fig. S13, S14). By careful examination of the isotopic distribution (see examples in Table S1, S2), we determined that the ^{13}C content in empty cages products is approximately 9.5 mol% ^{13}C content (Fig. S13). The ^{13}C content is 10.5 mol% in metallofullerenes Y_2C_{84} and 10.2 mol% in Y_2C_{86}, respectively (Fig. S14). The subtle difference between the overall ^{13}C content in empty-cage fullerenes and metallofullerenes could be due to the geometry of the carbon rod, in which the spatial location of the metal source is more intimately associated to the ^{13}C labeled amorphous carbon (inside) than natural abundance graphite (outside). More importantly, empty cage fullerenes and metallofullerenes exhibit very similar overall ^{13}C isotopic patterns (Fig. S13, S14). As a direct comparison shown in Fig. 4, empty cage fullerene C_{84} and metallofullerene Y_2C_{84} (same number of carbon atoms) share nearly identical isotopic pattern except for a slight difference in ^{13}C mol% content.

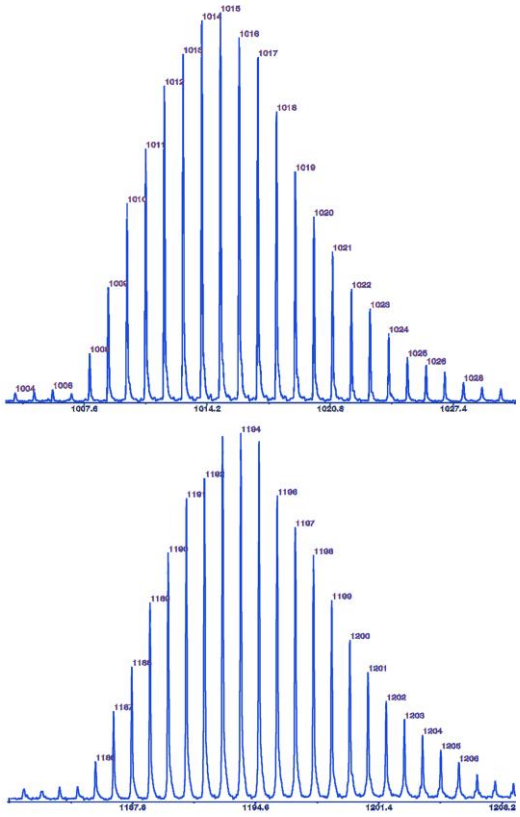

Figure 4. The isotopic distribution for ^{13}C enriched (a) fullerene C_{84} and (b) metallofullerene Y_2C_{84}. The similar pattern in (a) and (b) suggests that empty cage fullerenes and metallofullerenes are formed via similar pathway under our electric-arc conditions.

5.5 Discussion

The fullerene cages described in Fig. 3 and Fig. S12 involve a large fraction of the known metallofullerenes and cover all classes of encapsulated atoms and clusters, including traditional metallic fullerenes, metal nitride (the TNT EMF), metal carbide, metal sulfide, metal oxide, metal cyanide, and methanide clusterfullerenes, as shown in Table 1.[8] These cages account for the majority of the solvent-extractable yield of metallofullerenes. Metallofullerenes containing large endohedral groups need a large cage initially in order to fit the cluster inside without huge

energy expenditure, and the more plausible explanation for the distorted endohedral clusters (e.g. metal carbide cluster[25]) is that the corresponding metallofullerenes are formed from top-down cage shrinkage. In particular, the C_s(6)-C_{82}, C_{2v}(9)-C_{82} and C_{3v}(8)-C_{82} cages represent the three cage isomers found in the metal carbide C_{82} EMFs.[35] Furthermore, as suggested by Shinohara, the presence of endohedral carbide clusters (M_2C_2) can be viewed as a result of a favorable "envelopment" process by encapsulated metal atoms, as opposed to extrusion of C_2 from the fullerene cage,[35] making metal carbide clusters an especially important family in the cascade process. Depending on the size and charge of the endohedral units, the fullerene cage will choose different routes in the transformation scheme. For example, while the metal carbide cluster can stabilize C_1(51383)-C_{84} cage or induce the cage to adopt the routes converting to C_{2v}(9)-C_{82}, C_{3v}(8)-C_{82}, or C_s(6)-C_{82}, the TNT cluster would more inclined to convert the cage to C_s(39663)-C_{82}, I_h(7)-C_{80} and D_{5h}(6)-C_{80}. Distribution of the four C_{82} fullerene cages C_{2v}(9)-C_{82}, C_{3v}(8)-C_{82}, C_s(6)-C_{82} and C_s(39663)-C_{82} as a function of temperature has been computationally derived using their Gibbs free energy values with different charges associated (Fig. S15). The relative concentrations of each isomer are in reasonably good agreement with the experimental findings, but the size of the clusters will also influence these predictions.

Table 1. List of metallofullerenes involved in the pathways shown Figure 3 and Figure S7.

cage isomer	molecule
C_1(51383)-C_{84}	**M_2C_2@C_{84}**, M=Y, Gd (this work)
C_s(51365)-C_{84}	**M_3N@C_{84}**, M=Tb, Tm, Gd, Y
C_s(39663)-C_{82}	**M_3N@C_{82}**, M=Gd, Y
C_s(6)-C_{82}	**M_2C_2@C_{82}**, M=Sc, Y, Er, ErY, Dy; **M@C_{82}**, M=Ca, Tm, Yb, Eu, Sm, La; **Er_2@C_{82}**, **Sc_2S@C_{82}**, **Sc_2O@C_{82}**,
C_{2v}(9)-C_{82}	**M_2C_2@C_{82}**, M=Sc, Y, Er, Dy; **M@C_{82}**, M=Ca, Tm, Yb, Eu, Sm, Sc, La, Y, Ce, Gd, Dy; **M_2@C_{82}**, M=Er, Tm, TmHo
C_{3v}(8)-C_{82}	**M_2C_2@C_{82}**, M=Sc, Y, Er, ErY, Dy, **M_2@C_{82}**, M=Er, Sc, Y, Tm, TmHo; **M_2S@C_{82}**, M=Sc, Y, Lu, Dy
I_h(7)-C_{80}	**M_3N@C_{80}**, M=Sc, Y, Gd, Lu, Dy, Tm, Tb, mixed metals; **M_2@C_{80}**, M=La, Ce; **Sc_3CH@C_{80}**, **Sc_4O_2@C_{80}**, **Sc_4O_3@C_{80}**, **Sc_3C_2@C_{80}**, **Sc_3CN@C_{80}**
D_{5h}(6)-C_{80}	**M_3N@C_{80}**, M=Sc, Y, Tm, Tb, mixed metals; **Ce_2@C_{80}**

The mass-spectral data for ^{13}C enriched empty cage fullerenes and metallofullerenes exhibit nearly equivalent isotopic patterns (Fig. 4, S13, S14), which suggests that under our experimental conditions the formation mechanism for empty-cage fullerenes and metallofullerenes are very similar. However, it is possible that fullerenes and metallofullerenes have different specific pathways and intermediates due to the influence of metal cluster geometry, size or charge. The isotopic distributions represent enhanced C_2 insertion and extrusion in both the fullerenes and metallofullerenes in the electric-arc plasma,[36] which explains why separate 1.1% (natural abundance) and 99% ^{13}C products were not observed (Fig. S13, S14) even assuming a top-down process. Furthermore, C_2 extrusion as proposed in Fig. 3 is a necessary process to explain the high isotopic levels of fullerenes and metallofullerenes with odd-numbered ^{13}C atoms (odd-numbered mass). Since C_2 carbide formed from the natural abundance (1.1% ^{13}C) graphite source would consist mainly (99%) of ^{12}C-^{12}C, and the amorphous carbon source would yield mainly (99%) ^{13}C-^{13}C carbide, insertion of C_2 can only change the molecular mass by an even number. That is, significant intensities of the odd mass number in the isotopic distributions must relate to C_2 extrusion processes. For example, $^{12}C_{83}{}^{13}C_1$ (m/z = 841 in Fig. 4) must form from 2n ^{13}C atoms present or entering a fullerene cage and 2n-1 ^{13}C atoms leaving the molecule (together with odd number of ^{12}C atoms). It should also be noted that the mass-spectral isotopic distribution patterns are significantly broader than the computational average distribution (Fig. S13, S14), indicating that in the plasma the fullerenes and metallofullerenes are formed from an inhomogeneous carbon source.

Although our current study suggests a top-down mechanistic pathway, we acknowledge that the bottom-up mechanism cannot be excluded especially under different experimental conditions. For example, the capture of halogenated fullerene derivatives smaller than C_{60},[37-39]

although can be explained by a halogen-induced top-down process,[17] is more plausible with bottom-up pathway. In addition, Kroto and coworkers have shown that when fullerenes are exposed to a high concentration of C_2 they can grow via bottom-up process under laser ablation.[5] Considering the reversibility of C_2 insertion/extrusion, the local C_2 concentration could be a major factor,[36] i.e. extrusion (top-down) dominates in low C_2 concentration conditions as shown previously[7,10,17,18] and in Fig. S11, while insertion (bottom-up) dominates in high C_2 concentrations.[5] Moreover, when the plasma reaction mixture contains components such as metal oxides, or halogen sources,[17,34,37-39] the mechanistic pathway could be significantly affected. Therefore, further experimental and theoretical efforts with consideration of specific reaction conditions are needed to unambiguously unravel the formation mechanism of fullerenes and metallofullerenes.

5.6 Conclusion

In conclusion, we have found a missing link, the C_1(51383)-C_{84} fullerene cage, as a molecular structural evidence consistent with "top-down" formation of fullerene structures by illustration of its transformation pathways to a number of common, high-symmetry, IPR-allowed fullerene cages. Mass-spectral data for ^{13}C enriched fullerenes and metallofullerenes suggest they are formed via very similar mechanism under our experimental conditions. The formation of I_h-C_{80} and D_{5h}-C_{80} may shed light on the formation of I_h-C_{60} and D_{5h}-C_{70}, as they share same symmetric point group. While fullerene formation is still an open question, further study of other less stable missing link fullerenes and metallofullerenes will help to establish a detailed picture of the mechanistic pathway for fullerene formation from simple carbon sources.

5.7 Experimental methods and supplementary information

5.7.1 Experimental methods

Preparation of $Y_2C_2@C_1(51383)\text{-}C_{84}$ and $Gd_2C_2@C_1(51383)\text{-}C_{84}$. Both samples were obtained from the same synthetic and isolation procedure. *LUNA Innovations* was commissioned to do the electric-arc synthesis as described.*(17)* In the case of $Y_2C_2@C_1(51383)\text{-}C_{84}$, 99% ^{13}C labeled amorphous carbon was packed inside the rod which accounts for 25% mass of the total reacting carbon content (overall ^{13}C content is 26 w% or 24 mol%) from the packed rod, and approximately 10% ^{13}C enrichment was found in the product. Empty cages were removed by selective reaction with cyclopentadiene. Multistage HPLC separations were performed to give the purified product (see SI for details). The purity of the $Y_2C_2@C_1(51383)\text{-}C_{84}$ and $Gd_2C_2@C_1(51383)\text{-}C_{84}$ was examined with HPLC and mass spectrometry.

Isolation of $Y_2C_2@C_1(51383)\text{-}C_{84}$ and $Gd_2C_2@C_1(51383)\text{-}C_{84}$. The soot containing ^{13}C enriched fullerenes and yttrium metallofullerenes was extracted with o-xylene. The resulting solution was stirred with cyclopentadiene functionalized silica (~1g per 100 mL solution) for 12 hours and then filtered. The filtrate was treated by the same cyclopentadiene method for one more time, and then was loaded onto HPLC for separation. The first stage was performed on a 5 cm-diameter PBB column (Figure S1) and 8 fractions, named as Y-1 to Y-8, were collected. The major components for these 8 fractions are C_{84} and $Y_2@C_{79}N$, $Y_3N@C_{80}$, $Y_3N@C_{82}$, $Y_3N@C_{84}$, $Y_3N@C_{86}$, $Y_3N@C_{88}$, $Y_2C_2@C_{92}$, and larger fullerene and metallofullerenes, respectively.[29] $Y_2C_2@C_1(51383)\text{-}C_{84}$ was co-eluted with $Y_3N@C_{82}$ in the Y-3 fraction. The Y-3 fraction was injected onto a 1 cm-diameter PYE column for second stage separation (Figure S2). $Y_2C_2@C_1(51383)\text{-}C_{84}$ has a retention time of 78 minutes, which is very different from other members in the Y-3 fraction. The amount of $Y_2C_2@C_1(51383)\text{-}C_{84}$ is about 22% compared to the previously reported $Y_3N@C_{82}$.[29] Further chromatographic purification was performed to give the purified $Y_2C_2@C_1(51383)\text{-}C_{84}$ (Figure S3).

The soot containing fullerenes and gadolinium metallofullerenes was extracted with o-xylene. The resulting solution was subject to extensive cyclopentadiene functionalized silica treatment until all empty cage fullerenes were removed, and the filtrate was loaded onto HPLC for separation. The first stage was performed on a 5 cm-diameter PBB column (Figure S4) and 8 fractions, named as Gd-1 to Gd-8, were collected. The major components of these 8 fractions are $Gd_2@C_{79}N$, $Gd_3N@C_{80}$, $Gd_3N@C_{82}$, $Gd_3N@C_{84}$, $Gd_3N@C_{86}$, $Gd_3N@C_{88}$, $Gd_2C_2@C_{92}$, and larger fullerene and metallofullerenes, respectively. $Gd_2C_2@C_1$(51383)-C_{84} was co-eluted with $Gd_3N@C_{82}$ in the Gd-3 fraction. The Gd-3 fraction was injected onto a 1 cm-diameter PYE column for second stage separation (Figure S5). $Gd_2C_2@C_1$(51383)-C_{84} has a retention time of 78 minutes, which is very different from most other members in the Gd-3 fraction. The amount of $Gd_2C_2@C_1$(51383)-C_{84} is about 37% compared to the previously reported $Gd_3N@C_{82}$.[32] Further chromatographic purification was performed to give the purified $Gd_2C_2@C_1$(51383)-C_{84} (Figure S6).

^{13}C NMR characterization of $Y_2C_2@C_1$(51383)-C_{84}. The $Y_2C_2@C_1$(51383)-C_{84} sample was dissolved in 90% CS_2/10% CD_3COCD_3 and approximately 8mg $Cr(acac)_2$ was added as a relaxation agent. The 200MHz ^{13}C NMR spectrum was obtained after 180 hours of scan utilizing a Bruker 800 MHz instrument.

Mass-spectrometry method: Low resolution mass-spectral data (Fig. S3, S6 insets) were laser desorption/ionization time-of-flight spectra obtained on a Kratos SEQ instrument without matrix. High resolution mass-spectral data (Fig. 4, S11, S14, S15) were laser desorption/ionization time-of-flight spectra obtained on an AB Sciex 4800 MALDI TOF instrument without matrix. To investigate the isotopic distribution of fullerenes and metallofullerenes (Fig. 4, S14, S15), 60% laser power was used. For the laser ablation experiment of $Gd_2C_2@C_1$(51383)-C_{84} (Fig. S11),

60% and full laser power was used, respectively.800 MHz (Hollings Marine Laboratory facility) at 298K.

5.7.2 Supplementary figures

Supplementary Figures.

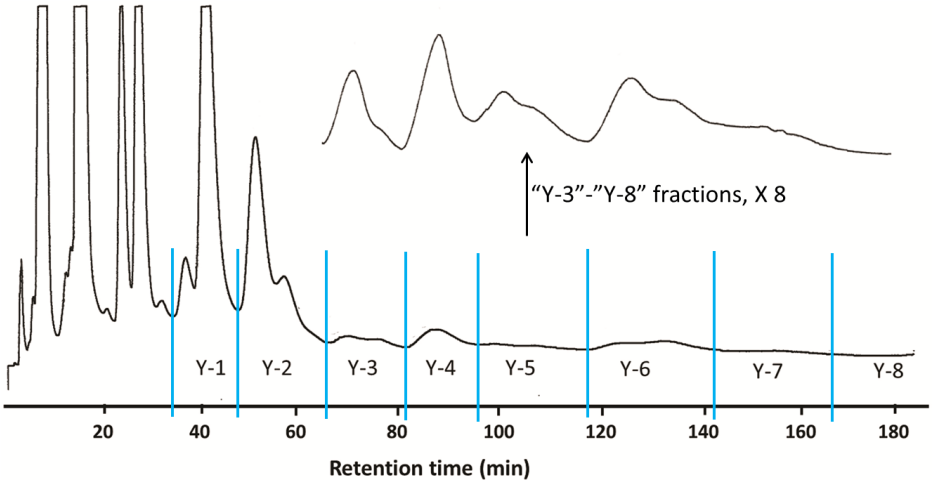

Figure S1. First-stage HPLC separation of ^{13}C enriched fullerenes and yttrium metallofullerenes on a 5 cm-diameter PBB column at room temperature, using toluene as eluent at 24 mL/min.

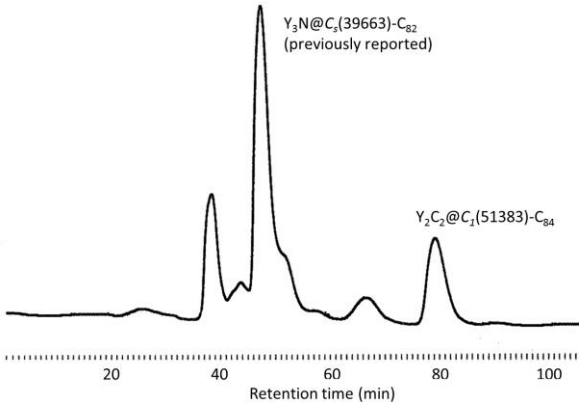

Figure S2. HPLC separation of the "Y-3" fraction on a 1 cm-diameter PYE column at room temperature, using toluene as eluent at 2 mL/min.

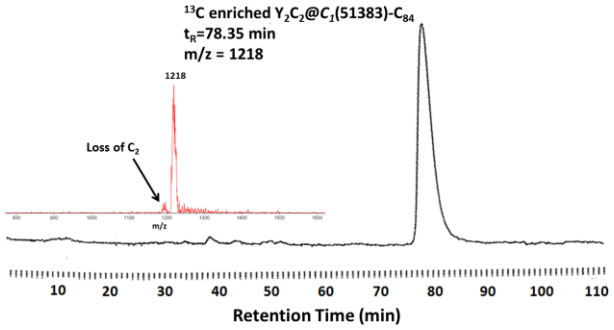

Figure S3. HPLC and mass-spectrum of ^{13}C enriched $Y_2C_2@C_1$(51383)-C_{84}.

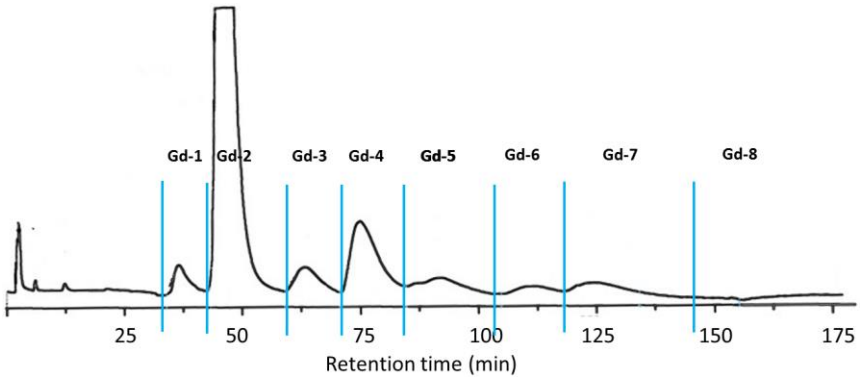

Figure S4 First-stage HPLC separation of gadolinium metallofullerenes on a 5 cm-diameter PBB column at room temperature, using toluene as eluent at 24 mL/min.

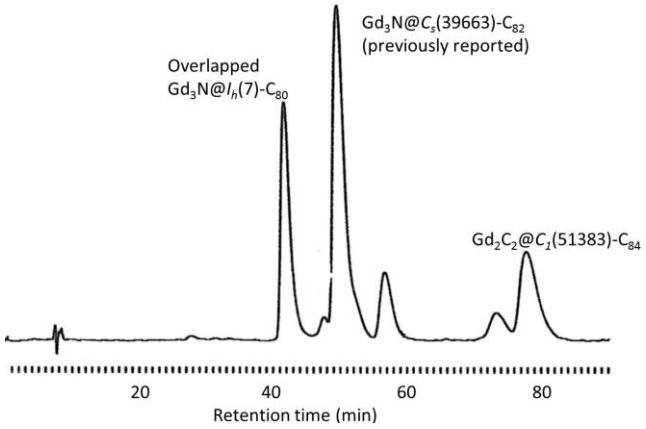

Figure S5. HPLC separation of the "Gd-3" fraction on a 1 cm-diameter PYE column at room temperature, using toluene as eluent at 2 mL/min.

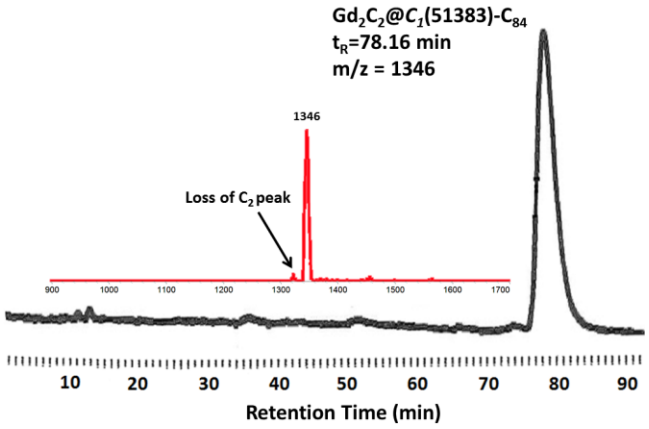

Figure S6. HPLC and mass-spectrum of $Gd_2C_2@C_1(51383)\text{-}C_{84}$.

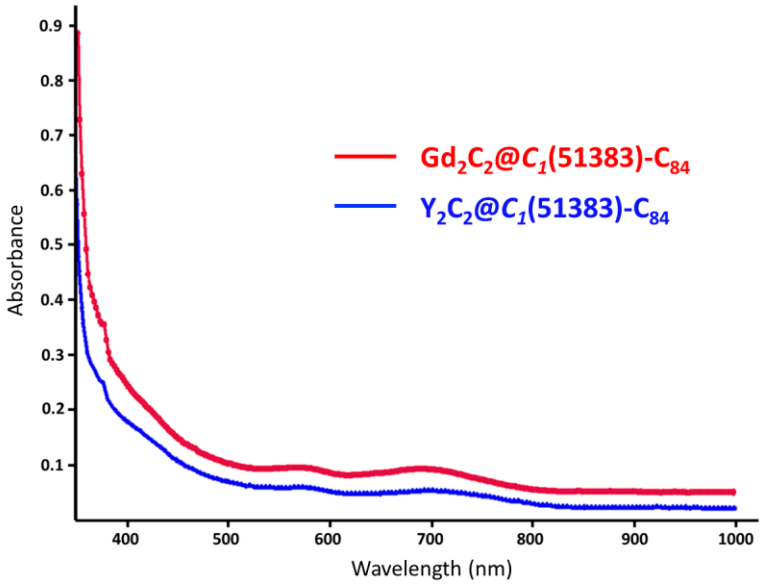

Figure S7. Stacked UV-vis spectra of $M_2C_2@C_1(51383)\text{-}C_{84}$ (M=Y, Gd) in toluene solution.

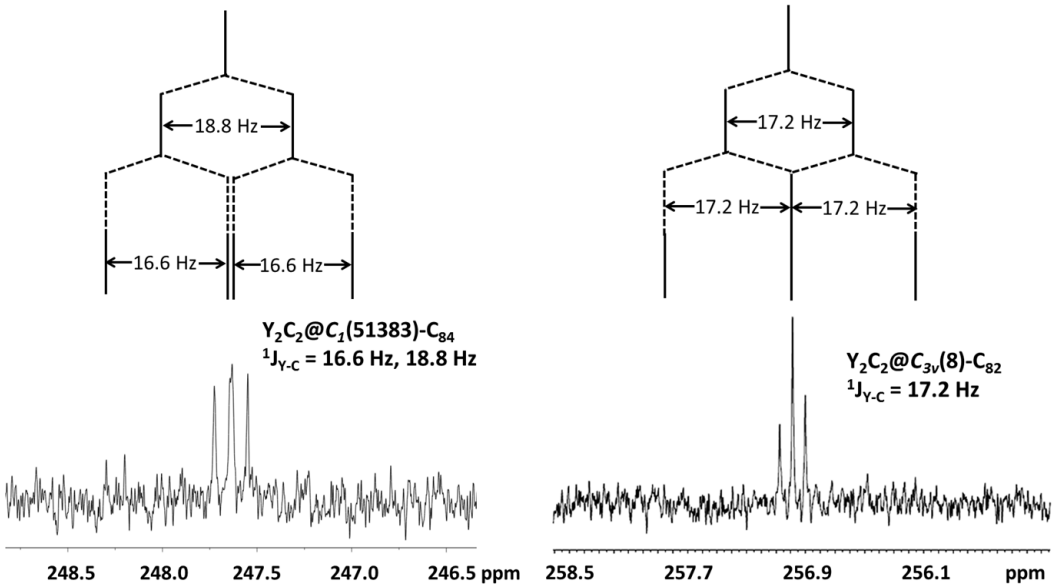

Figure S8. Expanded region of ^{13}C NMR spectrum for the cluster signal of $Y_2C_2@C_1(51383)\text{-}C_{84}$ (left) in comparison of that of $Y_2C_2@C_{3v}(8)\text{-}C_{82}$.

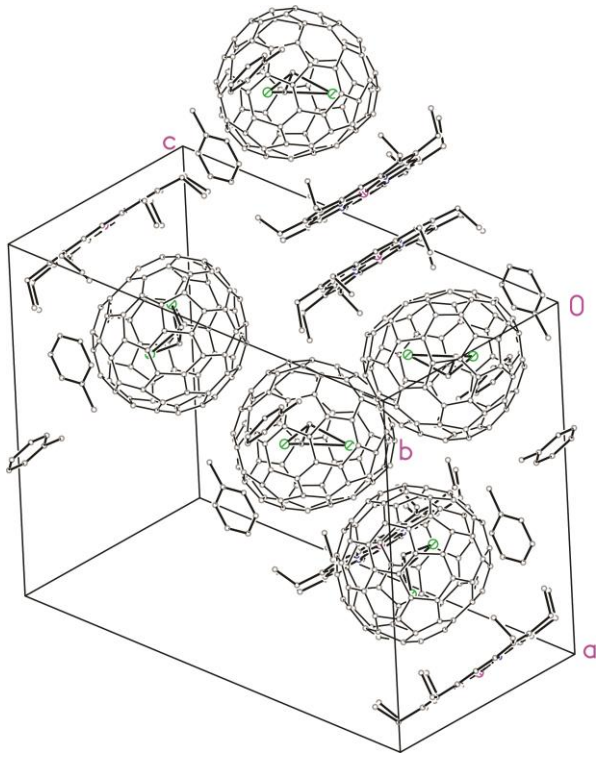

Figure S9. A view of the packing of $Gd_2C_2@C_1(51383)\text{-}C_{84}$•Ni(OEP)•2(toluene) with disorder omitted for clarity.

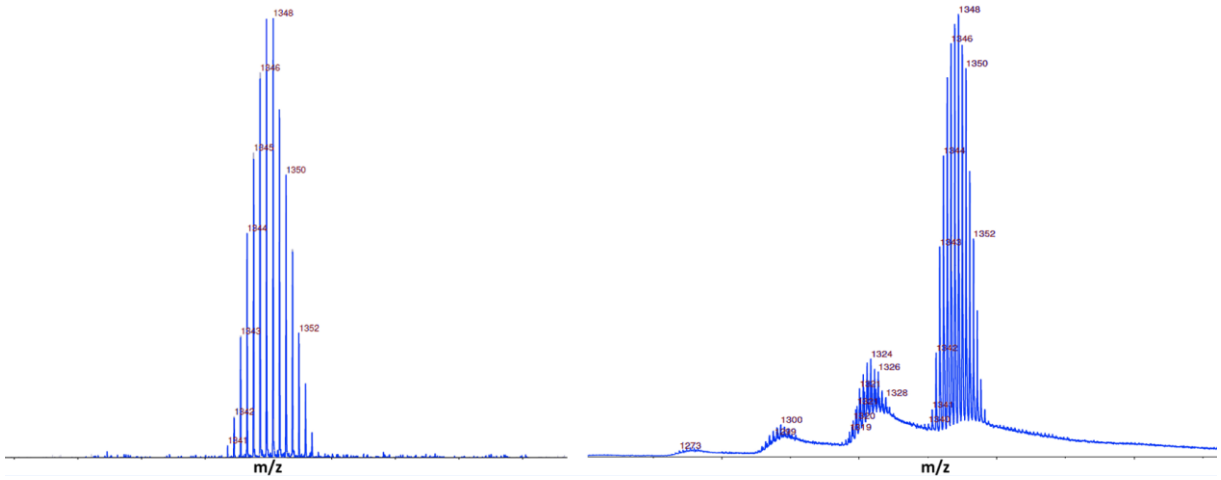

Figure S10. Laser desorption/ionization time-of-flight spectrum of $Gd_2C_2@C_1$(51383)-C_{84} under different power level. Left: 60% power. Right: full power.

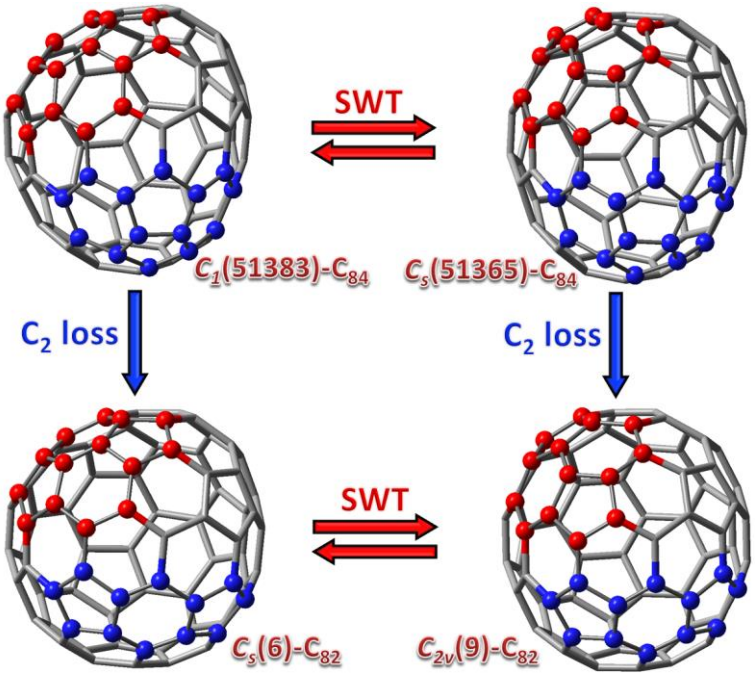

Figure S11. Interconversion map of C_1(51383)-C_{84} (this work), C_s(51365)-C_{84},*(27)* C_s(6)-C_{82},*(23)* and C_{2v}(9)-C_{82}.*(23)*

REFERENCE

(1) Kroto, H. W.; Heath, J. R.; Obrien, S. C.; Curl, R. F.; Smalley, R. E.: C_{60} - Buckminsterfullerene. *Nature* **1985**, *318*, 162-163.

(2) Ross, R. B.; Cardona, C. M.; Guldi, D. M.; Sankaranarayanan, S. G.; Reese, M. O.; Kopidakis, N.; Peet, J.; Walker, B.; Bazan, G. C.; Van Keuren, E.; Holloway, B. C.; Drees, M.: Endohedral Fullerenes for Organic Photovoltaic Devices. *Nature Mater.* **2009**, *8*, 208-212.

(3) Shultz, M. D.; Wilson, J. D.; Fuller, C. E.; Zhang, J.; Dorn, H. C.; Fatouros, P. P.: Metallofullerene-based Nanoplatform for Brain Tumor Brachytherapy and Longitudinal Imaging in a Murine Orthotopic Xenograft Model. *Radiology* **2011**, *261*, 136-143.

(4) Gan, L.-H.; Yuan, R.: Influence of Cluster Size on the Structures and Stability of Trimetallic Nitride Fullerenes $M_3N@C_{80}$. *Chem. Phys. Chem.* **2006**, *7*, 1306-1310.

(5) Dunk, P. W.; Kaiser, N. K.; Hendrickson, C. L.; Quinn, J. P.; Ewels, C. P.; Nakanishi, Y.; Sasaki, Y.; Shinohara, H.; Marshall, A. G.; Kroto, H. W.: Closed Network Growth of Fullerenes. *Nature Commun.* **2012**, *3*.

(6) Yamada, M.; Nakahodo, T.; Wakahara, T.; Tsuchiya, T.; Maeda, Y.; Akasaka, T.; Kako, M.; Yoza, K.; Horn, E.; Mizorogi, N.; Kobayashi, K.; Nagase, S.: Positional Control of Encapsulated Atoms Inside a Fullerene Cage by Exohedral Addition. *J. Am. Chem. Soc.* **2005**, *127*, 14570-14571.

(7) Chuvilin, A.; Kaiser, U.; Bichoutskaia, E.; Besley, N. A.; Khlobystov, A. N.: Direct Transformation of Graphene to Fullerene. *Nature Chem.* **2010**, *2*, 450-453.

(8) Popov, A. A.; Yang, S.; Dunsch, L.: Endohedral Fullerenes. *Chem. Rev.* **2013**.

(9) Cami, J.; Bernard-Salas, J.; Peeters, E.; Malek, S. E.: Detection of C_{60} and C_{70} in a Young Planetary Nebula. *Science* **2010**, *329*, 1180-1182.

(10) Berné, O.; Tielens, A. G. G. M.: Formation of Buckminsterfullerene (C_{60}) in Interstellar Space. *Proc. Nat. Aca. Sci.* **2012**, *109*, 401-406.

(11) Li, Z.; Cheng, Z.; Wang, R.; Li, Q.; Fang, Y.: Spontaneous Formation of Nanostructures in Graphene. *Nano Lett.* **2009**, *9*, 3599-3602.

(12) Shenoy, V. B.; Reddy, C. D.; Zhang, Y.-W.: Spontaneous Curling of Graphene Sheets with Reconstructed Edges. *ACS Nano* **2010**, *4*, 4840-4844.

(13) Kurihara, H.; Lu, X.; Iiduka, Y.; Mizorogi, N.; Slanina, Z.; Tsuchiya, T.; Nagase, S.; Akasaka, T.: $Sc_2@C_{3v}(8)$-C_{82} vs. $Sc_2C_2@C_{3v}(8)$-C_{82}: Drastic Effect of C_2 Capture on the Redox Properties of Scandium Metallofullerenes. *Chemical Commun.* **2012**, *48*, 1290-1292.

(14) Wang, T.-S.; Chen, N.; Xiang, J.-F.; Li, B.; Wu, J.-Y.; Xu, W.; Jiang, L.; Tan, K.; Shu, C.-Y.; Lu, X.; Wang, C.-R.: Russian-doll-type Metal Carbide Endofullerene: Synthesis, Isolation, and Characterization of $Sc_4C_2@C_{80}$. *J. Am. Chem. Soc.* **2009**, *131*, 16646-16647.

(15) Fowler, P. W., Manolopolous, D.E.: *An atlas of fullerenes*; Feb 27, 2007 ed.; Dover Publications, 2007.

(16) Murry, R. L.; Strout, D. L.; Odom, G. K.; Scuseria, G. E.: Role of sp^3 Carbon and 7-Membered Rings in Fullerene Annealing and Fragmentation. *Nature* **1993**, *366*, 665-667.

(17) Troshin, P. A.; Avent, A. G.; Darwish, A. D.; Martsinovich, N.; Abdul-Sada, A. K.; Street, J. M.; Taylor, R.: Isolation of Two Seven-membered Ring C_{58} Fullerene Derivatives: $C_{58}F_{17}CF_3$ and $C_{58}F_{18}$. *Science* **2005**, *309*, 278-281.

(18) Bolskar, R. D.; Benedetto, A. F.; Husebo, L. O.; Price, R. E.; Jackson, E. F.; Wallace, S.; Wilson, L. J.; Alford, J. M.: First Soluble M@C_{60} Derivatives Provide Enhanced Access to Metallofullerenes and Permit in Vivo Evaluation of Gd@$C_{60}[C(COOH)_2]_{10}$ as a MRI Contrast Agent. *J. Am. Chem. Soc.* **2003**, *125*, 5471-5478.

(19) Kroto, H. W.: The Stability of the Fullerenes C_n, with n = 24, 28, 32, 36, 50, 60 and 70. *Nature* **1987**, *329*, 529-531.

(20) Wang, C. R.; Kai, T.; Tomiyama, T.; Yoshida, T.; Kobayashi, Y.; Nishibori, E.; Takata, M.; Sakata, M.; Shinohara, H.: Materials science - C_{66} Fullerene Encaging a Scandium Dimer. *Nature* **2000**, *408*, 426-427.

(21) Stevenson, S.; Fowler, P. W.; Heine, T.; Duchamp, J. C.; Rice, G.; Glass, T.; Harich, K.; Hajdu, E.; Bible, R.; Dorn, H. C.: Materials science - A Stable Non-classical Metallofullerene Family. *Nature* **2000**, *408*, 427-428.

(22) Tan, Y.-Z.; Xie, S.-Y.; Huang, R.-B.; Zheng, L.-S.: The Stabilization of Fused-pentagon Fullerene Molecules. *Nature Chem.* **2009**, *1*, 450-460.

(23) Shi, Z. Q.; Wu, X.; Wang, C. R.; Lu, X.; Shinohara, H.: Isolation and characterization of $Sc_2C_2@C_{68}$: A Metal-carbide Endofullerene with a Non-IPR Carbon Cage. *Angew. Chem. Int. Ed.* **2006**, *45*, 2107-2111.

(24) Gorny, K. R., Pennington, C. H., Martindale, J. A., Philips, J. P., Stevenson, S. S., Heinmaa, I., Stern, R.: Molecular Orientational Dynamics of the Endohedral Fullerene $Sc_3N@C_{80}$ as Probed by ^{13}C and ^{45}Sc NMR. *Condensed Matter* **2006**, *arXiv:cond-mat/0604365*, arXiv:cond-mat/0604365.

(25) Zhang, J.; Fuhrer, T.; Fu, W.; Ge, J.; Bearden, D. W.; Dallas, J.; Duchamp, J.; Walker, K.; Champion, H.; Azurmendi, H.; Harich, K.; Dorn, H. C.: Nanoscale Fullerene Compression of an Yttrium Carbide Cluster. *J. Am. Chem. Soc.* **2012**, *134*, 8487-8493.

(26) Fu, W.; Zhang, J.; Fuhrer, T.; Champion, H.; Furukawa, K.; Kato, T.; Mahaney, J. E.; Burke, B. G.; Williams, K. A.; Walker, K.; Dixon, C.; Ge, J.; Shu, C.; Harich, K.; Dorn, H. C.: $Gd_2@C_{79}N$: Isolation, Characterization, and Monoadduct Formation of a Very Stable Heterofullerene with a Magnetic Spin State of S=15/2. *J. Am. Chem. Soc.* **2011**, *133*, 9741-9750.

(27) Olmstead, M. M.; Lee, H. M.; Stevenson, S.; Dorn, H. C.; Balch, A. L.: Crystallographic Characterization of Isomer 2 of $Er_2@C_{82}$ and Comparison with Isomer 1 of $Er_2@C_{82}$. *Chemical Commun.* **2002**, *0*, 2688-2689.

(28) Yang, T.; Zhao, X.; Li, S.-T.; Nagase, S.: Is the Isolated Pentagon Rule Always Satisfied for Metallic Carbide Endohedral Fullerenes? *Inorg. Chem.* **2012**, *51*, 11223-11225.

(29) Fu, W.; Xu, L.; Azurmendi, H.; Ge, J.; Fuhrer, T.; Zuo, T.; Reid, J.; Shu, C.; Harich, K.; Dorn, H. C.: ^{89}Y and ^{13}C NMR Cluster and Carbon Cage Studies of an Yttrium Metallofullerene Family, $Y_3N@C_{2n}$ (n=40-43). *J. Am. Chem. Soc.* **2009**, *131*, 11762-11769.

(30) Yang, H.; Lu, C.; Liu, Z.; Jin, H.; Che, Y.; Olmstead, M. M.; Balch, A. L.: Detection of a Family of Gadolinium-containing Endohedral Fullerenes and the Isolation and Crystallographic Characterization of One Member as a Metal-carbide Encapsulated inside a Large Fullerene Cage. *J. Am. Chem. Soc.* **2008**, *130*, 17296-17300.

(31) Rodriguez-Fortea, A.; Alegret, N.; Balch, A. L.; Poblet, J. M.: The Maximum Pentagon Separation Rule Provides a Guideline for the Structures of Endohedral Metallofullerenes. *Nature Chem.* **2010**, *2*, 955-961.

(32) Mercado, B. Q.; Beavers, C. M.; Olmstead, M. M.; Chaur, M. N.; Walker, K.; Holloway, B. C.; Echegoyen, L.; Balch, A. L.: Is the Isolated Pentagon Rule Merely a Suggestion for Endohedral Fullerenes? The Structure of a Second Egg-shaped Endohedral Fullerene - $Gd_3N@C_s$(39663)-C_{82}. *J. Am. Chem. Soc.* **2008**, *130*, 7854-7855.

(33) Beavers, C. M.; Zuo, T.; Duchamp, J. C.; Harich, K.; Dorn, H. C.; Olmstead, M. M.; Balch, A. L.: Tb3N@C-84: An Improbable, Egg-shaped Endohedral Fullerene that Violates the Isolated Pentagon Rule. *J. Am. Chem. Soc.* **2006**, *128*, 11352-11353.

(34) Kurotobi, K.; Murata, Y.: A Single Molecule of Water Encapsulated in Fullerene C_{60}. *Science* **2011**, *333*, 613-616.

(35) Inoue, T.; Tomiyama, T.; Sugai, T.; Okazaki, T.; Suematsu, T.; Fujii, N.; Utsumi, H.; Nojima, K.; Shinohara, H.: Trapping a C_2 Radical in Endohedral Metallofullerenes: Synthesis and Structures of $Y_2C_2@C_{82}$ (Isomers I, II, and III). *J. Phys. Chem. B* **2004**, *108*, 7573-7579.

(36) Iiduka, Y.; Wakahara, T.; Nakajima, K.; Tsuchiya, T.; Nakahodo, T.; Maeda, Y.; Akasaka, T.; Mizorogi, N.; Nagase, S.: ^{13}C NMR Spectroscopic Study of Scandium Dimetallofullerene, $Sc_2@C_{84}$ vs. $Sc_2C_2@C_{82}$. *Chemical Commun.* **2006**, 2057-2059.

(37) Xie, S. Y.; Gao, F.; Lu, X.; Huang, R. B.; Wang, C. R.; Zhang, X.; Liu, M. L.; Deng, S. L.; Zheng, L. S.: Capturing the Labile Fullerene 50 as $C_{50}Cl_{10}$. *Science* **2004**, *304*, 699-699.

(38) Tan, Y.-Z.; Han, X.; Wu, X.; Meng, Y.-Y.; Zhu, F.; Qian, Z.-Z.; Liao, Z.-J.; Chen, M.-H.; Lu, X.; Xie, S.-Y.; Huang, R.-B.; Zheng, L.-S.: An Entrant of Smaller Fullerene: C_{56} Captured by Chlorines and Aligned in Linear Chains. *J. Am. Chem. Soc.* **2008**, *130*, 15240-15241.

(39) Ziegler, K.; Mueller, A.; Amsharov, K. Y.; Jansen, M.: Capturing the Most-stable C_{56} Fullerene Cage by *in situ* Chlorination. *Chem. Asian J.* **2011**, *6*, 2412-2418.

Chapter 6 Functionalization of Gadolinium Based Endohedral Metallofullerenes by the Bingel Reaction

Part of this chapter is adopted from the manuscript published on *Journal of the American Chemical Society* with appropriate modifications with the permission of the American Chemical Society. Full text of the published manuscript entitled "$Gd_2@C_{79}N$: isolation, characterization and monoadduct formation of a very stable heterofullerene with a magnetic spin state of S=15/2", by Wujun Fu, Jianyuan Zhang, Tim Fuhrer, Hunter Champion, Ko Furukawa, Tatsuhisa Kato, James E. Mahaney, Brian G. Burke, Keith A. Willaims, Kenneth Walker, Caitlyn Dixon, Jiechao Ge, Chunying Shu, Kim Harich, and Harry C. Dorn, can be obtained at http://pubs.acs.org/doi/pdf/10.1021/ja202011u.

6.1 Introduction

The functionalization of gadolinium based endohedral metallofullerenes (EMFs) has been a fascinating topic. Although the paramagnetism of the Gd^{3+} precludes the ^{13}C NMR as an approach to characterize the products, it is also the paramagnetism that provides the products intriguing promise, including the application as magnetic resonance imaging (MRI) contrast agents[1] and other possibilities.

In the family of gadolinium based EMFs, two members are very special and may lead to novel properties of their derivatives. One of them is the $Gd_2@C_{79}N$. Similar to $Tb_2@C_{79}N$ and $Y_2@C_{79}N$,[2] $Gd_2@C_{79}N$ is a special EMF produced in the arc-synthesis[3] when metal oxide and nitrogen gas are both present, but in much higher yield. These EMFs have a nitrogen atom on the cage and form a sub-group of EMF, the endohedral heterofullerenes (EHFs). The two metal ions in $M_2@C_{79}N$ (M = Tb, Y, Gd) molecules transfer 5 electrons to the azafullerene cage and trap an unpaired electron between the two metal ions. Therefore, they are electronic paramagnetic resonance (EPR) active at room temperature. In other word, they can be viewed as room temperature radicals that are much more stable than TEMPO because the spin is trapped inside the cage. Among the three, $Gd_2@C_{79}N$ is the most interesting because it has 15/2 spin due to the contribution of the 7 unpaired electrons from each Gd^{3+} ion. The derivatives of the $Gd_2@C_{79}N$

may be applied in molecular electronics where a stable radical is wanted. Also, no derivative of EHFs had been reported so the functionalization of $Gd_2@C_{79}N$ would be an important endeavor by its own right.

The $Gd_3N@C_s(51365)\text{-}C_{84}$[4] is a special member of the TNT-EMF family. It is the most abundant "large cage" (over 80 carbons) TNT-EMF and also the most abundant non-IPR EMF of all kinds. The reactivity of both series has not been very well understood yet. Moreover, it has an egg-shape with a gadolinium ion associated with the pentalene motif; therefore, an enhanced dipole moment can be predicted for this molecule which could open the possibility of special features for its derivatives as molecular electronics and MRI contrast agents (see previous chapter). In this chapter, I present the attempts to functionalize $Gd_2@C_{79}N$ and $Gd_3N@C_{84}$ via Bingel Reactions.

6.2 Functionalization of $Gd_2@C_{79}N$

6.2.1 The inert nature of the $Gd_2@C_{79}N$ as a radical

As a radical the $Gd_2@C_{79}N$ did not show reactivity to form dimers or react with radical scavengers, as found out in our preliminary study by our group member Wujun Fu. The reactions he tried are summarized in Figure 1.

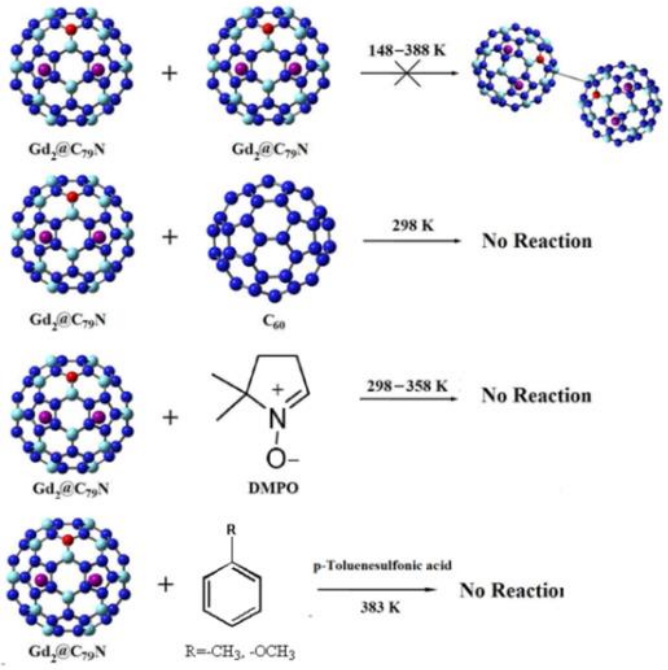

Figure 1. Reaction attempts made by Wujun Fu that showed the inert property of $Gd_2C_{79}N$ as a radical.

6.2.2 Comparative Diels-Alder reactivity study of $Y_2@C_{79}N$ and $Gd_2@C_{79}N$

Although the enhanced stability of the icosahedral $(C_{80})^{6-}$ cage is well documented, the stability of the isoelectronic $(C_{79}N)^{5-}$ cage is not as well recognized. As noted above, a surprising feature of $Gd_2@C_{79}N$ was the significantly higher yield of $Gd_2@C_{79}N$ obtained in the separation process in comparison with $Y_2@C_{79}N$. This enhanced yield is either due to a higher inherent yield in the K-H electric-arc generator process and/or lower chemical Diels-Alder reactivity of $Gd_2@C_{79}N$ in comparison with $Y_2@C_{79}N$ during the chemical cyclopentadiene Merrifield resin separation process.[5] To test between these alternatives, we prepared a two-component mixture (in toluene) containing nearly equal quantities of pure $Gd_2@C_{79}N$ and $Y_2@C_{79}N$ samples; the overall process is outlined in Figure 2. As expected, these two heterofullerenes have very similar chromatographic retention times and are only slightly resolved on a PYE column. A two-

component mixture of $Gd_2@C_{79}N$ and $Y_2@C_{79}N$ was applied a second time to the CPDE-MPR column as summarized in Figure 2. Greater than 70% of the mixture was recovered from the (CPDE-MPR) column and the resulting mixture exhibits a slight enhancement (~5-10%) in the concentration of the $Gd_2@C_{79}N$ species. This preferential reaction of the $Y_2@C_{79}N$ species was confirmed by heating the recovered cyclopentadiene-functionalized Merrifield peptide resin under reflux in toluene for 12 h. The resulting toluene solution was concentrated and mass spectral analysis on the recovered sample indicates a preponderance of the $Y_2@C_{79}N$ species (Figure 3c). These results confirm the very low chemical reactivity of both $Gd_2@C_{79}N$ and $Y_2@C_{79}N$ toward the cyclopentadiene moiety on the Merrifield peptide supported column. Also, I observed a slightly enhanced Diels-Alder chemical reactivity of the $Y_2@C_{79}N$ species in comparison with $Gd_2@C_{79}N$ toward the supported cyclopentadiene moiety. I could also conclude that Diels-Alder reaction would not be a good choice for the functionalization of $Gd_2@C_{79}N$.

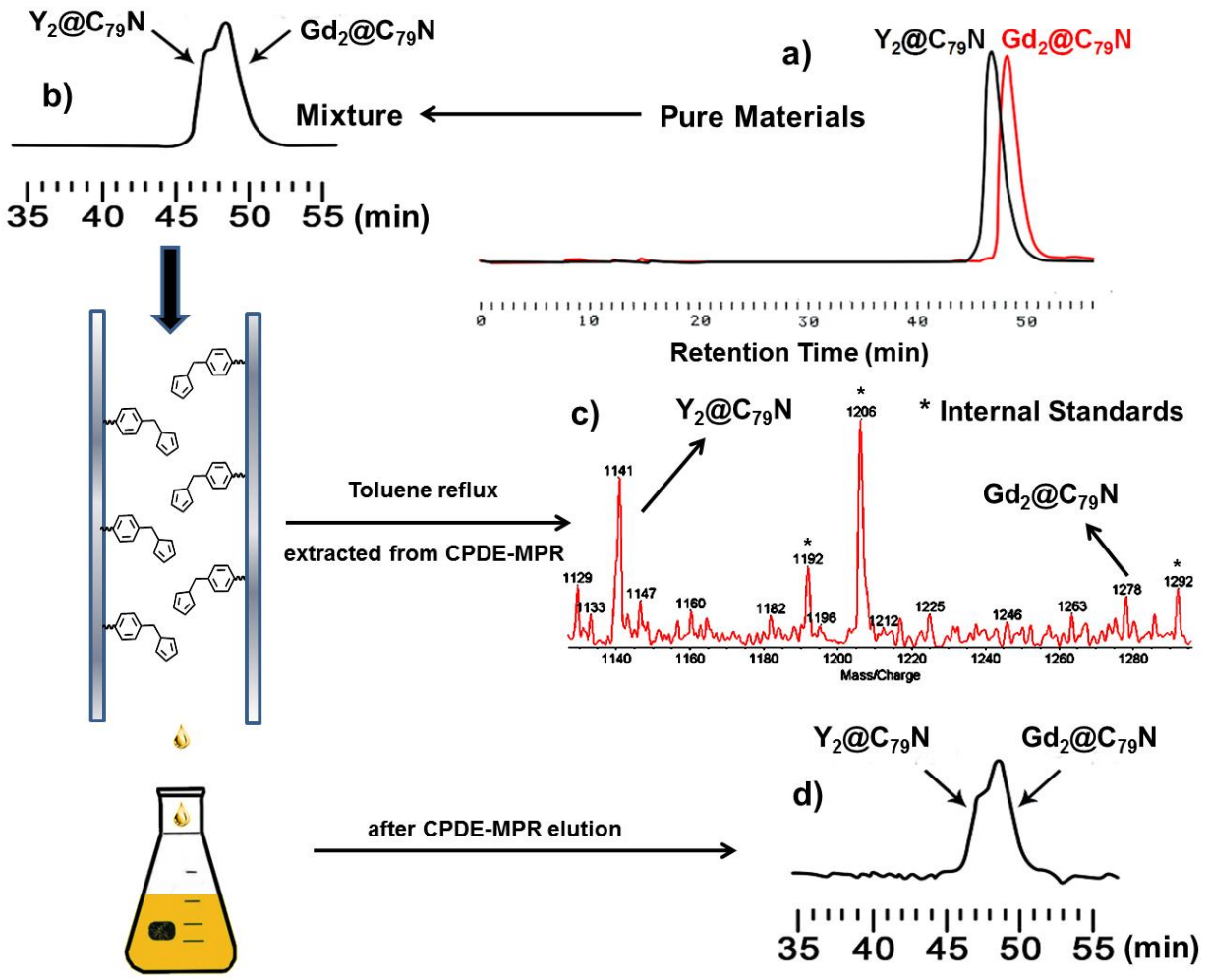

Figure 2. Reactivity comparison between $Y_2@C_{79}N$ and $Gd_2@C_{79}N$ towards Diels-Alder reaction. a) Overlapped chromatograms of pure $Gd_2@C_{79}N$ (red) and $Y_2@C_{79}N$ (a 4 x 250 mm 5-PYE column; λ=390 nm; flow rate 2.0 mL/min; toluene as eluent; 25 ℃). b) Chromatogram of the mixture of $Gd_2@C_{79}N$ and $Y_2@C_{79}N$ in nearly equal amounts. C) Negative ionization LD-TOF mass spectrum of recovered $Gd_2@C_{79}N$ and $Y_2@C_{79}N$ mixture from CPDE-MPR by heating at 110 ℃, with internal standards added (1192= $C_{22}H_{13}O_6N_3P_3F_{36}$, 1206= $C_{23}H_{15}O_6N_3P_3F_{36}$, 1292=$C_{24}H_{13}O_6N_3P_3F_{40}$). d) Chromatogram of the mixture of $Gd_2@C_{79}N$ and $Y_2@C_{79}N$ after the reaction.

6.2.3 Synthesis of the Bingel monoadduct of the $Gd_2@C_{79}N$

In spite of this low chemical reactivity, the first successful functionalization of $Gd_2@C_{79}N$ was achieved via a Bingel cyclopropanation with diethyl bromomalonate, but only in the presence of DMF which could catalyze the reaction.[6] Approximately 100 μg of $Gd_2@C_{79}N$ was dissolved in 2 mL toluene, and ~20 equivalent of diethyl bromomalonate (Aldrich Chemical Co.) and ~10 equivalents of 1,8-diazabicycloundec-7-ene (DBU, Aldrich Chemical Co.) was added for the synthetic preparation and reactivity comparison study, respectively. Finally, a drop of DMF was added as a catalyst. The reaction mixtures were degassed and subsequently stirred at room temperature for 60 min. The product was isolated by HPLC and mass spectrometry as shown in Figure 3 below. However due to the very small amount of the product obtained I was not able to conduct further structural characterization the reaction site.

To directly compare the reactivity of $Gd_3N@C_{80}$, $Sc_3N@C_{80}$ and $Gd_2@C_{79}N$, we prepared toluene solutions of these three purified metallofullerenes in nearly equal molarities and performed Bingel reactions under the same conditions as stated above. All three reaction mixtures were stirred for 1 h and then subjected to HPLC analysis. As summarized in Figure 3, significantly higher reactivity was observed for $Gd_3N@C_{80}$ as seen in a higher overall yield of monoadduct and significant multiadduct formation (Figure 3a). This reaction was previously reported for $Gd_3N@C_{80}$ even in the absence of DMF.[7] In contrast, a lower yield of the $Gd_2@C_{79}N$ monoadduct was obtained after DMF was added to the reaction mixture (Figure 3c). Similar low reactivity was also observed for the $Sc_3N@C_{80}$ (Figure 3e). The HPLC chromatograms also show that $Gd_3N@C_{80}$ was completely consumed, while about 73% $Sc_3N@C_{80}$ and 83% $Gd_2@C_{79}N$ were retained based on respective peak areas. This suggests that $Gd_3N@C_{80}$ has much higher reactivity toward this Bingel reaction than $Sc_3N@C_{80}$ and $Gd_2@C_{79}N$, which reacts in a similar fashion, but to very limited extent. $Gd_2@C_{79}N$ has even

slightly lower reactivity than $Sc_3N@C_{80}$, which had been reported to be unreactive towards Bingel reaction.[8] Hitherto, the reason for the high stability of $Gd_2@C_{79}N$ has not been clearly understood.

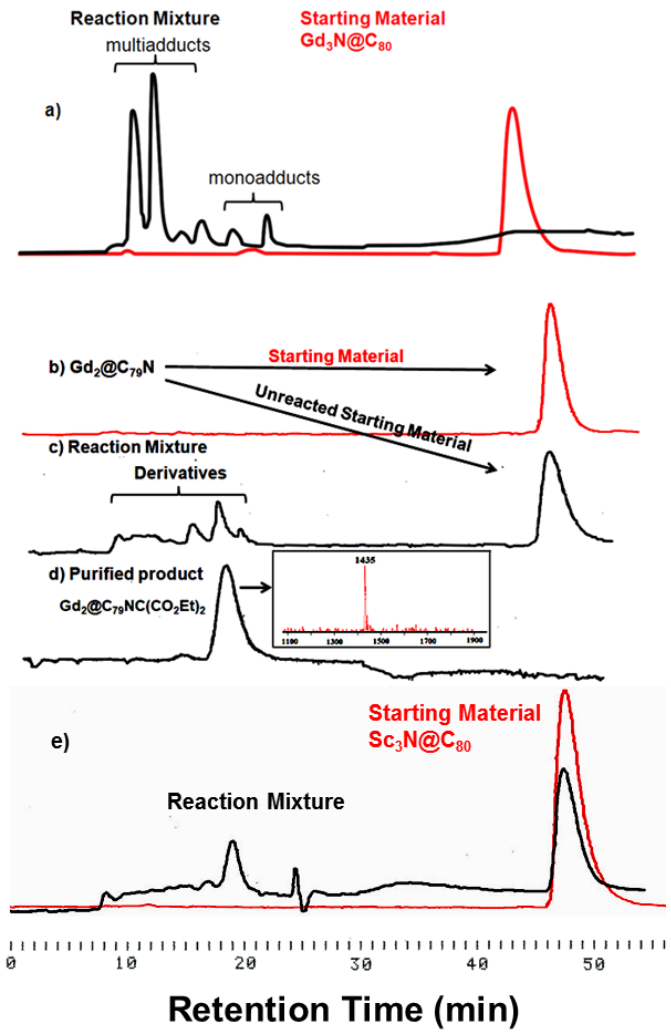

Figure 3. HPLC on 5-PYE column using toluene as eluent with 2 mL/min flow rate for a) $Gd_3N@C_{80}$ (red) and its reaction mixture (black) in Bingel reaction. b) pure $Gd_2@C_{79}N$. c) the reaction mixture of $Gd_2@C_{79}N$ from the Bingel reaction. d) the purified monoderivative, $Gd_2@C_{79}NC(CO_2Et)_2$ (inset: MALDI-TOF spectrum of the monoderivative). e) $Sc_3N@C_{80}$ (red) and its reaction mixture (black) in Bingel reaction.

6.3 Functionalization of $Gd_3N@C_{84}$.

The reactivity of the large cage gadolinium EMFs had been preliminarily studied by Echegoyen and coworkers.[7,9] They performed the Bingel reaction on a series of gadolinium TNT-EMFs by stirring the TNT-EMF with DBU and diethyl bromomalonate in o-dichlorobenzene under argon. They concluded that in contrast to the higher reactivity of $Gd_3N@C_{80}$ which forms multiadducts, the large cages had much lower reactivity. Even under elevated temperatures and for longer reaction times, the $Gd_3N@C_{82}$ and $Gd_3N@C_{84}$ only formed monoadducts, and $Gd_3N@C_{88}$ did not react. The addition sites of the monoadduct for $Gd_3N@C_{82}$ and $Gd_3N@C_{84}$ were not clear either.

Aiming to reveal the reaction sites on $Gd_3N@C_{84}$, I repeated the Bingel reaction for a single-crystal analysis of the derivative. I substituted the diethyl bromomalonate with the dibenzyl bromomalonate (obtained via a single transesterification step) which might help the crystallization process. The reaction procedure was basically the same as Echegoyen's report with small modifications. About 500 μg $Gd_3N@C_{84}$ was dissolved in 5 mL toluene (instead of o-dichlorobenzene, reason *vide infra*) and the solution was deaerated by argon flow for 15 minutes. Approximately 30-40 equivalents of dibenzyl bromomalonate (~4 mg) were injected in toluene solution followed by the addition of 1 drop of DBU. The reaction mixture was deaerated for 3 additional minutes and stirred for another 60 minutes. Due to very limited sample amount, I did not use flash chromatography as described in the literature. Alternatively, I reduced the solvent amount with nitrogen blowing to ~1 mL and filtered the mixture with a 0.2 μm pore-sized syringe filter. For a faster solvent evaporation I used toluene instead of o-dichlorobenzene as the reaction solvent. Although Echegoyen and coworkers used o-dichlorobenzene in their reaction,[7]

toluene had been used as reaction solvent for the earliest Bingel reactions by Bingel[10*] and Hirsch.[11,12] The toluene solution was injected onto a 5-PYE column for HPLC analysis and product purification (Figure 4). I found, surprisingly, despite the incomplete reaction described by Echegoyen group, all the starting $Gd_3N@C_{84}$ was consumed. Moreover, only a small portion of the products appeared in the expected "monoadduct region" (30-50 min); instead, large peaks appeared between 20 and 30 minutes, indicating the formation of multiadducts. The huge peak at 15-17 minutes was ascribed to the dibenzyl bromomalonate and its byproduct (dibenzyl malonate), which were removed by flash chromatography in the literature.

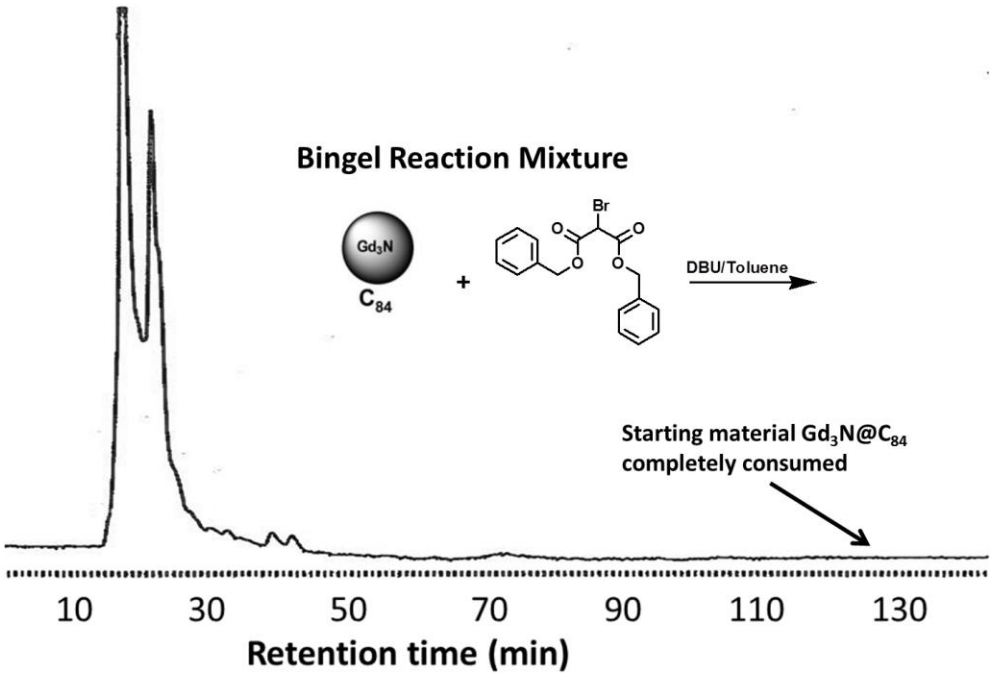

Figure 4. Chromatogram of the Bingel reaction mixture of $Gd_3N@C_{84}$, on a 5-PYE column at room temperature using toluene as eluent with 1 mL/min flow rate.

* Ref. 10 was written in German.

The multiadducts that were eluted between 20 and 30 minutes were collected and further separated by multi-stage HPLC. Two purified derivatives were obtained (Figure 5). MALDI-TOF mass-spectra of these purified products showed that they are two isomers of triadducts.

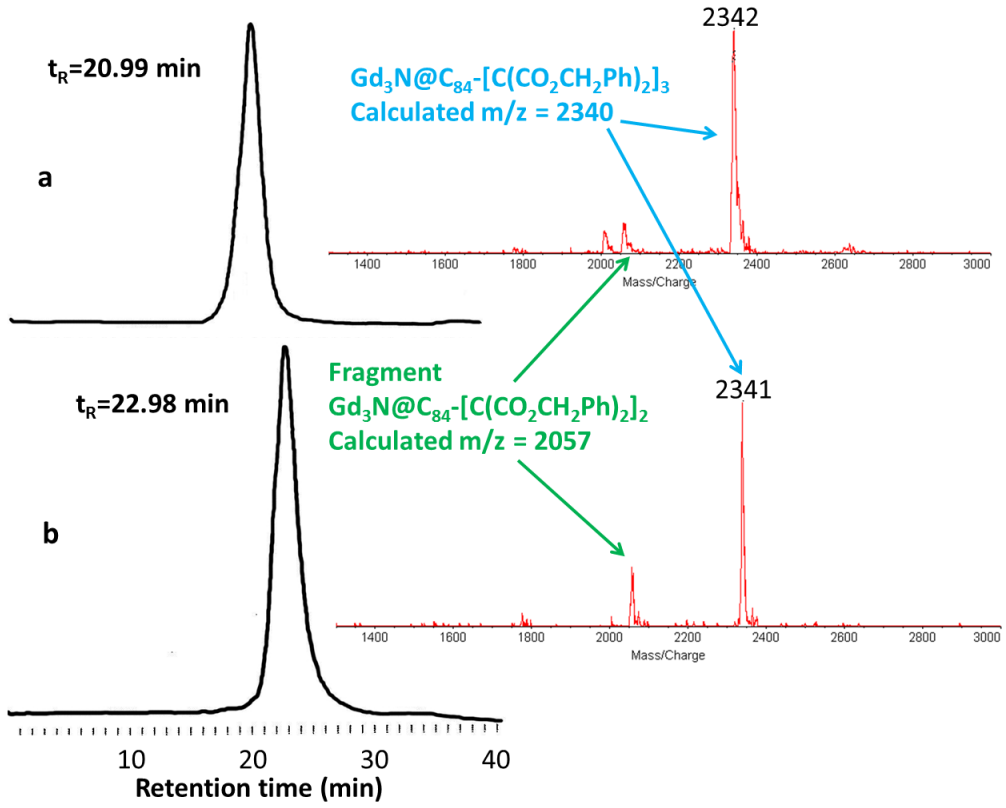

Figure 5. HPLC traces and mass spectra of the purified Bingel triadducts of $Gd_3N@C_{84}$. a) chromatogram and mass-spectrum of triadduct 1. b) chromatogram and mass-spectrum of triadduct 2.

The reason that I obtained triadducts following the reaction conditions that the Echegoyen group used only to get monoadduct remains mysterious to me. Three possible explanations are: 1) dibenzyl bromomalonate is more reactive than diethyl bromomalonate; 2) toluene could enhance the reaction compared to o-dichlobenzene; and 3) during the nitrogen flow the concentration of the reactants significantly increased that helped the reaction go completion. The latter 2

explanations are more plausible in my opinion. With higher availability of the starting material, the mystery of enhanced reactivity could be figured out by parallel experiments.

Another important factor left for future work is the structural characterization of the two regioisomers. These two purified derivatives, approximately 100-200 μg each (triadduct 1 is in higher abundance), are being analyzed by our collaborators in the Balch laboratory at UC Davis with single crystal structural determination. Alternatively, ^{13}C enriched $Y_3N@C_{84}$ could be functionalized in the same fashion and the derivatives could be analyzed by ^{13}C NMR.

REFERENCE

(1) Mikawa, M.; Kato, H.; Okumura, M.; Narazaki, M.; Kanazawa, Y.; Miwa, N.; Shinohara, H.: Paramagnetic Water-soluble Metallofullerenes Having the Highest Relaxivity for MRI Contrast Agents. *Bioconjugate Chem.* **2001**, *12*, 510-514.

(2) Zuo, T.; Xu, L.; Beavers, C. M.; Olmstead, M. M.; Fu, W.; Crawford, T. D.; Balch, A. L.; Dorn, H. C.: $M_2@C_{79}N$ (M = Y, Tb): Isolation and Characterization of Stable Endohedral Metallofullerenes Exhibiting M-M Bonding Interactions inside Aza[80]fullerene Cages. *J. Am. Chem. Soc.* **2008**, *130*, 12992-12997.

(3) Kratschmer, W.; Lamb, L. D.; Fostiropoulos, K.; Huffman, D. R.: Solid C_{60} - A New Form Of Carbon. *Nature* **1990**, *347*, 354-358.

(4) Zuo, T.; Walker, K.; Olmstead, M. M.; Melin, F.; Holloway, B. C.; Echegoyen, L.; Dorn, H. C.; Chaur, M. N.; Chancellor, C. J.; Beavers, C. M.; Balch, A. L.; Athans, A. J.: New Egg-shaped Fullerenes: Non-Isolated Pentagon Structures of $Tm_3N@C_s(51365)$-C_{84} and $Gd_3N@C_s(51365)$-C_{84}. *Chem. Comm.* **2008**, 1067-1069.

(5) Ge, Z. X.; Duchamp, J. C.; Cai, T.; Gibson, H. W.; Dorn, H. C.: Purification of Endohedral Trimetallic Nitride Fullerenes in a Single, Facile Step. *J. Am. Chem. Soc.* **2005**, *127*, 16292-16298.

(6) Pinzon, J. R.; Zuo, T.; Echegoyen, L.: Synthesis and Electrochemical Studies of Bingel-Hirsch Derivatives of $M_3N@I_h$-C_{80} (M = Sc, Lu). *Chem. Eur. J.* **2010**, *16*, 4864-4869.

(7) Chaur, M. N.; Melin, F.; Athans, A. J.; Elliott, B.; Walker, K.; Holloway, B. C.; Echegoyen, L.: The Influence of Cage Size on the Reactivity of Trimetallic Nitride Metallofullerenes: a Mono- and Bis-Methanoadduct of $Gd_3N@C_{80}$ and a Monoadduct of $Gd_3N@C_{84}$. *Chem. Comm.* **2008**, *0*, 2665-2667.

(8) Cardona, C. M.; Kitaygorodskiy, A.; Echegoyen, L.: Trimetallic Nitride Endohedral Metallofullerenes: Reactivity Dictated by the Encapsulated Metal Cluster. *J. Am. Chem. Soc.* **2005**, *127*, 10448-10453.

(9) Alegret, N.; Chaur, M. N.; Santos, E.; Rodriguez-Fortea, A.; Echegoyen, L.; Poblet, J. M.: Bingel-Hirsch Reactions on Non-IPR $Gd_3N@C_{2n}$ (2n=82 and 84). *J. Org. Chem.* **2010**, *75*, 8299-8302.

(10) Bingel, C.: Cyclopropanierung von Fullerenen. *Ber.* **1993**, *126*, 1957-1959.

(11) Hirsch, A.; Lamparth, I.; Karfunkel, H. R.: Fullerene Chemistry in Three Dimensions: Isolation of Seven Regioisomeric Bisadducts and Chiral Trisadducts of C_{60} and Di(ethoxycarbonyl)methylene. *Angew. Chem. Int. Ed.* **1994**, *33*, 437-438.

(12) Hirsch, A.; Lamparth, I.; Groesser, T.; Karfunkel, H. R.: Regiochemistry of Multiple Additions to the Fullerene Core: Synthesis of a Th-Symmetric Hexakis adduct of C_{60} with Bis(ethoxycarbonyl)methylene. *J. Am. Chem. Soc.* **1994**, *116*, 9385-9386.

Chapter 7 Magnetic Moments of Gadolinium Endohedral Metallofullerenes

7.1 Introduction

As mentioned in Chapter 1, gadolinium endohedral metallofullerenes (EMFs) are excellent candidates for next generation magnetic resonance imaging (MRI) contrast agents for their super high relaxivity,[1,2] non-cytotoxicity and longer retention near the tumor.[3] Also in Chapter 4 I discussed the electronic dipole moment of trimetallic nitride template (TNT) EMFs and predicted that the enhanced dipole moment caused by pentalene group may have profound influence in their MRI. In this regard, there is a more direct factor that is essential to the MRI contrast agent candidates: the magnetic moment. The experimental magnetic moment is often referred as the effective magnetic moment, or μ_{eff}. It is a measure of the local magnetism generated by paramagnetic materials under an external magnetic field, and probably is the most important physical property to describe paramagnetism. The μ_{eff} is defined as:

$$\mu_{eff} = (3k/N)^{1/2}(\chi T)^{1/2} = [g^2 s(s+1)]^{1/2}\ \mu_B$$

in which k is the Boltzmann constant, N is the Avogadro's number, χ is the magnetic susceptibility, g is electronic g factor, s is the spin of the nuclei, and μ_B is the Bohr magneton. The unit of μ_{eff} is μ_B.

Relaxivity r_1 is the physical term to reflect the effectiveness of T_1 weighted MR imaging, which is obtained from experimentally measured T_1. According to the Solomon-Bloembergen-Morgan equation,[4] the relaxation rate, $1/T_1$, is consist of two terms which are dipole-dipole interaction and scalar contact (SC) interaction:

$$\frac{1}{T_1} = \frac{1}{T_1^{DD}} + \frac{1}{T_1^{SC}}$$

The two terms are determined by the equations below:

$$\frac{1}{T_1^{DD}} = \frac{2}{15}\frac{\gamma_1^2 g^2 \mu_B^2 s(s+1)}{r^6}\left[\frac{3\tau_{c1}}{(1+\omega_I^2 3\tau_{c1}^2)} + \frac{7\tau_{c2}^2}{(1+\omega_s^2\tau_{c2}^2)}\right]$$

$$\frac{1}{T_1^{SC}} = \frac{2}{3}s(s+1)\left(\frac{A}{\hbar}\right)^2\left[\frac{\tau_e^2}{(1+\omega_s^2\tau_{e2}^2)}\right]$$

In the case of gadolinium EMFs, the dipole-dipole term is more important. From the definition of μ_{eff}, it can be derived that

$$\mu_{eff}{}^2 \propto \frac{1}{T_1^{DD}}$$

Therefore, it is important to investigate the molecular magnetic moment of gadolinium EMFs. The μ_{eff} of $Gd@C_{82}$ has been experimentally measured to be 6.90 μ_B.[5] However, as the gadolinium TNT-EMFs become more promising in MRI than gadolinium monometallic EMF, their molecular magnetic moment study has fallen behind. In this chapter, I describe our investigation of the magnetic properties of gadolinium TNT-EMFs with a superconducting quantum interference device (SQUID) in collaboration with Dr. Gorden Yee.

7.2 Experimental Methods

7.2.1 Purification of samples

Gadolinium based EMFs were synthesized in commission at LUNA Innovations and the empty cages were removed by chemical separation[6] as described in previous chapters. The HPLC traces for the raw soot extract and for the resulting mixture after the chemical separation are displayed

in Figure 1. Only the two species with higher yield, namely, the $Gd_3N@C_{80}$ and $Gd_3N@C_{84}$, were in sufficient amounts for SQUID experiment.

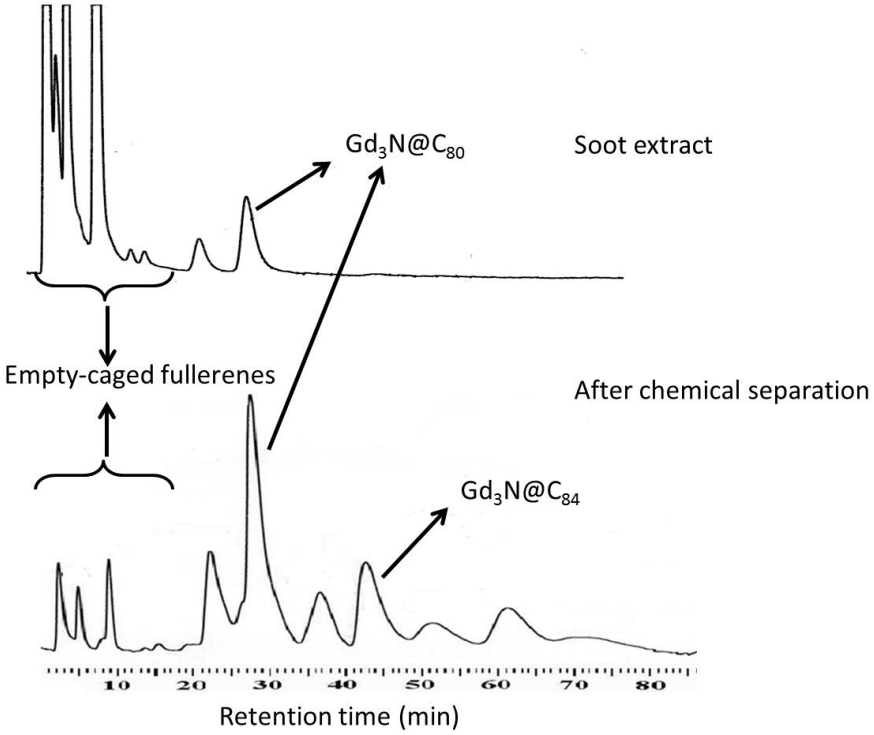

Figure 1. HPLC traces of gadolinium EMFs before (top) and after (bottom) chemical separation.

After further multi-stage HPLC process, $Gd_3N@C_{80}$ and $Gd_3N@C_{84}$ samples were isolated and the purity of both were checked with chromatography and mass-spectrometry (Figure 2).

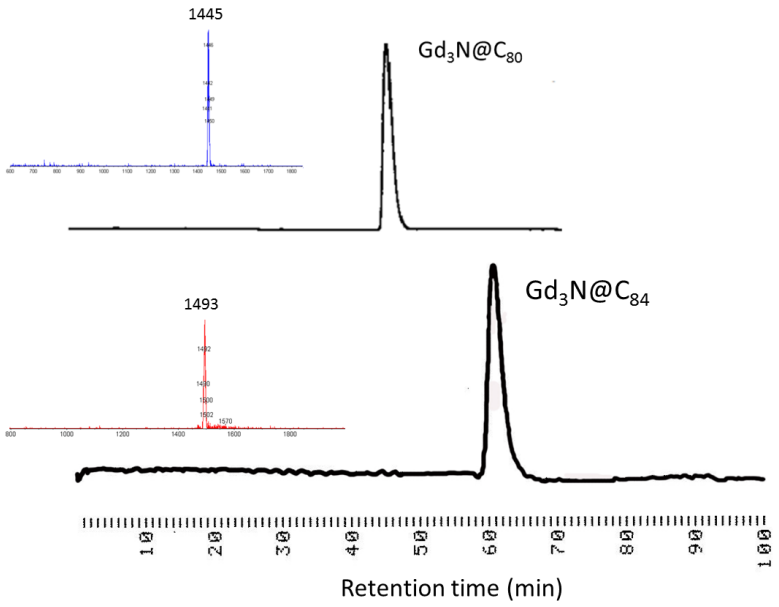

Figure 2. HPLC and mass spectral characterization of purified $Gd_3N@C_{80}$ (top) and $Gd_3N@C_{84}$ (bottom).

7.2.2 The SQUID measurements

The SQUID measurements were performed in NMR tubes. Four samples were prepared for the measurements: $Gd_3N@C_{80}$, $Gd_3N@C_{84}$, $Gd_3N@C_{80}$ diluted with C_{60}, and $Gd_3N@C_{84}$ diluted with C_{60}. As a general method, the solvent was removed from toluene solution of the samples and diethyl ether was added to wash away the oily residuals. The suspension of fullerene and EMF in diethyl ether was filtered with a fine fritted funnel (pore size 4.0-5.5 μm) under reduced pressure. The dry powder left in the funnel was collected and used for the SQUID measurements.

The magnetization of the sample was measured at temperatures from 5K to 300K, in increments of 5K. Independent measurements of an empty NMR tube and an NMR tube with C_{60} was performed in same fashion for diamagnetic corrections.

7.3 Results and Discussion

The magnetization was plotted vs temperature as shown in Figure 3. As expected for paramagnetic materials, all samples showed high magnetization at low temperature and low magnetization as the temperature went up. Meanwhile, I also note that for the pure samples the magnetization went all the way down and for the C_{60} diluted samples, both curves showed a peak at low temperature.

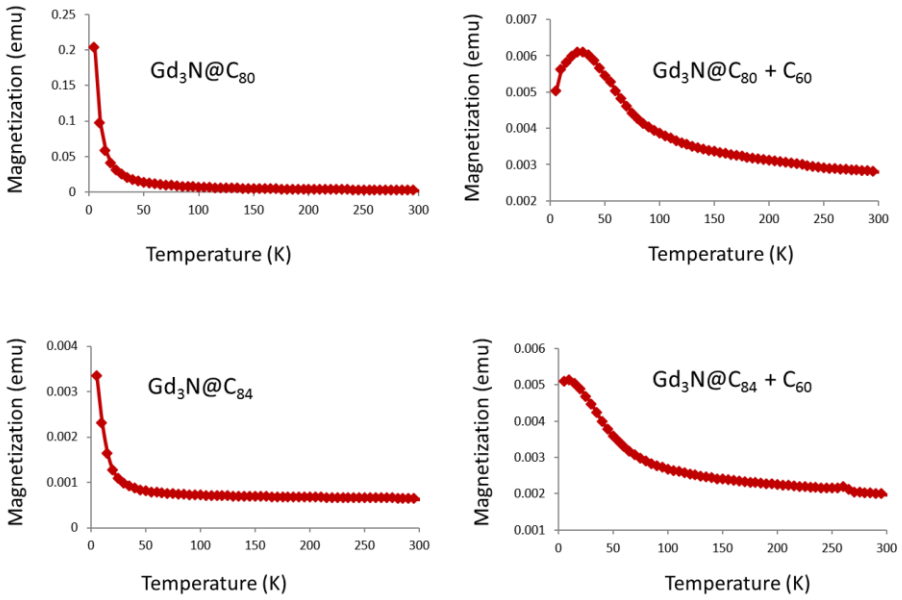

Figure 3. Magnetization of gadolinium EMFs as a dependence of temperature.

According to the Curie-Weiss law,

$$\chi^{-1} = \frac{T - \theta}{C}$$

where χ is the molar magnetic susceptibility, T is the temperature, C is a material specific Curie constant, and θ is a correct factor called Curie temperature. When θ is positive, it is called ferromagnetic in sign. When θ is negative, it is called antiferromagnetic in sign.

The experimental χ values contain three factors:

$$\chi_{obs} = \chi + \chi_d + \alpha$$

where χ is the intrinsic magnetic susceptibility of the molecule of interest, χ_d is a small negative contribution from diamagnetic material. In the data for Gd EMFs, this term is very negligibly small. Term α is the contribution from residual ferromagnetic material in the samples (e.g. iron content at the nanogram scale), which could be mathematically corrected by fitting the data into Curie-Weiss law.[7] After correction for the diamagnetic and ferromagnetic content in the sample, the χ for the paramagnetic content is used to make the χ^{-1} vs T graphs in Figure 4.

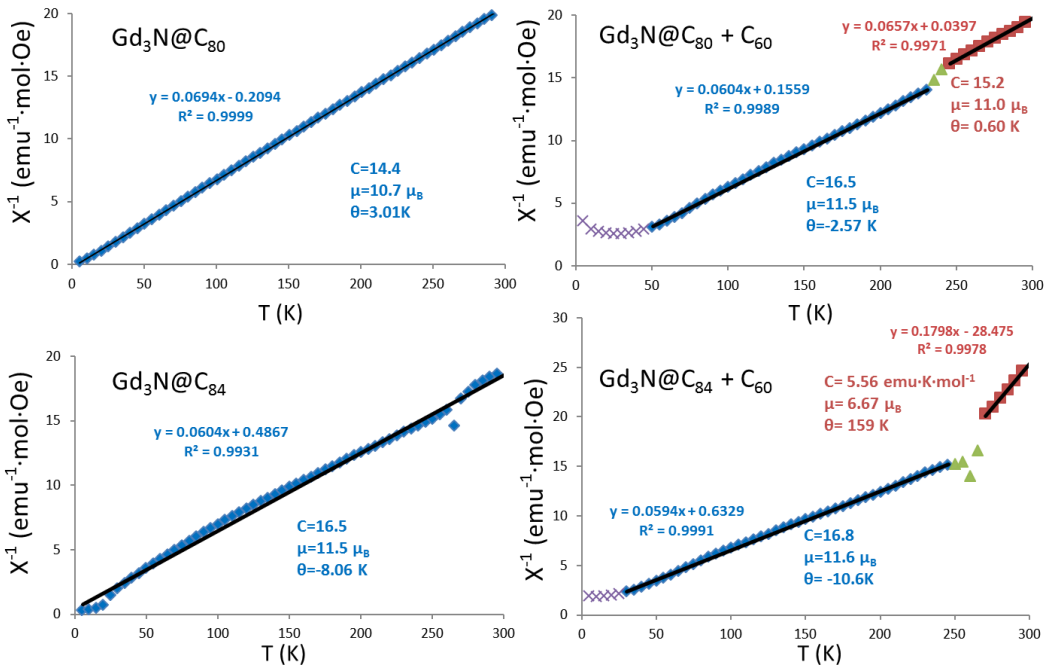

Figure 4. χ^{-1} vs T plots for Gd EMFs. The Curie constant C, effective magnetic moment μ_B, and Curie temperature θ are displayed in respective plot.

Both pure sample of $Gd_3N@C_{80}$ and $Gd_3N@C_{84}$ showed good linear relationships between the reciprocal of magnetic susceptibility and temperature. I note that there is one data point off the

line for $Gd_3N@C_{84}$ at 265K, which is repeatable in different trials. This is possibly due to the cessation of cluster rotation, which will be discussed further below. The effective magnetic moment for $Gd_3N@C_{80}$ is 10.7 μ_B, and the effective magnetic moment for $Gd_3N@C_{84}$ is slightly higher 11.5 μ_B. Compared to the reported value of 6.90 μ_B for $Gd@C_{82}$, the values for the TNT EMFs are 1.55 and 1.67 fold higher respectively, corresponding to expected 2.4 fold higher T_1 relaxivity for $Gd_3N@C_{80}$ and 2.8 fold higher T_1 relaxivity for $Gd_3N@C_{84}$. This result is in excellent agreement with our experimental study,[3] in which functionalized $Gd_3N@C_{80}$ showed 2.3-2.5 fold higher T_1 relaxivity compered to functionalized $Gd@C_{82}$. The higher T_1 relaxivity of functionalized $Gd_3N@C_{80}$ was attributed to the 3:1 Gd^{3+} ratio compared to $Gd@C_{82}$ at same concentration, but my study showed that it is more likely due to the intrinsic difference in effective magnetic moment, and the previous explanation could be just a mathematical coincidence which was not very close nevertheless. However the relaxivity values are also dependent on the functional groups attached; therefore, investigation of the TNT EMFs functionalized by the same reaction as reported for $Gd@C_{82}$ should be conducted to further validate the comparison.

In the samples diluted with C_{60}, the curves in Figure 4 are divided to 3 parts. In the low temperature region (below 50 K for $Gd_3N@C_{80}$ and below 30 K for $Gd_3N@C_{84}$, shown in purple), there was a small increase in magnetic susceptibility, and this region does not obey the Curie-Weiss law. In the middle region (50-235 K for $Gd_3N@C_{80}$, and 30-245 K for $Gd_3N@C_{84}$, shown in blue), both samples showed good Curie paramagnetic behavior, and effective magnetic moment of 11.5 μ_B and 11.6 μ_B were calculated for $Gd_3N@C_{80}$ and $Gd_3N@C_{84}$, respectively, which are very close to each other. After a transition (shown in green), in the high temperature

region (245-300 K for $Gd_3N@C_{80}$, 270-300 K for $Gd_3N@C_{84}$, shown in red) a linear relationship was recovered with lower calculated effective magnetic moments.

Although diamagnetic C_{60} has no direct contribution to magnetization, it can separate Gd TNT EMF molecules and reduce intermolecular interactions. Therefore, any change in intramolecular interaction among the three Gd^{3+} inside a cage is magnified. In the results from the pure samples, the curve for $Gd_3N@C_{80}$ showed linearity through the whole temperature range, while the curve for $Gd_3N@C_{84}$ showed very minor deviation from linearity, which is however consistent with that of the C_{60} diluted $Gd_3N@C_{84}$ sample in terms of both direction and corresponding temperature. In aqueous solutions of functionalized Gd TNT EMFs, the buckyballs are stacked together to form over 100-1,000 nm sized aggregates[2,8] (Figure 5) in which exist the intermolecular interactions among the Gd_3N clusters; therefore, the results for pure TNT EMFs may be a better model to discuss the relaxation behavior of the functionalized Gd EMFs. Meanwhile, the results for C_{60} diluted TNT EMFs give more insight about the influence of the molecular or cluster motion.

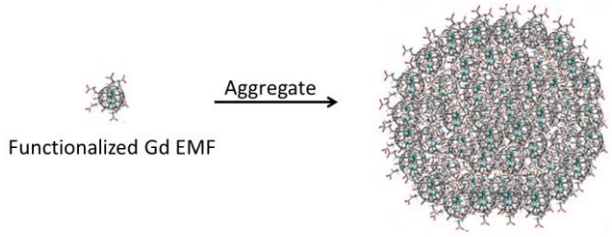

Figure 5. Aggregation of functionalized Gd EMF in aqueous solution

The change of the curves for C_{60} diluted samples can be explained by cluster motion in the TNT EMFs. At low temperature the clusters are frozen from motion, and at 30-50 K, the clusters start ammonia-like nitrogen inversion and the magnetic behavior reflects an average position of the

nitrogen atom, which is in the tri-metal plane. As seen in Figure 4, this factor has a larger effect in $Gd_3N@C_{80}$ which has a pyramidal cluster[9] than in $Gd_3N@C_{84}$ which has a planer cluster.[10] At 230-250 K, the clusters start to rotate, which accounts for the change in magnetic behavior in that region. The cluster rotation in $Gd_3N@C_{80}$ is in-plane rotation of the three Gd^{3+} ions (Figure 6, top), and the influence of rotation is averaged on the time scale of magnetization measurement; therefore, the observed magnetic behavior for $Gd_3N@C_{80}$ with and without cluster rotation is similar. In the cluster rotation of $Gd_3N@C_{84}$, nevertheless, one Gd^{3+} ion (Gd1) is fixed near the pentalene unit, while the other two Gd^{3+} ions (Gd2 and Gd3) rotate about the Gd1-N axis perpendicular to the tri-metal plane (Figure 6, bottom). In such rotation, the magnetic contribution from Gd2 and Gd3 are canceled by the cluster rotation, and only Gd1 contributes to the molecular effective magnetic moment, which resembles the situation in $Gd@C_{82}$. Therefore, the 6.67 μ_B effective magnetic moment for $Gd_3N@C_{84}$ is close to that of $Gd@C_{82}$, 6.90 μ_B. On the contrary, the magnetic susceptibility of pure $Gd_3N@C_{84}$ is not significantly affected by temperature, suggesting the cluster rotation is limited by intermolecular magnetic interactions.

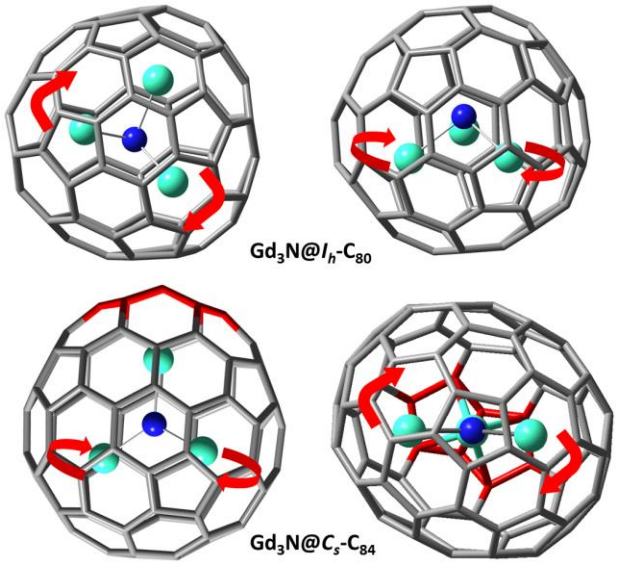

Figure 6 Cluster rotation in $Gd_3N@C_{80}$ and $Gd_3N@C_{84}$.

7.4 Conclusion

The magnetic behavior of $Gd_3N@C_{80}$ and $Gd_3N@C_{84}$ were investigated via SQUID measurements. Both TNT EMFs have higher effective magnetic moment than $Gd@C_{82}$, suggesting a 2.4-2.8 fold higher T_1 relaxivity in their water-soluble derivatives. The influence of cluster motion can be clearly seen in C_{60} diluted samples. Compared to $Gd_3N@C_{80}$, $Gd_3N@C_{84}$ is more significantly affected by cluster motion, and its derivative can be a good MRI contrast agent only when they aggregate. Experimental studies of $Gd_3N@C_{80}$ and $Gd_3N@C_{84}$ derivatives as MRI contrast should be performed to confirm the theory.

REFERENCE

(1) Mikawa, M.; Kato, H.; Okumura, M.; Narazaki, M.; Kanazawa, Y.; Miwa, N.; Shinohara, H.: Paramagnetic Water-Soluble Metallofullerenes Having the Highest Relaxivity For MRI Contrast Agents. *Bioconjugate Chem.* **2001**, *12*, 510-514.

(2) Zhang, J.; Fatouros, P. P.; Shu, C.; Reid, J.; Owens, L. S.; Cai, T.; Gibson, H. W.; Long, G. L.; Corwin, F. D.; Chen, Z.-J.; Dorn, H. C.: High Relaxivity Trimetallic Nitride (Gd_3N) Metallofullerene MRI Contrast Agents with Optimized Functionality. *Bioconjugate Chem.* **2010**, *21*, 610-615.

(3) Shu, C.; Corwin, F. D.; Zhang, J.; Chen, Z.; Reid, J. E.; Sun, M.; Xu, W.; Sim, J. H.; Wang, C.; Fatouros, P. P.; Esker, A. R.; Gibson, H. W.; Dorn, H. C.: Facile Preparation of a New Gadofullerene-Based Magnetic Resonance Imaging Contrast Agent with High ^1H Relaxivity. *Bioconjugate Chem.* **2009**, *20*, 1186-1193.

(4) Caravan, P.; Ellison, J. J.; McMurry, T. J.; Lauffer, R. B.: Gadolinium(III) Chelates as MRI Contrast Agents: Structure, Dynamics, and Applications. *Chem. Rev.* **1999**, *99*, 2293-2352.

(5) Funasaka, H.; Sakurai, K.; Oda, Y.; Yamamoto, K.; Takahashi, T.: Magnetic Properties of $Gd@C_{82}$ Metallofullerene. *Chem. Phys. Lett.* **1995**, *232*, 273-277.

(6) Ge, Z. X.; Duchamp, J. C.; Cai, T.; Gibson, H. W.; Dorn, H. C.: Purification of Endohedral Trimetallic Nitride Fullerenes In A Single, Facile Step. *J. Am. Chem. Soc.* **2005**, *127*, 16292-16298.

(7) Smirnova, T. I.; Smirnov, A. I.; Chadwick, T. G.; Walker, K. L.: Characterization of Magnetic and Electronic Properties of Trimetallic Nitride Endohedral Fullerenes by SQUID Magnetometry and Electron Paramagnetic Resonance. *Chem. Phys. Lett.* **2008**, *453*, 233-237.

(8) Shultz, M. D.; Wilson, J. D.; Fuller, C. E.; Zhang, J.; Dorn, H. C.; Fatouros, P. P.: Metallofullerene-based Nanoplatform for Brain Tumor Brachytherapy and Longitudinal Imaging in a Murine Orthotopic Xenograft Model. *Radiology* **2011**, *261*, 136-143.

(9) Stevenson, S.; Phillips, J. P.; Reid, J. E.; Olmstead, M. M.; Rath, S. P.; Balch, A. L.: Pyramidalization of Gd_3N inside a C_{80} Cage: the Synthesis and Structure of $Gd_3N@C_{80}$. *Chem. Commun.* **2004**, 2814-2815.

(10) Zuo, T.; Walker, K.; Olmstead, M. M.; Melin, F.; Holloway, B. C.; Echegoyen, L.; Dorn, H. C.; Chaur, M. N.; Chancellor, C. J.; Beavers, C. M.; Balch, A. L.; Athans, A. J.: New Egg-shaped Fullerenes: Non-Isolated Pentagon Structures of $Tm_3N@C_s(51365)\text{-}C_{84}$ and $Gd_3N@C_s(51365)\text{-}C_{84}$. *Chem. Commun.* **2008**, 1067-1069.

APPENDIX

Hydrogenation of endohedral metallofullerenes. The hydrogenation of TNT EMF was carried out by the Benkeser reduction following Wujun Fu's description. A representative experimental procedure is as follows: $Sc_3N@C_{80}$ (13.5 mg, 0.012mmol) was dissolved in 30 mL of ethylenediamine and 909 mg (12.3 mmol) of *t*-butanol was added. The resulting solution was deoxygenated with bubbling argon for 30 min, and 86 mg (12.3 mmol) of lithium metal was added. The mixture was stirred vigorously under a N_2 atmosphere. The dark brown solution slowly changed to yellow and then blue. The blue color disappeared gradually due to the decay of the solvated electrons. After 24 h, the solution turned pale yellow. The resulting solution was poured into 20 mL of ice water to destroy the excess lithium metal. The mixture was extracted with toluene and the toluene layer was washed with brine, dried over anhydrous Na_2SO_4 and evaporated under reduced pressure to obtain the hydrogenated product (~1.2 mg).

The product was purified on HPLC (PYE, 17 min, 2 mL/min toluene), and was subject to ^1H and ^{13}C NMR characterization. The NMR results as shown below are informative but not conclusive on the structure of the product.

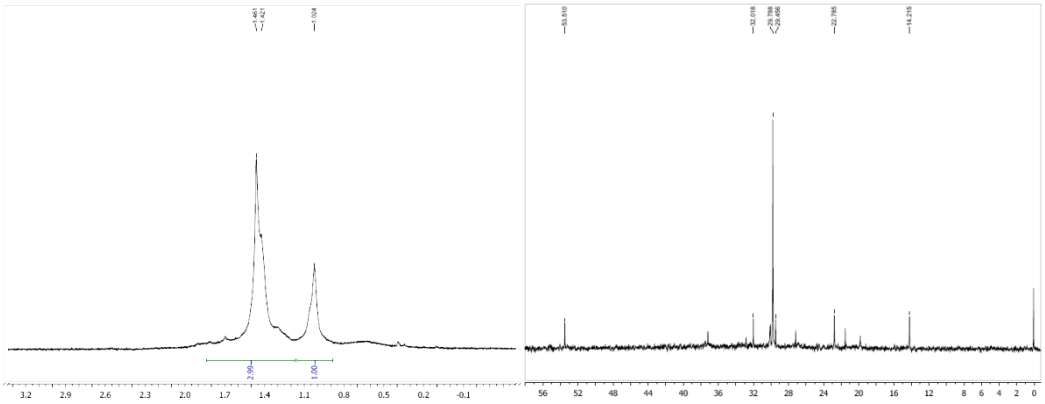

^1H and ^{13}C NMR results for hydrogenation products of $Sc_3N@C_{80}$.

Direct hydrogenation of the $Sc_3N@C_{80}$ was performed in toluene with Pd/C, and in ethanol with Pt/C, respectively. Both reactions were allowed for 7 days, and no hydrogenated product was detected from the reaction mixture.

Title: Trimetallic Nitride Template Endohedral Metallofullerenes: Discovery, Structural Characterization, Reactivity, and Applications

Author: Jianyuan Zhang, Steven Stevenson, and Harry C. Dorn

Publication: Accounts of Chemical Research

Publisher: American Chemical Society

Date: Jul 1, 2013

PERMISSION/LICENSE IS GRANTED FOR YOUR ORDER AT NO CHARGE

This type of permission/license, instead of the standard Terms & Conditions, is sent to you because no fee is being charged for your order. Please note the following:

- Permission is granted for your request in both print and electronic formats, and translations.
- If figures and/or tables were requested, they may be adapted or used in part.
- Please print this page for your records and send a copy of it to your publisher/graduate school.
- Appropriate credit for the requested material should be given as follows: "Reprinted (adapted) with permission from (COMPLETE REFERENCE CITATION). Copyright (YEAR) American Chemical Society." Insert appropriate information in place of the capitalized words.
- One-time permission is granted only for the use specified in your request. No additional uses are granted (such as derivative works or other editions). For any other uses, please submit a new request.

JOHN WILEY AND SONS LICENSE TERMS AND CONDITIONS

Dec 20, 2013

This is a License Agreement between Jianyuan Zhang ("You") and John Wiley and Sons ("John Wiley and Sons") provided by Copyright Clearance Center ("CCC"). The license consists of your order details, the terms and conditions provided by John Wiley and Sons, and the payment terms and conditions.

All payments must be made in full to CCC. For payment instructions, please see information listed at the bottom of this form.

License Number	3094281451612
License date	Feb 22, 2013
Licensed content publisher	John Wiley and Sons
Licensed content publication	Angewandte Chemie International Edition
Licensed content title	Isolation and Characterization of Sc2C2@C68: A Metal-Carbide Endofullerene with a Non-IPR Carbon Cage
Licensed copyright line	Copyright © 2006 WILEY-VCH Verlag GmbH & Co. KGaA, Weinheim
Licensed content author	Zhi-Qiang Shi,Xin Wu,Chun-Ru Wang,Xin Lu,Hisanori Shinohara
Licensed content date	Feb 24, 2006
Start page	2107
End page	2111
Type of use	Dissertation/Thesis
Requestor type	Author of this Wiley article
Format	Electronic
Portion	Full article
Will you be translating?	No
Total	0.00 USD
Terms and Conditions	

TERMS AND CONDITIONS

This copyrighted material is owned by or exclusively licensed to John Wiley & Sons, Inc. or one of its group companies (each a "Wiley Company") or a society for whom a Wiley Company has exclusive publishing rights in relation to a particular journal (collectively WILEY"). By clicking "accept" in connection with completing this licensing transaction, you agree that the following terms and conditions apply to this transaction (along with the billing and payment terms and conditions established by the Copyright Clearance Center Inc., ("CCC's Billing and Payment terms and conditions"), at the time that you opened your Rightslink account (these are available at any time at http://myaccount.copyright.com)

Terms and Conditions

1. The materials you have requested permission to reproduce (the "Materials") are protected by copyright.

2. You are hereby granted a personal, non-exclusive, non-sublicensable, non-transferable, worldwide, limited license to reproduce the Materials for the purpose specified in the licensing process. This license is for a one-time use only with a maximum distribution equal to the number that you identified in the licensing process. Any form of republication granted by this licence must be completed within two years of the date of the grant of this licence (although copies prepared before may be distributed thereafter). The Materials shall not be used in any other manner or for any other purpose. Permission is granted subject to an appropriate acknowledgement given to the author, title of the material/book/journal and the publisher. You shall also duplicate the copyright notice that appears in the Wiley publication in your use of the Material. Permission is also granted on the understanding that nowhere in the text is a previously published source acknowledged for all or part of this Material. Any third party material is expressly excluded from this permission.

3. With respect to the Materials, all rights are reserved. Except as expressly granted by the terms of the license, no part of the Materials may be copied, modified, adapted (except for minor reformatting required by the new Publication), translated, reproduced, transferred or distributed, in any form or by any means, and no derivative works may be made based on the Materials without the prior permission of the respective copyright owner. You may not alter, remove or suppress in any manner any copyright, trademark or other notices displayed by the Materials. You may not license, rent, sell, loan, lease, pledge, offer as security, transfer or assign the Materials, or any of the rights granted to you hereunder to any other person.

4. The Materials and all of the intellectual property rights therein shall at all times remain the exclusive property of John Wiley & Sons Inc or one of its related companies (WILEY) or their respective licensors, and your interest therein is only that of having possession of and the right to reproduce the Materials pursuant to Section 2 herein during the continuance of this Agreement. You agree that you own no right, title or interest in or to the Materials or any of the intellectual property rights therein. You shall have no rights hereunder other than the license as provided for above in Section 2. No right, license or interest to any trademark, trade name, service mark or other branding ("Marks") of WILEY or its licensors is granted hereunder, and you agree that you shall not assert any such right, license or interest with respect thereto.

5. NEITHER WILEY NOR ITS LICENSORS MAKES ANY WARRANTY OR REPRESENTATION OF ANY KIND TO YOU OR ANY THIRD PARTY, EXPRESS, IMPLIED OR STATUTORY, WITH RESPECT TO THE MATERIALS OR THE ACCURACY OF ANY INFORMATION CONTAINED IN THE MATERIALS, INCLUDING, WITHOUT LIMITATION, ANY IMPLIED WARRANTY OF MERCHANTABILITY, ACCURACY, SATISFACTORY QUALITY, FITNESS FOR A PARTICULAR PURPOSE, USABILITY, INTEGRATION OR NON-INFRINGEMENT AND ALL SUCH WARRANTIES ARE HEREBY EXCLUDED BY WILEY AND ITS LICENSORS AND WAIVED BY YOU.

6. WILEY shall have the right to terminate this Agreement immediately upon breach of this Agreement by you.

7. You shall indemnify, defend and hold harmless WILEY, its Licensors and their respective directors, officers, agents and employees, from and against any actual or threatened claims, demands, causes of action or proceedings arising from any breach of this Agreement by you.

8. IN NO EVENT SHALL WILEY OR ITS LICENSORS BE LIABLE TO YOU OR ANY OTHER PARTY OR ANY OTHER PERSON OR ENTITY FOR ANY SPECIAL, CONSEQUENTIAL, INCIDENTAL, INDIRECT, EXEMPLARY OR PUNITIVE DAMAGES, HOWEVER CAUSED, ARISING OUT OF OR IN CONNECTION WITH THE DOWNLOADING, PROVISIONING, VIEWING OR USE OF THE MATERIALS REGARDLESS OF THE FORM OF ACTION, WHETHER FOR BREACH OF CONTRACT, BREACH OF WARRANTY, TORT, NEGLIGENCE, INFRINGEMENT OR OTHERWISE (INCLUDING, WITHOUT LIMITATION, DAMAGES BASED ON LOSS OF PROFITS, DATA, FILES, USE, BUSINESS OPPORTUNITY OR CLAIMS OF THIRD PARTIES), AND WHETHER OR NOT THE PARTY HAS BEEN ADVISED OF THE POSSIBILITY OF SUCH DAMAGES. THIS LIMITATION SHALL APPLY NOTWITHSTANDING ANY FAILURE OF ESSENTIAL PURPOSE OF ANY LIMITED REMEDY PROVIDED HEREIN.

9. Should any provision of this Agreement be held by a court of competent jurisdiction to be illegal, invalid, or unenforceable, that provision shall be deemed amended to achieve as nearly as possible the same economic effect as the original provision, and the legality, validity and

enforceability of the remaining provisions of this Agreement shall not be affected or impaired thereby.

10. The failure of either party to enforce any term or condition of this Agreement shall not constitute a waiver of either party's right to enforce each and every term and condition of this Agreement. No breach under this agreement shall be deemed waived or excused by either party unless such waiver or consent is in writing signed by the party granting such waiver or consent. The waiver by or consent of a party to a breach of any provision of this Agreement shall not operate or be construed as a waiver of or consent to any other or subsequent breach by such other party.

11. This Agreement may not be assigned (including by operation of law or otherwise) by you without WILEY's prior written consent.

12. Any fee required for this permission shall be non-refundable after thirty (30) days from receipt.

13. These terms and conditions together with CCC's Billing and Payment terms and conditions (which are incorporated herein) form the entire agreement between you and WILEY concerning this licensing transaction and (in the absence of fraud) supersedes all prior agreements and representations of the parties, oral or written. This Agreement may not be amended except in writing signed by both parties. This Agreement shall be binding upon and inure to the benefit of the parties' successors, legal representatives, and authorized assigns.

14. In the event of any conflict between your obligations established by these terms and conditions and those established by CCC's Billing and Payment terms and conditions, these terms and conditions shall prevail.

15. WILEY expressly reserves all rights not specifically granted in the combination of (i) the license details provided by you and accepted in the course of this licensing transaction, (ii) these terms and conditions and (iii) CCC's Billing and Payment terms and conditions.

16. This Agreement will be void if the Type of Use, Format, Circulation, or Requestor Type was misrepresented during the licensing process.

17. This Agreement shall be governed by and construed in accordance with the laws of the State of New York, USA, without regards to such state's conflict of law rules. Any legal action, suit or proceeding arising out of or relating to these Terms and Conditions or the breach thereof shall be instituted in a court of competent jurisdiction in New York County in the State of New York in the United States of America and each party hereby consents and submits to the personal jurisdiction of such court, waives any objection to venue in such court and consents to service of process by registered or certified mail, return receipt requested, at the last known address of such party.

Wiley Open Access Terms and Conditions

All research articles published in Wiley Open Access journals are fully open access: immediately freely available to read, download and share. Articles are published under the terms of the Creative Commons Attribution Non Commercial License. which permits use, distribution and reproduction in any medium, provided the original work is properly cited and is not used for commercial purposes. The license is subject to the Wiley Open Access terms and conditions:
Wiley Open Access articles are protected by copyright and are posted to repositories and websites in accordance with the terms of the Creative Commons Attribution Non Commercial License. At the time of deposit, Wiley Open Access articles include all changes made during peer review, copyediting, and publishing. Repositories and websites that host the article are responsible for incorporating any publisher-supplied amendments or retractions issued subsequently.
Wiley Open Access articles are also available without charge on Wiley's publishing platform, **Wiley Online Library** or any successor sites.

Use by non-commercial users

For non-commercial and non-promotional purposes individual users may access, download, copy, display and redistribute to colleagues Wiley Open Access articles, as well as adapt,

translate, text- and data-mine the content subject to the following conditions:

- The authors' moral rights are not compromised. These rights include the right of "paternity" (also known as "attribution" - the right for the author to be identified as such) and "integrity" (the right for the author not to have the work altered in such a way that the author's reputation or integrity may be impugned).
- Where content in the article is identified as belonging to a third party, it is the obligation of the user to ensure that any reuse complies with the copyright policies of the owner of that content.
- If article content is copied, downloaded or otherwise reused for non-commercial research and education purposes, a link to the appropriate bibliographic citation (authors, journal, article title, volume, issue, page numbers, DOI and the link to the definitive published version on Wiley Online Library) should be maintained. Copyright notices and disclaimers must not be deleted.
- Any translations, for which a prior translation agreement with Wiley has not been agreed, must prominently display the statement: "This is an unofficial translation of an article that appeared in a Wiley publication. The publisher has not endorsed this translation."

Use by commercial "for-profit" organisations

Use of Wiley Open Access articles for commercial, promotional, or marketing purposes requires further explicit permission from Wiley and will be subject to a fee. Commercial purposes include:

- Copying or downloading of articles, or linking to such articles for further redistribution, sale or licensing;
- Copying, downloading or posting by a site or service that incorporates advertising with such content;
- The inclusion or incorporation of article content in other works or services (other than normal quotations with an appropriate citation) that is then available for sale or licensing, for a fee (for example, a compilation produced for marketing purposes, inclusion in a sales pack)
- Use of article content (other than normal quotations with appropriate citation) by for-profit organisations for promotional purposes
- Linking to article content in e-mails redistributed for promotional, marketing or educational purposes;
- Use for the purposes of monetary reward by means of sale, resale, licence, loan, transfer or other form of commercial exploitation such as marketing products
- Print reprints of Wiley Open Access articles can be purchased from: corporatesales@wiley.com

Other Terms and Conditions:

BY CLICKING ON THE "I AGREE..." BOX, YOU ACKNOWLEDGE THAT YOU HAVE READ AND FULLY UNDERSTAND EACH OF THE SECTIONS OF AND PROVISIONS SET FORTH IN THIS AGREEMENT AND THAT YOU ARE IN AGREEMENT WITH AND ARE WILLING TO ACCEPT ALL OF YOUR OBLIGATIONS AS SET FORTH IN THIS AGREEMENT.

v1.7

If you would like to pay for this license now, please remit this license along with your payment made payable to "COPYRIGHT CLEARANCE CENTER" otherwise you will be invoiced within 48 hours of the license date. Payment should be in the form of a check or money order referencing your account number and this invoice number 500962778. Once you receive your invoice for this order, you may pay your invoice by credit card. Please follow instructions provided at that time.

Make Payment To:
Copyright Clearance Center
Dept 001
P.O. Box 843006
Boston, MA 02284-3006

For suggestions or comments regarding this order, contact RightsLink Customer Support: customercare@copyright.com or +1-877-622-5543 (toll free in the US) or +1-978-646-2777.

Gratis licenses (referencing $0 in the Total field) are free. Please retain this printable license for your reference. No payment is required.

Title: Nanoscale Fullerene Compression of an Yttrium Carbide Cluster

Author: Jianyuan Zhang, Tim Fuhrer, Wujun Fu, Jiechao Ge, Daniel W. Bearden, Jerry Dallas, James Duchamp, Kenneth Walker, Hunter Champion, Hugo Azurmendi, Kim Harich, and Harry C. Dorn

Publication: Journal of the American Chemical Society

Publisher: American Chemical Society

Date: May 1, 2012

PERMISSION/LICENSE IS GRANTED FOR YOUR ORDER AT NO CHARGE

This type of permission/license, instead of the standard Terms & Conditions, is sent to you because no fee is being charged for your order. Please note the following:

- Permission is granted for your request in both print and electronic formats, and translations.
- If figures and/or tables were requested, they may be adapted or used in part.
- Please print this page for your records and send a copy of it to your publisher/graduate school.
- Appropriate credit for the requested material should be given as follows: "Reprinted (adapted) with permission from (COMPLETE REFERENCE CITATION). Copyright (YEAR) American Chemical Society." Insert appropriate information in place of the capitalized words.
- One-time permission is granted only for the use specified in your request. No additional uses are granted (such as derivative works or other editions). For any other uses, please submit a new request.

Title: Enhanced Dipole Moments in Trimetallic Nitride Template Endohedral Metallofullerenes with the Pentalene Motif

Author: Jianyuan Zhang, Daniel W. Bearden, Tim Fuhrer, Liaosa Xu, Wujun Fu, Tianming Zuo, and Harry C. Dorn

Publication: Journal of the American Chemical Society

Publisher: American Chemical Society

Date: Mar 1, 2013

PERMISSION/LICENSE IS GRANTED FOR YOUR ORDER AT NO CHARGE

This type of permission/license, instead of the standard Terms & Conditions, is sent to you because no fee is being charged for your order. Please note the following:

- Permission is granted for your request in both print and electronic formats, and translations.
- If figures and/or tables were requested, they may be adapted or used in part.
- Please print this page for your records and send a copy of it to your publisher/graduate school.
- Appropriate credit for the requested material should be given as follows: "Reprinted (adapted) with permission from (COMPLETE REFERENCE CITATION). Copyright (YEAR) American Chemical Society." Insert appropriate information in place of the capitalized words.
- One-time permission is granted only for the use specified in your request. No additional uses are granted (such as derivative works or other editions). For any other uses, please submit a new request.

Title: Gd2@C79N: Isolation, Characterization, and Monoadduct Formation of a Very Stable Heterofullerene with a Magnetic Spin State of S = 15/2

Author: Wujun Fu, Jianyuan Zhang, Tim Fuhrer, Hunter Champion, Ko Furukawa, Tatsuhisa Kato, James E. Mahaney, Brian G. Burke, Keith A. Williams, Kenneth Walker, Caitlyn Dixon, Jiechao Ge, Chunying Shu, Kim Harich, and Harry C. Dorn

Publication: Journal of the American Chemical Society

Publisher: American Chemical Society

Date: Jun 1, 2011

PERMISSION/LICENSE IS GRANTED FOR YOUR ORDER AT NO CHARGE

This type of permission/license, instead of the standard Terms & Conditions, is sent to you because no fee is being charged for your order. Please note the following:

- Permission is granted for your request in both print and electronic formats, and translations.
- If figures and/or tables were requested, they may be adapted or used in part.
- Please print this page for your records and send a copy of it to your publisher/graduate school.
- Appropriate credit for the requested material should be given as follows: "Reprinted (adapted) with permission from (COMPLETE REFERENCE CITATION). Copyright (YEAR) American Chemical Society." Insert appropriate information in place of the capitalized words.
- One-time permission is granted only for the use specified in your request. No additional uses are granted (such as derivative works or other editions). For any other uses, please submit a new request.